OPTIMIZING CONVENTIONAL COMBUSTION AND IMPLEMENTING LOW-TEMPERATURE COMBUSTION OF BIODIESEL IN A COMMON-RAIL HIGH-SPEED DIRECT-INJECTION ENGINE

BY

MICHAEL T. LEICK

THESIS

Submitted in partial fulfillment of the requirements
for the degree of Master of Science in Mechanical Engineering
in the Graduate College of the
University of Illinois at Urbana-Champaign, 2010

Urbana, Illinois

Adviser:

Professor Chia-Fon Lee

Abstract

Biodiesel and different biodiesel-diesel blends were run in a production compression ignition engine to determine optimized engine control module (ECM) settings for each fuel. Focus was placed on a combination of exhaust gas recirculation (EGR) ratio and start of injection (SOI) timing, as these parameters are easily modified and have significant effects on engine emissions. Tests were run at low to moderate engine load at different engine speeds. It was found that with the ECM's default settings, higher blends of biodiesel tended to result in higher NOx emissions and lower soot emissions, in line with previous studies. It was also found that increasing the EGR ratio to account for the different stoichiometric air-fuel ratio of biodiesel was effective in bringing NOx emissions to similar or lower levels compared with those of petroleum diesel. At low load conditions, improved fuel economy could also be achieved by advancing the start of injection relative to the ECM default timing.

Pure soybean biodiesel was also run with high rates of EGR and modified injection schemes in order to achieve simultaneous reduction of NOx and soot emissions consistent with low temperature combustion. At low load conditions, increasing the EGR ratio to high levels was sufficient to achieve very low NOx and soot emissions. As engine load increased, high levels of EGR brought NOx emissions to very low levels, but soot emissions increased substantially. The amount of EGR was increased to the point of combustion deterioration without seeing a reduction in soot emissions. Thus, the engine's default injection strategy needed to be modified in order to achieve low temperature combustion. Strategies found effective were a reduced amount of pre-injection, later injection timing, and a combination of the two. With these strategies, low temperature combustion was achieved through a moderate range of engine load. To see the effect of engine speed, cases were run at different speeds with a

constant load. Modifications to the injection strategy were found to be beneficial at different engine speeds.

Acknowledgements

I wish to thank the College of Engineering, the Department of Mechanical Science and Engineering, and my advisor, Professor Chia-Fon Lee, for their work in locating sources of funding for students such as myself. At times, I may have lost sight of what a blessing this has been. In the end, I appreciate the opportunity I have been given to further my theoretical understanding and gain practical research experience in an area of great interest to me. I would also like to thank Professor Alan Hansen and Professor Dimitrios Kyritsis for their guidance and helpfulness during the course of my study.

My predecessor, Tien Mun Foong, deserves credit for setting up much of the engine and teaching me how to use it. Thanks also go to Yu Liu, Alex Burnap, Matt Rosenberger, Xuan Feng, and Darren Ting for assisting me in working on the engine and taking data. I would like to thank my friends Jacob Walker, Brandon Logeman, Evan Williams, and James Doelling for helping me to maintain a portion of my social skills during this time in my life. Finally, I suppose no thesis is complete without the customary acknowledgment of one's wonderful family for their support in the difficult times.

Table of Contents

Chapter 1: Introduction 1

Chapter 2: Literature Review 3

2.1 Conventional Diesel Combustion 3

2.2 Exhaust Gas Recirculation 9

2.3 Low Temperature Combustion 13

2.4 Biodiesel Production and Life-Cycle Analysis 15

2.5 Biodiesel Combustion 17

Chapter 3: Experimental Methodology 20

3.1 Experimental Setup 20

3.2 Test Fuels 34

3.3 Measurement Devices 35

3.4 Calculations and Data Analysis 38

3.5 Experimental Procedures and Operating Conditions 43

Chapter 4: Experimental Results and Discussion 60

4.1 Conventional Combustion Study 60

4.2 Low Temperature Combustion Study 72

Chapter 5: Conclusions and Future Work 99

References 101

Appendix A: Incomplete List of Useful INCA Parameters 107

Appendix B: Selected Operating Parameters for LTC Study 109

Chapter 1:
Introduction

Biodiesel has become a common alternative fuel for use in compression-ignition engines. In the United States, biodiesel is predominantly produced from soybeans and blended into petroleum diesel, providing a more renewable fuel with reduced emissions of certain pollutants, specifically soot, hydrocarbons (HC), and carbon monoxide (CO). Though soybean-derived biodiesel is somewhat limited in quantity due to land constraints and the inevitable debate of food versus fuel, next-generation feedstocks such as algae are being researched and may provide a much more substantial supply of biodiesel. These advances on the production end of biodiesel must be matched with advances in utilization. Control modules for compression-ignition engines are typically optimized for use with petroleum diesel. However, biodiesel has different fuel properties which alter an engine's combustion characteristics. Therefore, the first part of the current study aims to optimize certain engine control parameters for use with biodiesel.

At the same time, increasingly strict emissions regulations have prompted much research on strategies to reduce engine emissions. For compression-ignition engines, soot and oxides of nitrogen (NOx) are the typical problematic pollutants. In conventional diesel combustion, these pollutants are particularly difficult to manage due to a soot-NOx tradeoff, whereby reduction of one pollutant generally results in an increase of the other. As a result, engine companies typically rely on aftertreatment systems in order to meet emissions regulations for soot and NOx. Meanwhile, research has shown the potential for simultaneous reduction of soot and NOx in a combustion strategy known as low temperature combustion. This strategy has its own set of issues to resolve, as HC and CO emissions tend to be higher, and combustion phasing may be unstable from cycle to cycle. Given that biodiesel tends to reduce HC and CO emissions, a study

of biodiesel combustion in the low temperature combustion regime is a logical choice for the second part of this study.

With this in mind, the remainder of this document is broken down as follows. First, a literature review of research relevant to this topic is presented. Next, the experimental methodology is presented, including a description of the engine setup, overview of measurement equipment, and explanation of experimental procedures. Following that, results and discussion will be presented for the conventional combustion optimization as well as the low temperature combustion study. Finally, conclusions of this study and suggestions for further work related to this engine will be offered.

Chapter 2:
Literature Review

2.1 Conventional Diesel Combustion

The fundamental aspects of diesel engines must be studied before any advanced work may be done in the area. Emphasis is given to the direct injection diesel engine, as it is most prevalent and relates to the test engine utilized in this study. Starting at the most basic level, a brief operating description of the diesel engine is given here. Air is inducted into the cylinder and compressed, creating a high pressure and temperature environment. As the piston approaches top dead center (TDC), fuel is injected into the cylinder. The fuel partially atomizes and vaporizes in the hot environment before self-igniting. The ensuing combustion can vary widely in character depending on the amount of mixing that occurs prior to auto-ignition.

Diesel combustion in general is an unsteady, heterogeneous, and quite complex phenomenon. For typical metal engines, it is difficult to know exactly what goes on during the combustion process. In-cylinder pressure transducers provide some information about the heat release as a whole, and are an important tool in engine research. Using the in-cylinder pressure data, the apparent heat release rate may be calculated, taking into account heat transfer to the chamber walls, by way of first law analysis. Robust calculations have been made possible through a wealth of literature on the subject, as described in [1]. A typical heat release rate plot for a direct injection diesel engine is shown in Figure 2.1. As indicated in the diagram, the heat release process may be divided into four general parts. First, the period after the start of injection (SOI) but before the start of combustion is known as the ignition delay. During this phase, fuel atomization and vaporization is occurring, and a dip into negative territory may be seen on the heat release rate diagram due to the energy required for vaporization. Next comes the premixed combustion phase, which is characterized by a rapid increase in heat release rate.

Following the premixed combustion phase, mixing-controlled combustion occurs. Here, the rate of heat release is controlled by how quickly the remaining fuel-air mixture becomes available for burning. Finally, during the late combustion phase, little fuel remains in the cylinder, and the heat release rate becomes much lower. During this phase, kinetic rates are slowing as well due to the expansion process and consequently lower temperatures.

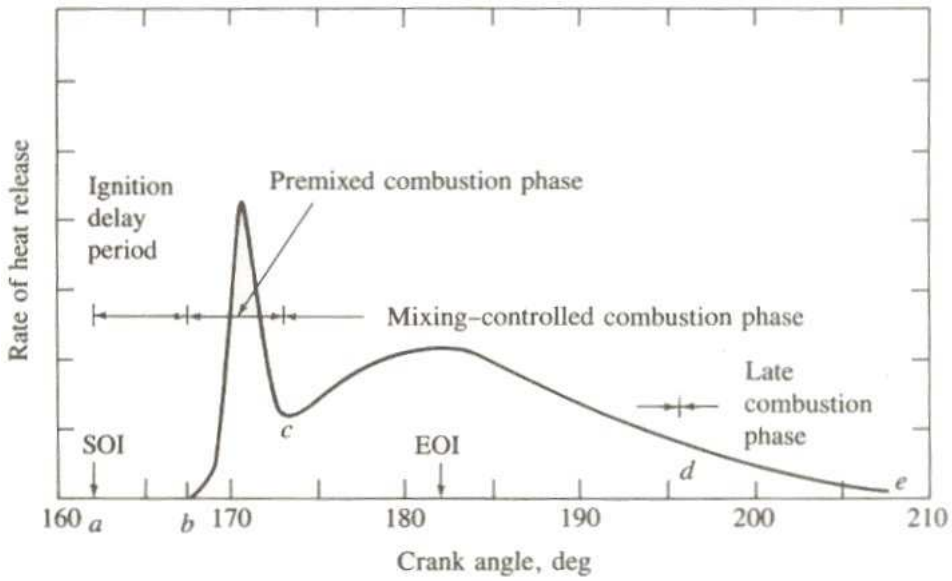


Figure 2.1: Typical heat release rate diagram for a direct injection diesel engine [2]

Beyond the in-cylinder pressure and calculated heat release rate, additional information about the combustion process is difficult to obtain using a typical metal engine. Constant volume combustion chambers and optically-accessible diesel engines have enabled much more insight into the combustion process through a wide variety of combustion imaging and laser diagnostic techniques. Recently, a conceptual model for diesel combustion has been proposed [3,4]. A diagram corresponding to this conceptual model is shown in Figure 2.2. According to the model, after the fuel is injected into the hot ambient air, fuel vaporization takes place in the

periphery of the liquid jet. The jet is enclosed by the air-fuel mixture as it penetrates further into the chamber. Auto-ignition occurs in the downstream portion of the jet in multiple points. At the same time, poly-cyclic aromatic hydrocarbon (PAH), a precursor of soot, is formed. Heat release from the fuel-rich mixture in the leading portion of the jet causes the premixed combustion. Meanwhile, diffusion combustion begins at the periphery of the fuel jet between the premixed combustion zone and the surrounding air. At the end of the premixed combustion, mixing-controlled combustion becomes dominant, and the main soot zone forms. At this point, the jet is almost fully developed, and the combustion reaches a quasi-steady condition as illustrated in Figure 2.2. It is during diffusion combustion that most of the soot is formed. Note that soot undergoes oxidation within the cylinder, and only a fraction of the soot produced is emitted in the engine exhaust. Oxides of nitrogen (NOx) also form during the diffusion combustion phase due to the high temperatures associated with near-stoichiometric combustion.

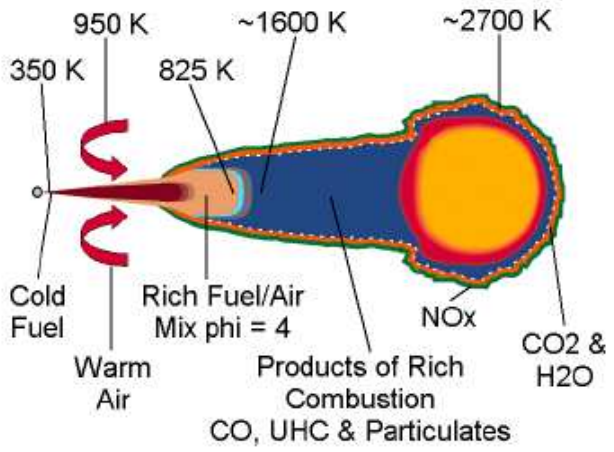


Figure 2.2: Conceptual model of quasi-steady burning jet proposed by John Dec [3]

The primary pollutants resulting from the diesel combustion process, therefore, are NOx and particulate matter, which is in part composed of soot. Emissions of carbon monoxide and

unburned hydrocarbons are generally rather small for diesel engines because the overall air-fuel ratio is sufficiently lean of stoichiometric. However, as the air-fuel ratio approaches its stoichiometric value, these emissions become more significant and need to be accounted for. A more detailed analysis of NOx and particulate matter emissions is included below, as these are the pollutants of focus in the current study.

The nitrogen oxide reaction mechanisms are relatively well known, and have been summarized in many sources, including [5]. A summary of the basic concepts is included here. The primary nitrogen oxide emitted from most combustion sources is nitric oxide (NO). There are three major sources of NO formed in combustion: oxidation of atmospheric nitrogen via the thermal NO (Zeldovich) mechanism, prompt NO mechanisms, and oxidation of nitrogen-containing organic compounds in fossil fuels via the fuel NO mechanism. The thermal NO mechanism is comprised of three reactions, whose rate constants have been accurately measured over a wide temperature range. Using these reactions, an equation may be written for the maximum NO formation rate. The resulting equation shows NO formation rate to be strongly dependent on burned gas temperature and dependent to a lesser degree on the oxygen concentration in the burned gas. In internal combustion engines, NO formed in the previously described processes begins to decompose after it is formed. However, as the piston expands and the cylinder temperature is reduced, NO decomposition is frozen at some point in the cycle, and the remaining quantity is emitted in the exhaust. For diesel engines, the high temperature burned gases mix with the remaining cooler air, reducing the cylinder temperature to a greater extent than gasoline engines. Therefore, the NO decomposition is lower, and relatively more NO is emitted in the exhaust.

Soot formation in diesel engines, meanwhile, is less well understood. Soot particles are thought to be formed in the locally rich region of combustion, where high temperature causes thermal cracking of the fuel. The general consensus is that the molecular precursor of soot forms in the process of breakdown and rearrangement of the fuel molecules, or pyrolysis [6]. As a result of pyrolysis, PAHs are formed, which subsequently generate soot particles through condensation, polymerization, and dehydrogenation. The newly-formed soot particles then grow in size through the addition of gas phase species like acetylene and PAH. Meanwhile, particle-particle collisions cause the soot particles to stick together, and coagulation takes place. Next, the amorphous soot particles are converted to a more graphite carbon material. Eventually, the soot particles go through an oxidation process. Soot formation is dominant in the initial combustion phase, during the premixed combustion and the beginning of diffusion combustion. However, in later portions of the cycle, soot oxidation becomes more prominent. Soot oxidation may be controlled either by the kinetics of the reaction or by surface diffusion, depending on the size of the particles. Higher in-cylinder temperature increases the oxidation rate during the late cycle, and only a small fraction of the initially formed soot is emitted in the exhaust [7].

The soot described above is only a portion of the regulated pollutant known as particulate matter. Particulate matter emitted from a typical diesel engine is composed of two types of particles: (1) fractal-like agglomerates of primary particles 15–30 nm in diameter, composed of carbon and traces of metallic ash, and coated with condensed heavier end organic compounds and sulfate; (2) nucleation particles composed of condensed hydrocarbons and sulfate [8]. An artist's representation of particulate matter according to this description is shown in Figure 2.3.

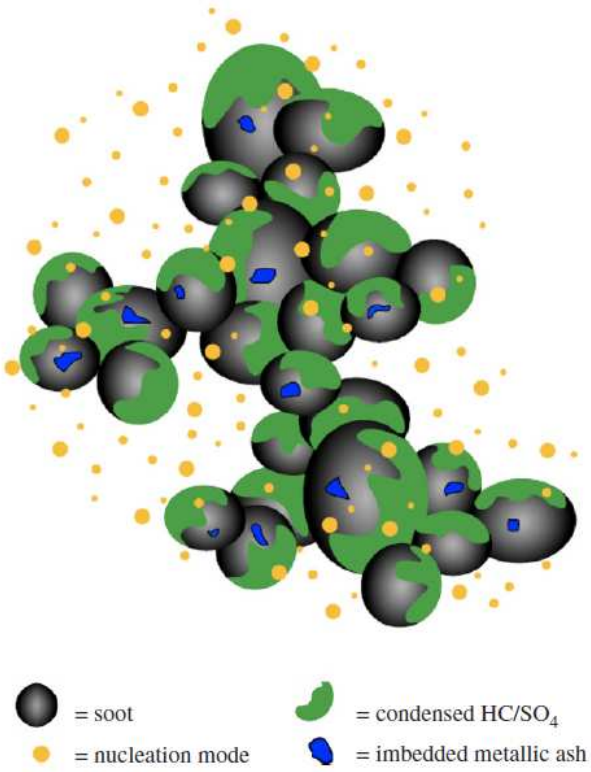


Figure 2.3: Artist's conception of particulate matter [8]

Measurement and characterization of this pollutant has become increasingly complex as engine-out emission levels continue to be regulated lower. In general, composition measurement is performed through offline chemical analysis. The collection substrate is first prepared before sampling the exhaust from the engine via a dilution tunnel. The particulate matter must then be removed from the substrate prior to chemical analysis. Conventional particulate matter mass measurements are made simply by passing a steady flow of diluted exhaust through a filter and recording the mass increase of the filter at the end of the test. Though this provides the overall particulate matter mass, it is not sufficient for chemical analysis [9]. No one system is sufficient to fully characterize the particulate matter. Rather, a wide variety of test equipment, each capable of characterizing certain components, is utilized to obtain the full characterization of

particulate matter. Due to the complexity and cost associated with full characterization, it will not be performed in the current study. Instead, the soot portion of particulate matter will be measured using a simple but well-developed filter paper method, as described in the measurement devices section. However, it is important to recognize the many constituents which fall under the category of particulate matter and acknowledge the limitations of the measurements made in this study.

2.2 Exhaust Gas Recirculation

Several modifications to the diesel engine have been made in recent years. A shift has been made from indirect to direct fuel injection, and high pressure common rail fuel systems [10] have become common. These advancements have helped to control engine noise, improve fuel economy, and reduce emissions [11]. For further control of NOx emissions, however, the use of cooled exhaust gas recirculation (EGR) has been adopted. In a cooled EGR system, a portion of burned exhaust gas is taken from the exhaust stream, run through a heat exchanger to reduce its temperature, and reintroduced at the intake of the engine. This has several effects on the combustion process, as described in [12]. The first consequence of EGR is the dilution effect. Since the exhaust gas contains CO_2 and H_2O, and therefore less oxygen, the oxygen concentration in the inlet charge is reduced. Studies have shown that by varying intake oxygen concentration, changes to the flame temperature had a major influence on NOx emissions [13,14]. The next consequence of EGR is the thermal effect. Because the burned exhaust gas has a higher specific heat capacity than the fresh air it displaces, the in-cylinder temperature is lowered, thereby decreasing NOx [15,16]. However, some have suggested that the effect of higher specific heat capacity is only a secondary effect compared with the reduction in oxygen

concentration, and that the thermal effect of EGR is offset by the rise in inlet charge temperature associated with EGR [17]. A third consequence of EGR is the chemical effect, suggesting that dissociation of the CO_2 introduced by EGR under the high temperatures of combustion may change the combustion process. Specifically, atomic oxygen is produced, which could increase NOx formation according to the Zeldovich mechanism [18]. Additionally, it has been suggested that the dissociation of CO_2 causes a reduction in soot production due to a longer ignition delay and a greater fraction of premixed combustion [19]. Finally, addition of EGR increases the intake charge temperature. Studies have found that introducing EGR cooling reduces NOx but increases unburned hydrocarbon emissions, though at high levels of EGR, NOx emissions are less sensitive to EGR temperature [16].

Negative aspects of EGR include decreased combustion efficiency and increased production of particulate matter [12]. In addition, EGR can potentially affect the durability of the engine due to corrosive products in the recirculated exhaust gas. It is important to note that exhaust gas composition from a diesel engine varies depending on the composition of the fuel utilized. The exhaust products of biodiesel, for example, are different from those of diesel. These differences may have an effect on the combustion process when exhaust gases are brought back to the intake through EGR. The current study will, among other things, attempt to provide some information on how engine emissions vary with EGR ratio when using biodiesel fuel.

Zheng et al [20] review the various methods of EGR implementation on modern diesel engines. EGR may be achieved either by retaining exhaust gas in the cylinder through control of the valves (internal EGR), or by installing a connection between the exhaust system and intake system and providing a pressure differential to drive the flow (external EGR). For turbocharged engines, external EGR systems fall into one of two categories, low pressure loop EGR or high

pressure loop EGR. In a low pressure loop EGR system, exhaust gas is routed from a point downstream of the turbocharger turbine, through a heat exchanger, to the inlet of the turbocharger compressor. The flow of exhaust in this system is driven by a pressure differential between the turbine outlet and compressor inlet which is typically present without modification. If necessary, the tailpipe pressure may be elevated by throttling the exhaust. A schematic of this type of EGR system is shown in Figure 2.4. The low pressure loop EGR system has been somewhat limited in application, as conventional compressors and intercoolers are not designed to endure the temperature and fouling of Diesel exhausts [20].

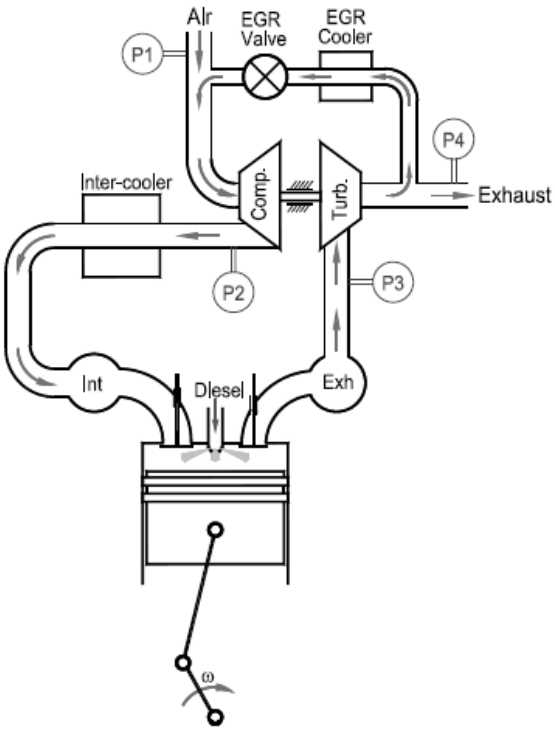


Figure 2.4: Low pressure loop EGR system [20]

A second external EGR option for turbocharged diesel engines is the high pressure loop. In this system, exhaust gas is routed from a point upstream of the turbocharger turbine, through a

heat exchanger, to a point downstream of the turbocharger compressor. Care must be taken to size the turbocharger appropriately to ensure a pressure differential sufficient to drive the EGR flow in this case. A variable geometry turbocharger (VGT) is often used with high pressure loop EGR systems to ensure proper driving pressure without sacrificing engine performance [20]. A diagram of a typical high pressure loop EGR system is shown in Figure 2.5. In this type of system, control of the EGR valve and VGT are closely related [21]. Consider a scenario in which the EGR valve is completely open, but an insufficient level of EGR is obtained. Adjusting the VGT to give a smaller flow area in the turbine will result in a higher pressure upstream of the turbine and a lower pressure downstream of the compressor, resulting in a higher pressure differential to drive EGR flow. The amount of EGR may then be controlled by adjusting the EGR valve. In the same sense, consider a scenario in which the EGR valve is almost closed, but the amount of EGR is too high. Adjusting the VGT to give a larger flow area in the turbine will result in a lower pressure upstream of the turbine and a higher pressure downstream of the compressor, reducing the pressure differential and decreasing the EGR flow. The flow rate of fresh air into the engine may be measured and used to approximate the amount of EGR since the recirculated exhaust gas displaces a portion of the fresh air flow. Target values for the fresh air flow rate at different speed and load conditions may be chosen, set into the engine control module (ECM), and used to provide the desired EGR levels throughout the operating range of the engine. Of course, this is a simplified explanation of a complicated system, but it is meant to give a general background on the control of high pressure loop EGR systems such as the one used in this study.

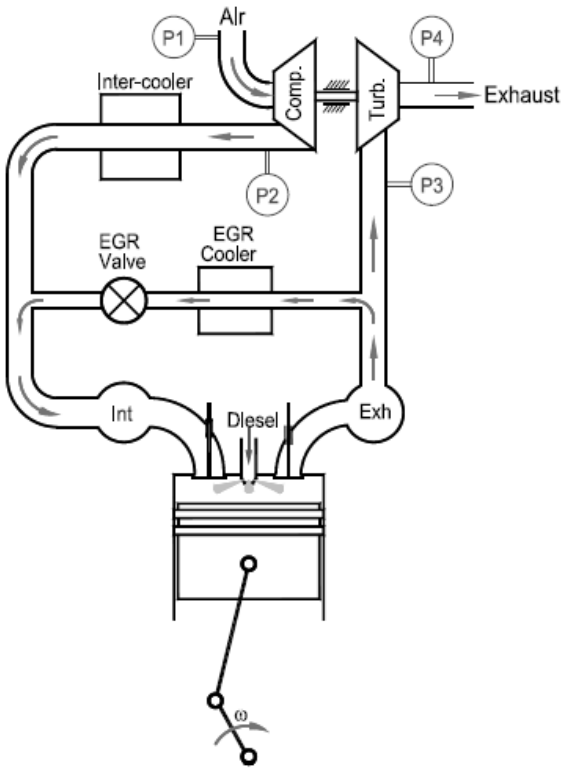


Figure 2.5: High pressure loop EGR system [20]

2.3 Low Temperature Combustion

Meeting emissions requirements while improving fuel economy has led engine manufacturers and researchers to develop new combustion techniques for simultaneous reduction of NOx and soot emissions. A few of these techniques have been implemented in production engines. One successful technique, known as MK combustion, relies on high swirl and long ignition delays with high exhaust gas recirculation and retarded injection timings to develop a highly premixed combustion [22]. Another successful technique is referred to as UNIBUS. This technique relies on early injection using a pintle injector with short duration to obtain well-mixed conditions prior to ignition [23]. These are examples of commercially-implemented low temperature combustion techniques. There are concerns being addressed considering low

temperature combustion, including higher UHC and CO emissions, cycle-to-cycle and cylinder-to-cylinder variations, and extending the operating range to the full range of engine load [24]. Nonetheless, it is a promising technique for meeting strict emissions regulations.

As discussed earlier, with conventional diesel combustion, a portion of the fuel typically mixes with air prior to ignition, but ignition occurs before the fuel is fully mixed. The fraction of fuel not consumed in the premixed combustion burns in a diffusion flame at near-stoichiometric conditions. It is in this diffusion flame where soot is primarily formed, and the high temperatures associated with near-stoichiometric combustion promote the formation of NOx as well. By contrast, low temperature combustion, as its name suggests, is characterized by overall cooler combustion temperature, in which NOx and soot emissions are avoided to a large extent.

Low temperature combustion is characterized by a two-stage combustion, including low-temperature oxidation and high-temperature oxidation. Auto-ignition is controlled by the low temperature oxidation, expected to occur at a temperature less than 950 K, while the bulk of the energy is released during high temperature oxidation, expected to occur at a temperature greater than 1000 K [25]. Some chemiluminescence can be seen during the low-temperature oxidation process, and weak flame propagation can be seen through the mixture [26]. The cool flame or low temperature oxidation process can be described by a kinetic mechanism according to Semenov [26]. This kinetic mechanism consists of four steps: chain initiation, chain propagation, branching degeneration, and chain termination. These mechanisms have been partly confirmed through various Laser Induced Fluorescence measurements in optically-accessible diesel engines [27,28]. Meanwhile, the high temperature oxidation of fuels such as diesel is characterized by three overlapping processes: conversion of alkanes to alkenes,

conversion of alkenes to carbon monoxide, and conversion of CO to CO_2, in which the bulk of the energy is released.

2.4 Biodiesel Production and Life-Cycle Analysis

Biodiesel is defined as the monoalkyl esters of vegetable oils and animal fats [29]. It is produced from raw oil or fat through a process called transesterification. Transesterification is the reaction of an oil or fat with an alcohol, typically catalyzed with alkalis, acids, or enzymes, to form esters and glycerol [30], as shown in Figure 2.6. By processing raw oils and fats in this way, a fuel is obtained which has properties quite similar to those of conventional petroleum diesel. The resulting product may then be utilized in a typical diesel engine with little or no modification.

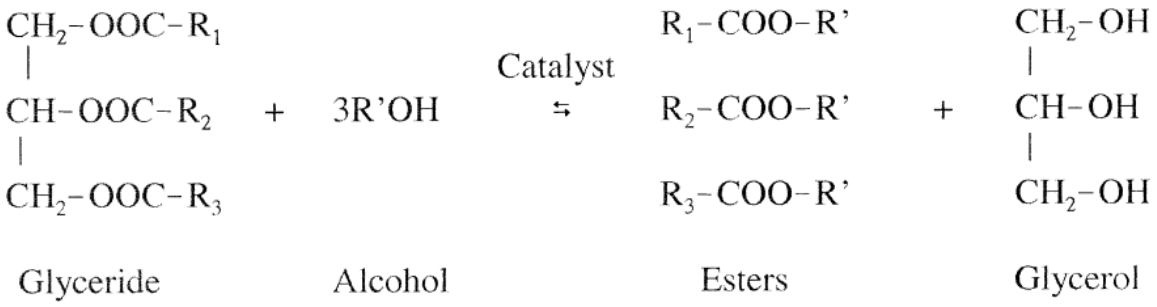


Figure 2.6: Transesterification of triglycerides with alcohol [30]

In the United States, biodiesel is typically produced through the transesterification of soybean oil. Several studies have aimed to address the net social benefit of soybean-derived biodiesel by carrying out a thorough accounting of the direct and indirect inputs and outputs for its full production and use life cycle. A recent study estimates that soybean biodiesel provides

93% more usable energy than the fossil energy needed for its production and reduces greenhouse gases by 41% compared with diesel [31]. Another study shows that soybean biodiesel provides net life cycle reductions of carbon monoxide (34.50%), total particulate matter (32.41%), and oxides of sulfur (8.03%) compared with petroleum diesel [32]. Clearly, there are benefits associated with replacing a portion of petroleum diesel with soybean biodiesel.

At the same time, soybean biodiesel has some limitations. Life cycle emissions of oxides of nitrogen were found to be 13.35% higher than for petroleum diesel due to higher tailpipe emissions [32], which will be discussed in more detail later. Perhaps more importantly, it cannot be produced in quantities large enough to offset a significant portion of diesel fuel consumption. One study reports that if all of the 2005 U.S. soybean production was devoted to producing biodiesel, it would have offset 6.0% of U.S. diesel demand, and taking into account the energy required to produce biodiesel, the switch would provide a net energy gain equivalent to just 2.9% of U.S. diesel consumption [31]. While this may be beneficial, different feedstocks must be found in order to replace any significant portion of diesel consumption.

To this end, several alternative feedstocks for biodiesel have been studied. A recent review [33] compiled experimental data on the potential productivity of various biodiesel feedstocks (see Figure 2.7). The feedstock with the highest potential for biodiesel productivity was reported to be microalgae. Production of biodiesel from this feedstock is not yet commercialized to any large extent because it is currently not economically competitive with petroleum diesel [33]. Ongoing research hopes to reduce production costs and refine the cultivation, harvesting, biomass processing, and oil extraction processes to realize the large potential for biodiesel production that microalgae holds. Further investigation into the production side of biodiesel is outside the scope of this study. However, the information

provided here gives a general background on where the fuel comes from, demonstrates the positive life cycle impacts of current biodiesel production, and offers evidence that biodiesel may be a feasible alternative energy source for years to come, albeit the primary feedstock will likely change.

Plant source	Seed oil content (% oil by wt in biomass)	Oil yield (L oil/ha year)	Land use (m^2 year/kg biodiesel)	Biodiesel productivity (kg biodiesel/ha year)
Corn/Maize (*Zea mays* L.)	44	172	66	152
Hemp (*Cannabis sativa* L.)	33	363	31	321
Soybean (*Glycine max* L.)	18	636	18	562
Jatropha (*Jatropha curcas* L.)	28	741	15	656
Camelina (*Camelina sativa* L.)	42	915	12	809
Canola/Rapeseed (*Brassica napus* L.)	41	974	12	862
Sunflower (*Helianthus annuus* L.)	40	1070	11	946
Castor (*Ricinus communis*)	48	1307	9	1156
Palm oil (*Elaeis guineensis*)	36	5366	2	4747
Microalgae (low oil content)	30	58,700	0.2	51,927
Microalgae (medium oil content)	50	97,800	0.1	86,515
Microalgae (high oil content)	70	136,900	0.1	121,104

Figure 2.7: Comparison of various biodiesel feedstocks [33]

2.5 Biodiesel Combustion

When used in unmodified conventional diesel engines, biodiesel has been shown to reduce tailpipe emissions of soot, unburned hydrocarbon, and carbon monoxide relative to petroleum diesel [34]. However, it also tends to increase tailpipe emissions of oxides of nitrogen [34]. Given the increasingly severe emissions regulations, this is a problem to be overcome before biodiesel can be implemented to a larger extent. Several studies have aimed to account for this increase in NOx, and several explanations have been given. One hypothesis relates to the higher bulk modulus of biodiesel compared with petroleum diesel [35]. By this hypothesis, the increase in bulk modulus and resulting increase in the speed of sound causes pressure waves between the pump and injector to move more quickly, causing the injector needle to lift earlier. The injection timing is thereby advanced for engines equipped with pump-line-nozzle fuel

injection systems, contributing to higher NOx emissions due to higher in-cylinder temperatures. However, in engines with common-rail fuel systems, this phenomenon has been shown not occur [36]. Another hypothesis suggests that the formation of prompt NOx is higher for biodiesel, suggested to be due to a higher concentration of fuel-derived radicals which are relevant to prompt NOx production [37]. Still others suggest that, since biodiesel tends to contain more molecules with double bonds, it burns with a slightly higher adiabatic flame temperature, thereby causing the increase in NOx [38]. Finally, it has been suggested that soot radiation from the flame zone may be able to lower the diffusion flame temperature, thereby reducing NOx emissions [39,40]. As biodiesel has been shown to produce less soot than diesel, less soot radiation can be expected, resulting in a higher flame temperature and higher NOx emissions.

To add further complication, biodiesels produced from different feedstocks are known to have different chemical compositions which affect the relevant fuel properties. In general, cetane number, heat of combustion, melting point, and viscosity of neat fatty compounds were found to increase with increasing chain length and decrease with increasing unsaturation [41]. Biodiesels produced from a variety of feedstocks were tested in a heavy-duty truck engine to determine the impact of biodiesel chemical structure on NOx and particulate matter emissions [42]. NOx emissions were found to increase with increasing density or decreasing cetane number. Increasing the number of double bonds was found to increase NOx emissions as well. For fully saturated fatty acid chains, NOx emissions increased with decreasing chain length. Particulate matter emissions, on the other hand, were hardly influenced by the aforementioned structural factors. Given the variability of fuel properties and the resulting impact on engine emissions, studies have been carried out intending to find an optimum fatty ester composition to address all fuel property issues simultaneously [43]. This type of information can be used to

guide the development of future biodiesel feedstocks with the end use in mind. For the current study, only soybean-derived biodiesel is utilized, but it is important to acknowledge the wide variety of chemical compositions associated with the term 'biodiesel' and recognize their effects on fuel properties and emissions.

Another effect of biodiesel on combustion and emissions is related to the engine's control module (ECM). Modern diesel engines utilize complex electronics to measure and control a variety of parameters affecting the combustion process. Control parameters are chosen experimentally for the full range of speed and load conditions and written to the ECM. The engine can then reference this data to determine how best to run under certain conditions. The two variables characterizing an engine operating condition are typically rotational speed and torque. The engine is typically equipped with a speed sensor, but has no direct measure of torque. Instead, the torque is characterized by the amount of fuel injected into the cylinders, which has been a simple but effective method. The problem arises when fuels of different energy content are utilized in the engine. An engine optimized to run on diesel will run differently when fueled with biodiesel, for example, because the lower heating values of these two fuels are different. This effect was studied in a precisely controlled single-cylinder engine fueled with a 20% volumetric blend of biodiesel in diesel [44]. This study reported that when a production diesel engine was fueled with biodiesel blends, injection timings changed due to the inability of the production ECM to adjust to the change of fuel heating value and hence the assumed engine torque was higher than it actually was. The assumed higher engine torque caused the ECM to work at a different operating point, and consequently changed the injection timings and the EGR rate. At higher load, NOx emissions were found to increase by 3% to 4% as a result of the changes in engine parameters.

Chapter 3:
Experimental Methodology

3.1 Experimental Setup

A Ford Lion 2.7L V6 compression-ignition engine is used in this study. This production engine is equipped with common rail injection system, piezoelectric injectors, variable geometry turbocharger, and a high pressure cooled EGR system. Detailed engine specifications are shown in Table 3.1 below.

Table 3.1: Specifications of Ford Lion engine

engine type	V-6, 4-stroke diesel
bore and stroke (mm)	81 x 88
displacement per cylinder (cm^3)	453.46
compression ratio	17.3:1
valves per cylinder intake / exhaust	2 / 2
combustion system	direct injection
induction system	variable geometry turbocharger
injection system	common rail
injector type	6 nozzle, piezoelectric
exhaust gas recirculation	high pressure, water-cooled

A large portion of the engine has previously been set up, and much of the following experimental setup is referenced from the thesis of Tien Mun Foong [45]. The Ford Lion engine was set up on an engine test bench and coupled with an eddy-current dynamometer. Various engine subsystems were set up to enable operation of the engine in a laboratory setting, as will be discussed below. The VGT normally used on the engine was not installed. Instead, a compressed air system was chosen to provide dry, heated, and pressurized intake air. A flow restricting valve on the exhaust allowed for proper functioning of the high pressure loop EGR system. The fuel supply and return for the engine were set up using lines resistant to the corrosive nature of biodiesel. The engine was instrumented with a variety of data acquisition

(DAQ) devices, including thermocouples and pressure transducers for monitoring relevant fluid properties. An in-cylinder pressure transducer was installed in place of the glow plug in one cylinder to monitor the combustion process and enable calculation of apparent heat release rate. The other five glow plugs remain in the engine, but have been disabled by removing their wires. A LabVIEW program was developed to monitor these various DAQ devices. An engine control module specifies and controls various operating parameters for the engine, including injection timings, injection durations, fuel rail pressure, intake manifold pressure, and amount of EGR. By default, the ECM operates according to Ford specifications. The common rail fuel system provides fuel at pressures ranging from 220 bar to 1650 bar, depending on engine operating conditions. Fuel is delivered to the cylinders using 6-nozzle piezoelectric injectors, capable of anywhere from 1 to 6 injections per cycle. Up to two pilot injections, two main injections, and two post injections may be utilized with this injection system, but the default injection strategy for this engine utilizes only one pre-injection and one main injection. ETAS INCA software was installed and connected to the ECM to enable monitoring and changing of the various parameters. It should be noted that enabling additional injections is not as simple as populating the tables found in INCA. Further advice from Ford should be sought if studies with additional injections are desired. The pre-injection, however, may be disabled to allow for single-injection studies. No exhaust aftertreatment devices are installed on the engine, and all emissions measurements are taken on the raw exhaust gases coming from the engine. To facilitate operation of the engine in a research environment, a variety of subsystems have been built and installed. Air supply, fuel supply, coolant, starting and motoring, and data acquisition and control systems were installed, as illustrated in Figure 3.1. These systems will be described in more detail below. Data acquisition and control is accomplished from a room adjacent to the test

cell. Many of these engine subsystems were built or modified by Mark Paul or Tien Mun Foong, and can be referenced in their theses [46,45].

3.1.1 Air Supply

The Ford Lion engine is normally equipped with a variable geometry turbocharger, but this has been removed in favor of a pressurized and heated intake air system to allow for better control of inlet air conditions. As described in the literature review, high pressure EGR systems such as this typically rely on a VGT to provide sufficient backpressure or exhaust flow restriction to drive the flow of exhaust gases through the EGR coolers and into the intake manifold. When using pressurized intake air, and having the exhaust at atmospheric pressure, little or no exhaust will be recirculated to the intake manifold. To correct this problem, an adjustable valve was installed in the exhaust pipe, allowing the flow to be restricted and sufficient backpressure to be created to drive the EGR flow.

The air supply system shown in Figure 3.2 was previously built for the Direct-Injection Natural Gas (DING) engine in the 1990's, and is capable of supplying clean, dry intake air at a specified temperature and pressure with a maximum flow rate of 7.36 m^3/min at standard conditions. The first component in the air supply system is an Ingersoll-rand SSR XF60 air compressor located in the lab bay area. The output pressure of the compressor cycles between 621 kPa and 689 kPa, as the compressor is set to turn on and shut off at these levels. From the compressor, the air supply is routed to the engine lab by way of 2" galvanized pipes. The pressure is then regulated down to 345 kPa by a heavy-duty air line regulator in order to minimize pressure fluctuations. The intake pressure to the engine is finally controlled by a Valtek Mark 1 air pressure controller. The valve was modified to optimally supply an intake

pressure that ranges from 89 to 269 kPa and the maximum intake mass flow rate is 7.36 m3/min at standard conditions. Pressure gauges are installed both upstream and downstream of the valve so that the pressure drop across the valve can be estimated. A brass ball valve is available upstream of the valve to shut down the air supply if service is needed.

The Valtek pressure regulator is controlled by a LabVIEW program. This program first monitors the air pressure using a Setra 280E (0-250 psia) pressure transducer installed upstream of the engine intake manifold. The transducer has a piston-type snubber installed in order to reduce pressure pulsation. Using a PI (proportional-integral) control, the program then outputs a 4 to 20 mA signal to the controller depending on the required air pressure that the user sets. With a signal of 4 mA, the pressure controller will be partially open. With a signal of 20 mA, the pressure controller will be fully open. Under certain conditions (low speed and high EGR), it is possible that the flow rate demanded by the engine is lower than the minimum flow rate through the pressure controller (4 mA signal). In these cases, the intake pressure will rise and eventually even out at a value higher than desired. For this reason, cases of low speed and high EGR were typically run naturally-aspirated using atmospheric air from the test cell.

An Odgen ACK5A 9kW circulation heater is used to simulate the inlet temperatures seen on turbocharged engines. An Omega SCR71Z-260, 60 A, 240 VAC single-phase power controller is coupled to the heater to provide the required amount of heating during engine operations. A PI control for the heating system is set up in the engine instrumentation LabVIEW program. A thermocouple is mounted upstream of the engine intake manifold, allowing LabVIEW to monitor the intake air temperature. The program subsequently outputs a 4 to 20 mA signal to the heater controller. The silicon-controlled rectifier heater controller then switches the power to the heater on and off according to the output signal from LabVIEW. When

LabVIEW supplies the minimum current, 4 mA, to the controller, the power to the heater will be completely turned off. With the maximum current, 20 mA, supplied to the controller, the heater will be turned on all the time. For supply currents between 4 mA and 20 mA, the controller will turn the heater on for a given number of cycles and then off for a given number of cycles. The heater controller runs with zero voltage switching to allow for low noise operation. Details about the LabVIEW controls of the valve and the heater will be discussed in the Data Acquisition and Control section. Following the heater, the compressed and heated air enters a Hankinson 1-micron air line filter (Model T850-24-5 G) where water, oil, and oil/water emulsions are removed. From here, the air supply is routed to the intake manifold of the engine using flexible couplers and PVC pipe.

The engine exhaust coming from the manifolds is routed through braided steel flexible couplers which isolate engine vibrations from the exhaust pipe. These come together into a 2" iron pipe, at which point a ball valve is installed to allow restriction of the exhaust flow. A turnbuckle connected to the valve handle enables fine adjustment of the valve and ensures that the valve does not change position unexpectedly. The exhaust then flows through another section of 2" iron pipe, a section of 3" iron pipe, and a muffler (Model Maxim M51 Silencer) hanging from the ceiling of the engine lab. From here, the exhaust flows through a final section of iron pipe before exiting the building through a stack on the roof. Instrumentation on the exhaust includes a J-type thermocouple installed at the outlet of the left exhaust manifold of the engine. Ports for exhaust gas analysis are available in the section of iron pipe near the engine. The sampling points for the exhaust gas analyzer and soot measurement system, as well as the sensor head for the non-sampling type NOx meter are located here.

3.1.2 Fuel Supply

The fuel supply system consists of a fuel pump, fuel filter, and radiator. Biodiesel is known to be incompatible with certain materials such as rubber and brass, and a long-term usage of incompatible materials in a biodiesel engine will result in material degradation or corrosion over time. The fuel system was built to be fully biodiesel compatible through careful selection of lines and fittings. A schematic of the fuel supply system is shown in Figure 3.3. Fuel is first drawn from the tank using an in-line 12V transfer pump, which is capable of delivering up to 125 psi of fuel pressure. Under normal usage the fuel pressure is about 40 to 50 psig. The fuel then enters a small 3-pass fluid cooler made by Flex-a-lite (part number FLX-4116). This is needed because the fuel returning to the tank is quite hot due to the energy input by the high pressure pump. From the radiator, the fuel goes through a Caterpillar 1R-0751 High Efficiency Fuel Filter to keep contaminants out of the high pressure pump. The fuel filter is positioned for ease of service on the engine test cell. Fuel then arrives at the high pressure pump, which is driven by the engine. A portion of the fuel is utilized by the engine, while the remainder flows back to the tank. The fuel tank (part number SUM-290101) from Summit is capable of storing a total of 5 gallons of fuel and it is made of high-density polyethylene, which is biodiesel compatible. The fuel lines are 3/8” in size and are made of nylon, while the fittings are all metal.

3.1.3 Coolant

The coolant system, shown in Figure 3.4, is a closed loop system that circulates coolant through the engine at a volumetric flow rate of 114 L/min. The coolant is a mixture of water and Caterpillar 3P-2044 supplemental coolant additive, which inhibits rust and corrosion, and prevents scale deposits. Coolant is stored in a vessel measuring 31 cm in diameter and 64 cm in

height. A Price Pump Company EC E100B centrifugal pump circulates the coolant within the closed loop. In order to prevent air from entering the pump and to deal with suction lift problems, the pump is placed below the coolant level of the vessel. The pump has an outlet pressure of 207 kPa, resulting in a flow rate of 114 L/min. A 0 to 60 psig gage is installed at the outlet of the pump. From the pump, the coolant enters the Young Radiator Company F-302-EY-1P single-pass shell-and-tube heat exchanger for cooling purposes. Engine coolant flows on the tube side, while building water flows on the shell side to lower the coolant temperature. The flow of building water is controlled by a pneumatic temperature control system to maintain a set constant coolant temperature.

The coolant then flows from the heat exchanger to the engine through copper and steel pipes. Typically, the coolant would flow first through the engine block, including various coolant passages and a heat exchanger for engine oil cooling. Then, a portion of the coolant would run through the EGR coolers before going back to the radiator. To allow for better cooling of the recirculated exhaust gases, coolant flow from the heat exchanger was split so that a portion goes to the engine block and a portion goes directly to the EGR coolers. A ball valve on the line to the engine block allows adjustment of the fraction of coolant flowing through each path. Coolant outlets from the engine block and EGR coolers are then routed back to the storage vessel. To monitor coolant temperature, a J-type thermocouple is mounted at the outlet of the engine coolant.

3.1.4 Starting, Motoring, and Power Absorbing

The starting, motoring, and power absorbing system is an important subsystem of the engine as it provides the ability to start the engine, motor the engine at a given speed, apply a

load to the engine while it is running at a given speed, and change the engine speed at a given load. The components making up this system include a Midwest Dynamometer 310, Dyne Systems DYN-LOC IV controller, a flywheel assembly, a Baldor electric motor, and an Asea Brown Boveri (ABB) adjustable frequency alternating current drive. Figure 3.5 illustrates the overall starting, motoring, and power absorbing system.

The Midwest Dynamometer 310 is connected to the flywheel of the engine through a Model 1810 drive shaft assembly made by Johnson Power. The eddy-current dynamometer is rated for a maximum power of 300 hp at speeds between 2500 and 6000 rpm. Building water flows through the dynamometer for cooling and exits into a drain pan mounted below the dynamometer. The flow rate of cooling water can be adjusted using a ball valve located on the north wall of the engine lab. Depending on the power being absorbed, the flow rate of cooling water can be fairly small as long as the water pressure is high enough to engage the water pressure safety switch and close the dynamometer controller circuit. This is to protect the dynamometer from overheating by loading the engine without proper cooling. With the dynamometer operating at its maximum rated power, the cooling water flow rate should be 22 gpm. Cooling water is pumped out of the drain pan using a Little Giant 1/6 hp submersible sump pump, which is capable of a maximum flow rate of 77 L/min and is turned on and off automatically according to the water level. Care must be taken not to open the building water ball valve too much, as the flow of water into the dynamometer can exceed the maximum flow rate of the sump pump, causing water to flood the test cell. To monitor the cooling water temperature, a thermocouple is installed near its outlet from the dynamometer. The maximum temperature of the cooling water should not exceed 60° C.

A Dyne Systems DYN-LOC IV controller is placed in the engine control room and connected to the field wires of the dynamometer to allow for control of engine speed or load. Engine speed is sensed by an Electro Kinetics 3030 AN25 magnetic sensor which produces a quasi-sinusoidal signal from a rotating 60-toothed wheel spinning at the same speed as the engine. Meanwhile, a Lebow Products Model 3132 load cell with a maximum capacity of 4450 N is used to determine the torque being produced by the engine. From these devices, the controller computes and displays the engine speed, torque, and power. Analog outputs on the back of the controller pass the engine speed and torque information to LabVIEW for further engine control and management. This will be discussed in details in the Data Acquisition and Control section.

The Midwest Dynamometer 310 is capable of absorbing but not motoring, so a starting and motoring system was integrated into the dynamometer setup. The dynamometer is connected to a 30-hp Baldor high-efficiency electric motor through a custom clutch assembly. The clutch is an International Harvester 915 combine clutch, which is mounted on a custom shaft and is engaged or disengaged using a 12 VDC power supply switched from the control room. The electric motor is rated for a speed of 1760 rpm at a frequency of 60 Hz and a normal operating current of 38 A at 460 VAC. Speed control of the motor is achieved using an ABB variable frequency drive, which can output a frequency between 0 and 120 Hz, and is capable of supplying a momentary torque boost of up to 72 A when starting the engine from a stationary position. If the torque boost is used for more than 1 min, the electric motor will tend to overheat. An ABB SAGS 700 PAN remote control for the variable frequency drive is installed in the engine control room for safer, remote operation. The ABB variable frequency drive is configured such that the engine is motored at 800 rpm.

3.1.5 Data Acquisition and Control

Data acquisition devices such as thermocouples and pressure transducers, as well as computer-based measurement and control, comprise the data acquisition and control system. A schematic of this system is provided in Figure 3.6. A National Instruments signal conditioning chassis (Model SCXI-1000) was installed to amplify, filter, and isolate the signals. In addition, it serves as a switching system which multiplexes the signals from all thermocouples and pressure transducers into a single channel on the data acquisition (DAQ) board. In this way, only two input channels are needed even though there are more than six input signals. The chassis houses two different modules and a feedthrough panel. One module (Model SCXI-1100) is a 32-channel differential multiplexer/amplifier used primarily for signal conditioning and switching related to the thermocouples. A terminal block (Model SCXI-1303) is included with this module, which is used to provide an accurate measurement of the cold-junction reference voltage for the thermocouples through a built-in temperature sensor. Six J-type thermocouples are connected to this module, as illustrated in Figure 3.7. The second module (Model SCXI-1120) has eight isolated input channels and is used for signal conditioning all pressure transducers except the in-cylinder pressure transducer. A connection diagram for the pressure transducers is also shown in Figure 3.7. A feedthrough panel (SCXI-1180) passes all unconditioned signals directly to and from the DAQ board, which will be discussed in more detail below. The unconditioned signals include the in-cylinder pressure transducer, engine speed and torque from the dynamometer, and the pedal signals to the engine to control the load and speed.

A PC-based computer system was set up for the data acquisition and control system. The computer contains two National Instruments devices, including a 16-channel data acquisition

board (Model PCI-MIO-16E-4) and a 2-channel analog current output card (Model PC-AO-2DC). The analog current output card controls the air intake system for the engine, while the remaining signals are processed using the data acquisition board. Signals acquired by the data acquisition board come from the thermocouples, pressure transducers, dynamometer, and shaft encoder. At the same time, the board generates output voltages to simulate the accelerator pedal position. The data acquisition board also works as a bridge of communication between computer and signal conditioning chassis. Meanwhile, the analog current output card generates the current necessary to control the intake air pressure valve and the heater. Each of these systems requires a control current between 4 and 20 mA. To provide the accelerator pedal position to the engine, a physical pedal was originally purchased from a Land Rover dealer. This approach, however, was cumbersome, and the pedal position is now simulated in LabVIEW. Two pedal signals are sent by LabVIEW to the ECM. The first signal ranges from 0.732 to 3.774 V, while the second signal is just half of the first. These signals are delivered by LabVIEW to the ECM via the feedthrough panel mentioned above. An AVL pressure transducer (GU13P) is used to measure in-cylinder pressure for cylinder #6. The transducer has a bore of 3 mm and fits into the glow plug hole using a glow plug adaptor, also made by AVL. The transducer has a sensitivity of 15.37 pC/bar, and was recently calibrated on 12/09/2008. To install the transducer into the glow plug adaptor, a custom-made wrench with a hex size of 4 mm has to be used. The pressure transducer is connected to a Kistler charge amplifier (Model 5004) to amplify the signal, which is then passed to the data acquisition board for further processing. A BEI shaft encoder (Model - BEI H25D-SS-1440-ABZC-7406R-LEB-SM18) is used to determine the engine timing for proper measurement of in-cylinder pressure. The shaft encoder provides ¼ crank angle degree resolution, and thus outputs 2880 pulses per engine cycle. It also outputs a signal corresponding

to TDC for each engine revolution. The shaft encoder is mounted to the crank shaft at the front of the engine. LabVIEW 8.6, an object-oriented programming language, is used both for data acquisition and control. A virtual instrument program called Engine_Control_022709.vi was developed to monitor and control the inputs and outputs of the boards, acquire and record data, and compute engine performance parameters. The program is made up of 3 main sections: low-speed data acquisition, high-speed in-cylinder pressure data acquisition, and control signal generation. For low-speed data acquisition, the program monitors and acquires the data of all steady-state inputs, including temperatures, torque and engine speed from the dynamometer, and intake pressure. The second section of the code performs the high-speed data acquisition for in-cylinder pressure data. When the acquisition button is pressed, the pressure data acquisition will start when the computer receives a TDC pulse from the shaft encoder. Pressure data are then recorded for the full engine cycle as triggered by the shaft encoder. A post-processing code calculates the corresponding cylinder volume based on the crank angle at which the pressure is acquired, and also average and adjust the data by incorporating the effect of the intake pressure. Expansion, compression, and pumping work are then calculated from the averaged pressure data. The last section of the program involves signal generation for the external devices. Four output signals are generated, two of which are supplied to the ECM for simulation of the pedal position. The other two signals are generated by PI (proportional-integral) controls to maintain the intake air pressure and temperature at the chosen values.

A separate DAQ system was developed for averaging and recording emissions and fuel consumption measurements, making some calculations, and writing the results to a data file. Results from the exhaust gas analyzer and NOx meter had previously been written down manually, which proved to be an inefficient and error-prone method. A shortage of analog input

channels prevented the analog output channels of these units from being wired into the existing DAQ system. Instead, they were wired into an additional DAQ card (National Instruments PCI-MIO-16E-4) on a separate computer, and another LabVIEW program (emissions_v5.vi) was developed for averaging the results, making calculations, and saving the data to a text file.

Analog outputs from the Horiba MEXA-554JU and Horiba MEXA-720NOx were wired into analog input channels on the DAQ card by way of a connector block (National Instruments CB68LP). The exhaust gas analyzer outputs an analog signal ranging from 0-1 V for each of four measurements, corresponding linearly with concentration through the measureable range. These ranges are 0-10,000 ppm for HC, 0-20% for CO_2, 0-10% for CO, and 0-25% for O_2. The NOx meter outputs an analog signal ranging from 0-5 V corresponding to 0-5000 ppm NOx. The program starts by prompting the user to connect the exhaust gas sampling line to the analyzer, ensure that the analyzer is drawing a sample, wait for measurements to stabilize, and then press a button to continue. The program then reads in the analog signals once every 100 ms for a user defined number of iterations. It multiplies the voltage signals according to their respective scaling factors to obtain concentration data and outputs this to the front panel of the LabVIEW program. While the program is outputting instantaneous emissions values, it is also averaging them using a feedback loop and the iteration number. Once it has finished reading in exhaust emissions, it prompts the user to switch the sampling line to the mixed intake (fresh air and EGR) stream, and gas composition for the mixed intake air is obtained. Various calculations are then carried out based on these data. Specifically, emissions measurements from the exhaust gas analyzer are corrected to account for water content, and EGR ratio is calculated based on CO_2 measurements. At this point, instantaneous emissions are plotted to ensure that measurements were taken during steady-state operation.

Meanwhile, digital output signals from the liquid level sensors of the fuel consumption measurement system are wired into digital input channels on the DAQ card by means of the same connector block. Another loop in the same LabVIEW program detects when the fuel falls below the first liquid level sensor based on the digital voltage signal, and a timer is started. Once the fuel drops below the lower liquid level sensor, the timer is stopped. The sampling tank may then be refilled to take additional measurements. The first measurement is thrown out due to observed inconsistency, and the remaining measurements are averaged. Therefore, at least two measurements of fuel consumption should be made for each engine operating condition. The fuel flow rate is then calculated based on the known sample volume and the user-supplied fuel specific gravity. When the desired number of measurements has been taken, the fuel flow rate and all emissions data are written to a text file. This file may be opened using a spreadsheet, allowing easy access to the data for further calculations and plotting.

To establish communication with the engine ECM, ETAS INCA is installed in a second computer. INCA is used for the development and calibration of control and diagnostic parameters in engine ECM's, and allows data acquisition and real-time recording of many engine operating parameters present in the ECM. An ETAS ES580 interface card provides the hardware connection between computer and ECM. This PCMCIA interface card is installed in one of the PCI slots on the motherboard using a PCMCIA-to-PCI converter. The setup of the ECM control and management system is shown in Figure 3.8.

The ECM works by first receiving inputs from all the sensors placed around the engine. From there it processes the signals using its internal calibrations, and then outputs the necessary control signals for proper engine operation. This particular ECM is different from production ECM's in that it can be reconfigured. In other words, the internal calibrations of the ECM can be

changed as desired by the user. The engine runs with the default calibrations supplied by Ford until a connection is established between INCA and the ECM, at which point the various calibrations can be modified. An incomplete list of INCA parameters found useful for this study is included in Appendix A.

3.2 Test Fuels

3.2.1 Conventional Combustion Study

The fuels used in this study are U.S. ultra-low sulfur diesel (B0), soybean biodiesel (B100) and blends of the two. B20 (20% vol biodiesel and 80% vol diesel) and B50 (50% vol biodiesel and 50% vol diesel) were obtained through splash-blending. The ultra-low sulfur diesel was obtained through a local fuel supplier (Illini FS), who provided general fuel specifications. The soybean biodiesel was provided by Incobrasa Industries, who provided results from fuel testing. Fuel properties are shown in Table 3.2 below.

Table 3.2: Fuel properties

	Ultra Low Sulfur Diesel (B0)	Soybean Biodiesel (B100)
specific gravity	0.845	0.8853
sulfur (ppm)	7.0 - 15.0	< 3
viscosity (cSt @40°C)	2.0 - 3.0	4.11
cetane number	43-47	47.1
stoichiometric air-fuel ratio	14.6	12.6

3.2.2 Low Temperature Combustion Study

Only pure soybean biodiesel was tested in this portion of the project. Fuel could not be obtained from the same producer as the previous study, so it was acquired through a local fuel

supplier (Illini FS). Detailed test results were not available for this fuel. However, it was run under the same conditions, and the results were compared with those obtained when using the fuel from Incobrasa. Similar trends were seen, indicating similarity between the fuels. However, it is acknowledged that different supplies of fuel can have differences in properties that affect the results obtained. Therefore, care should be taken in making direct comparisons between the conventional combustion study and low temperature combustion study.

3.3 Measurement Devices

3.3.1 Fuel Consumption Measurement

A volumetric system for fuel consumption measurement was set up to allow steady-state fuel consumption measurement. A small sampling tank was constructed from PVC pipe, which is resistant to biodiesel and other fuels. Three liquid level sensors (Honeywell LLE102101) detect the presence of fuel at different levels in the sampling tank, outputting a logic high voltage in air and a logic low voltage in liquid. Only two of the three sensors are used at a time, but having a third sensor allows for different sampling volumes to be chosen, as shown in Figure 3.9. The repeatability of the sensors is ±1 mm, while the minimum distance between any two sensors is approximately 150 mm. A timer is started as the fuel drops below the upper sensor and stopped as it drops below the lower sensor. The response time of the sensors in falling liquid is up to 1 second depending on viscosity. However, the two sensors are expected to have the same response time since the fuel properties are constant throughout the measurement duration. This was confirmed by testing the device for consistency under a constant fuel flow rate. The volume contained between the two sensors is known, allowing a volumetric measurement of net fuel flow to the engine. Mass flow rate is then calculated based on the user-input fuel specific

gravity. Measurements are not taken until the fuel temperature becomes constant near the engine coolant temperature, preventing the results from being skewed due to different fuel densities.

Two solenoid valves (Hydraforce SV10-31) control fuel flow to and from the sampling tank. In normal operation, the solenoid valves are configured to draw fuel from the main fuel tank and return excess fuel to the same tank. To fill the sampling tank, a selector switch is flipped, and the solenoid valve for the return fuel line switches to the sampling tank. Once the fuel level rises above the upper liquid level sensor, an electronic circuit switches off power to the solenoid valve, connecting the return line back to the main tank and preventing the sampling tank from overflowing. To make a fuel consumption measurement, the selector switch is flipped, and the solenoid valves for the supply line and return line are connected to the sampling tank. As the engine uses the fuel, the fuel level drops until it gets below the lower liquid level sensor, at which point an electronic circuit switches off power to the solenoid valves, connecting the supply and return lines to the main tank and preventing the fuel pump from being run dry.

3.3.2 Soot Measurement

Soot measurement was performed using a standard filter paper method. A JB Industries model DV-85N deep-vacuum pump was used to draw a sample of raw exhaust gas through a 7/8" round filter paper. The filter holder was taken from a Bacharach True-Spot smoke meter and adapted to the new setup. Filter paper discs were no longer available from the manufacturer, so rectangular strips of filter paper, available from Grainger Industrial Supply (item #6T167), were cut into discs. A line filter (McMaster item #4958K34) was installed after the vacuum pump to remove any oil or condensed water which may affect the flow measurement. A Brooks flow meter, tube size R-6-25-B, with stainless steel ball was used to monitor the sampling flow

rate. The meter reads from 0 to 25, in increments of 0.1. The maximum flow rate is 2349 L/h for air at standard conditions according to manufacturer data. The flow rate for sampling was controlled using a needle valve on the inlet of the vacuum pump. Based on the expected soot content, the flow rate and duration were chosen to achieve moderate darkening of the filter paper. Results can then be used to determine a filter smoke number.

3.3.3 NOx Measurement

Measurement of NOx emissions was made on the raw exhaust gases using a Horiba MEXA-720NOx non-sampling type meter. A new sensor head had recently been installed, and the factory calibration data was considered sufficient, as the general trends are of most interest to this work. The sensor's measurement range is 0 to 3000 ppm NO_X concentration, with ±30 ppm accuracy for the 0-1000 ppm range, ±3% accuracy for the 1000-2000 ppm range, and ±5% accuracy for the 2000-3000 ppm range. All measurements for this study fell in the range of 0-1000 ppm. This analyzer uses a zirconia sensor, which operates according to the following principle [47], which is also illustrated in Figure 3.10. Sample gas flows into the first internal cavity, where an ion pump is utilized to keep the oxygen concentration low. The oxygen concentration in the sample gas is calculated by measuring the pumping current. Meanwhile, NO_2 in this chamber is broken down into NO and O_2. The sample gas then enters the second internal cavity, where NO is split into N_2 and O_2. Oxygen generated by this reaction is removed using an ion pump, and the overall NOx (NO and NO_2) is calculated by measuring the pumping current. According to the manufacturer, this is a wet-basis measurement, and no correction for the water content of the exhaust is required.

3.3.4 CO_2, CO, and O_2 Measurement

Measurements of other raw exhaust gas components and of the mixed intake gas components were made using a Horiba MEXA-554JU exhaust gas analyzer. Ice baths were installed in the sampling lines to condense the water vapor, and compressed air line dryers (McMaster item #4958K34) were installed to filter out the condensed water before the sample entered the analyzer. In this way, all water vapor is considered to be removed from the sample, and the results are considered to be dry-basis measurements.

3.4 Calculations and Data Analysis

3.4.1 Correction for Water Content and Calculation of Brake-Specific Emissions

As described in the measurement section, the exhaust gas analyzer measures emissions on a dry basis, so the water content in the exhaust must be taken into account when interpreting data. Knowing the fuel composition and equivalence ratio, the exhaust gas composition for the case with no EGR can be calculated. For all cases studied, the overall mixture of air and fuel was lean of the stoichiometric ratio, where CO and H_2 in the exhaust products may typically be considered negligible. This assumption becomes less valid for air-fuel ratios near stoichiometric and for high EGR ratios. The highest measured CO concentration in this study was well under 1%, so the assumption of lean combustion with negligible CO and H_2 was considered adequate. The general equation for lean combustion without EGR is given as:

$$C_xH_yO_z + \frac{1}{\varphi}\left(x + \frac{y}{4} - \frac{z}{2}\right)(O_2 + 3.76N_2)$$

$$\rightarrow \frac{3.76}{\varphi}\left(x + \frac{y}{4} - \frac{z}{2}\right)N_2 + xCO_2 + \frac{y}{2}H_2O + \left(\frac{1}{\varphi} - 1\right)\left(x + \frac{y}{4} - \frac{z}{2}\right)O_2$$

Since tests were conducted at steady state, the recirculated exhaust gases from the previous cycle have the same composition as the products of the current cycle. Thus, the general combustion equation without EGR can be used to calculate the exhaust composition for the case with EGR. These exhaust components may be added to the fresh intake air, and the combustion equation with EGR may be solved as shown below.

$$C_xH_yO_z + \frac{1}{\varphi}\left(x + \frac{y}{4} - \frac{z}{2}\right)(O_2 + 3.76N_2)$$

$$+ \frac{n_{EGR}}{n_{fresh}}\left[\frac{3.76}{\varphi}\left(x + \frac{y}{4} - \frac{z}{2}\right)N_2 + xCO_2\right.$$

$$\left. + \left(\frac{1}{\varphi} - 1\right)\left(x + \frac{y}{4} - \frac{z}{2}\right)O_2 + \frac{y}{2}H_2O\right]_{exhaust}$$

$$\rightarrow \frac{7.52}{\varphi}\left(x + \frac{y}{4} - \frac{z}{2}\right)N_2 + 2xCO_2 + yH_2O + 2\left(\frac{1}{\varphi} - 1\right)\left(x + \frac{y}{4} - \frac{z}{2}\right)O_2$$

Here, $\frac{n_{EGR}}{n_{fresh}}$ is the molar ratio of recirculated exhaust gases to fresh air, which can be written in terms of the the commonly used EGR ratio. With the EGR ratio defined as $EGR(\%) = \frac{m_{EGR}}{m_{EGR}+m_{fresh}}$, the following equation may be used to replace the molar ratio of recirculated exhaust gases to fresh air.

$$\left(\frac{n_{EGR}}{n_{fresh}}\right) = \left(\frac{EGR(\%)}{100 - EGR(\%)}\right)\left(\frac{MW_{fresh}}{MW_{exhaust}}\right)$$

From the combustion equation with EGR as written above, it can be seen that water vapor is produced on a molar basis at a ratio of $\frac{y/x}{2}$ times that of CO_2. Thus, water vapor concentrations were calculated based on measured dry-basis CO_2 concentrations, and wet-basis mole fractions were calculated for the relevant gas species. The overall wet-basis molecular weight of each gas

stream may then be calculated according to the following equation, where $\tilde{n}_{species}$ is the mole fraction of the designated species.

$$MW = \tilde{n}_{N2}MW_{N2} + \tilde{n}_{CO2}MW_{CO2} + \tilde{n}_{O2}MW_{O2} + \tilde{n}_{H2O}MW_{H2O}$$

Thus, to account for water content in the exhaust gases, a correction factor relating the number of dry moles of exhaust gas to the number of wet moles of exhaust gas was applied.

$$\%\ wet\ basis = \%\ dry\ basis * \frac{n_{dry\ exhaust}}{n_{wet\ exhaust}} = \frac{\%\ dry\ basis}{1 + (\%\ dry\ basis\ water\ vapor/100)}$$

With the wet-basis emissions results, the air and fuel flow rates, and the power output, brake-specific emissions (NOx, for example) were then calculated according to the following equation.

$$\frac{ppm_{NO}}{10^6} * \frac{MW_{NO}}{MW_{wet\ exhaust}} * \frac{(\dot{m}_{air} + \dot{m}_{fuel})}{P_b}$$

3.4.2 EGR Ratio Calculation

For calculation of EGR, a CO_2 balance on the mixed intake air was considered. A sampling line on the mixed intake air downstream of the point of EGR addition allowed for sampling of the mixed intake air as well as the exhaust. These two streams were sampled sequentially during steady state operation using the same exhaust gas analyzer, and the CO_2 concentrations were used for calculation of EGR within the LabVIEW emissions and fuel consumption DAQ program. The initial mass balance equation for CO_2 is given below.

$$\dot{m}_{fresh}\left(\frac{MW_{CO2}}{MW_{fresh}}\right)[CO_2]_{fresh} + \dot{m}_{EGR}\left(\frac{MW_{CO2}}{MW_{exhaust}}\right)[CO_2]_{exhaust}$$

$$= (\dot{m}_{fresh} + \dot{m}_{EGR})\left(\frac{MW_{CO2}}{MW_{mix}}\right)[CO_2]_{mix}$$

Rearranging to group the $\dot{m}_{fresh}$ and $\dot{m}_{EGR}$ terms gives

$$\dot{m}_{fresh}\left(\frac{[CO_2]_{fresh}}{MW_{fresh}}-\frac{[CO_2]_{mix}}{MW_{mix}}\right)=\dot{m}_{EGR}\left(\frac{[CO_2]_{mix}}{MW_{mix}}-\frac{[CO_2]_{exhaust}}{MW_{exhaust}}\right)$$

Solving for $\dot{m}_{EGR}/\dot{m}_{fresh}$ gives

$$\frac{\dot{m}_{EGR}}{\dot{m}_{fresh}}=\frac{[CO_2]_{mix}/MW_{mix}-[CO_2]_{fresh}/MW_{fresh}}{[CO_2]_{exhaust}/MW_{exhaust}-[CO_2]_{mix}/MW_{mix}}$$

Then, solving for the EGR ratio,

$$EGR(\%)=\frac{\dot{m}_{EGR}}{\dot{m}_{fresh}+\dot{m}_{EGR}}=\frac{[CO_2]_{mix}/MW_{mix}-[CO_2]_{fresh}/MW_{fresh}}{[CO_2]_{exhaust}/MW_{exhaust}-[CO_2]_{fresh}/MW_{fresh}}$$

Practically speaking, the CO_2 concentration of fresh intake air is negligible compared with typical mixed intake and exhaust CO_2 concentrations, especially with higher rates of EGR. In addition, the difference in molecular weight between mixed intake and exhaust is minimal, so a sufficiently accurate calculation of EGR ratio for these experiments is

$$EGR(\%)\approx\frac{[CO_2]_{mix}}{[CO_2]_{exhaust}}$$

3.4.3 Filter Smoke Number Calculation

The functional principle of a filter smoke number measurement is described in [48]. The important parameter for filter smoke number is the exhaust gas volume relative to the loaded filter area, which is referred to as the 'effective sampling length'. The effective sampling length is defined as

$$effective\ sampling\ length=\frac{sampled\ volume-dead\ volume-leakage\ volume}{filter\ area}$$

where the *dead volume* is the volume contained between the sampling point and the filter paper, and the *leakage volume* is caused by transverse currents of the filter at the suction unit and by leakages in the sampling system. In this study, the system was checked for leaks periodically,

and the filter was tightly contained in the holder, ensuring that all gas flow went through the filter. Therefore, the leakage volume was assumed to be negligible. The dead volume consisted of ten inches of 3/8" OD copper tubing, a quick connector, and the upstream end of the filter holder, totaling less than 20 mL. The minimum sampled volume in the study was 2 L, so the dead volume, representing at most 1% of the sampled volume, was also considered negligible. Thus, the effective sampling length for this study was taken as

$$effective\ sampling\ length = \frac{sampled\ volume}{filter\ area}$$

The darkened filter area for this study was measured to be 16.7 mm in diameter, or 2.19 cm^2. Sampled volumes ranged from 2.1 to 3.9 L, depending on the soot content of the exhaust gases.

In the standards for filter smoke number, the filter blackening is to be measured with a reflectometer. The paper blackening is defined as

$$PB = \frac{100 - R_R}{10}$$

where

$$R_R = \frac{R_P}{R_F} \cdot 100\%$$

and

R_P = reflectometer value of sample

R_F = reflectometer value of the unblackened paper

R_R = relative brightness of the sample (relative radiance factor)

Then, if the effective sampling length is 405 mm, with the sampled volume related to 298 K and 1 bar,

$$FSN = PB$$

No reflectometer was available for use in this study, so optical analysis was instead performed using a computer scanner. Images of the filter papers were first obtained using an HP PSC1210 scanner, set to scan in 256 gray shades, where completely black corresponds to a pixel value of 0, and completely white, 255. A square area was cropped from the darkened region of each filter paper and saved in jpeg format. These cropped images were then processed using MATLAB. A Bacharach oil burner smoke scale, made to assess filter paper blackening, was scanned using the same settings as the filter papers and used as a reference for soot processing (see Figure 3.11). An average pixel value for each paper blackening number was obtained, and the series of data was plotted. In order to translate average pixel value to paper blackening, a polynomial fit was employed, as shown in Figure 3.12. Finally, to obtain filter smoke number (FSN) results, all paper blackening numbers were scaled based on an effective sampling length of 405mm. Thus, for the lowest sample volume (2.1 L), the correction factor is 1/23.7, while for the highest sample volume (3.9 L), the correction factor is 1/44.

3.5 Experimental Procedures and Operating Conditions

3.5.1 General Operating Procedures

Some suggestions regarding general engine maintenance are included here for future reference. Prior to engine operation, the following items should be addressed: (1) ensure sufficient fuel for the planned duration of testing; (2) check the engine oil level; (3) visually inspect the engine and stand for anything unusual, including loose wires, material in contact with the exhaust system, puddles of fluid under the engine, etc.; (4) fill ice bath used for water removal from sampling lines. The following items need not be addressed at each startup, but should be checked periodically on a weekly or monthly basis depending on how much the engine

is used: (1) check oil level in dynamometer oilers; (2) check coolant level in reservoir; (3) check engine stand for loose bolts potentially caused by engine vibration; (4) grease universal joints on driveshaft; (5) drain water from line dryers on soot measurement and exhaust gas measurement systems. Finally, some maintenance should be performed on an as-needed basis: (1) change engine oil and filter at reasonable intervals; (2) change fuel filter when switching fuels or if it becomes clogged; (3) clean EGR valves if they are found to be sticking; (4) replace filters on the MEXA-554JU exhaust gas analyzer whenever they become dirty, which may be several times during a test.

The engine was allowed to warm up before any data acquisition. A rather large volume (approximately 15 gallons) is contained in the tank and pipes of the coolant system, so full warm-up can take a long time (up to 45 minutes) depending on engine speed and load. The building water supply was kept off during this time for quicker warm-up. Once the coolant temperature attained its desired value (75°C), the building water supply was turned on, and it was regulated by the pneumatic system described in the experimental setup. The oil and fuel temperatures typically followed closely along the coolant temperature, achieving stable values prior to data acquisition.

As the VGT was not installed, conditions for the fresh intake air were set manually to simulate appropriate conditions. The manifold absolute pressure (MAP) was controlled using the compressed intake air system described in the experimental setup. As the engine speed or load changes, the ECM would typically adjust the VGT to achieve a set MAP value. This value was read from INCA and manually input to the compressed air system controller, thereby achieving appropriate intake pressures consistent with those of the turbocharged engine. As for the intake temperature, a constant value of 30°C was chosen, based on data from Ford, to

account for heating during the turbocharging process. This temperature is reasonable for the low- to mid-load conditions considered in this study, as the designated boost pressure was low (less than 0.5 bar) for all cases tested. Under high-load conditions, this temperature should be increased to ensure realistic operating conditions for the engine.

Adjustment of EGR was accomplished by one of two methods. The first method uses the engine's normal control strategy, which is described here. On the stock engine equipped with VGT, the EGR rate is controlled by the ECM through an electrically-controlled valve in each of the two EGR coolers. A table of mass air flow (MAF) setpoints dictates the fresh air flow at each engine operating condition. The EGR valves open or close to decrease or increase, respectively, the fresh air flow rate and maintain a value near the setpoint. Though the VGT is typically an important part of the EGR control system, the current tests are performed at steady state conditions, where the exhaust restrictor can be adjusted to simulate the backpressure normally supplied by the VGT. The on-board EGR controller is thus able to function properly, provided that the exhaust backpressure is set to an appropriate level.

Under certain operating conditions, the EGR control system and the pressurized intake air control system were found to interfere with one another and create wide oscillations in intake pressure. For these cases, the position of the EGR valves on the engine was set manually through INCA to constant values. The intake pressure would then stabilize, and the exhaust flow restrictor and EGR valves were adjusted as needed to achieve the desired amount of EGR. Another problem found relates to sticking EGR valves. If the engine is run for extended periods under conditions producing high amounts of soot, the EGR valves will occasionally stick upon engine shutdown. This becomes apparent upon subsequent startup, when the EGR valves will be completely closed as observed from their control signal voltages. If this happens, the EGR

valves should be cleaned. The metal tube with flexible joint running from EGR cooler to intake manifold should first be removed from the EGR cooler, allowing access to the EGR valve seat. The valve seat may then be soaked in alcohol or similar solvent and broken loose. The EGR valve movement may be observed without starting the engine by turning on the engine ignition and then shutting it off. Upon engine shutdown, the ECM is programmed to open and close the valves several times to avoid sticking. A properly working valve can be observed opening and closing using a flashlight. If a valve is stuck, it can be heard trying to open and close, but will not be moving.

3.5.2 Conventional Combustion Study Operating Conditions

For the studies in conventional combustion, several speed and load combinations were run, as indicated in Table 3.3. In each case, the load was adjusted to constant bmep by adjusting the fueling rate. For the biodiesel blends, delayed main injection timings were investigated for reducing NOx. For B50 and B100 in the light load (3 bar bmep) cases, where NOx levels were similar to diesel to begin with, earlier main injection timings at one increased EGR ratio were studied to determine if a reduction in NOx could be attained along with lower fuel consumption. For B50 and B100 at moderate load (5 bar bmep), the MAF setpoint was changed to account for the lower stoichiometric air-fuel ratio of biodiesel.

Note that, throughout this study, default conditions are referenced. These correspond to the operating conditions of the unaltered ECM, set up according to Ford's specifications. While absolute numbers will not be given, the trends in some relevant ECM parameters are shown in Figures 3.13 through 3.15 to put the results in perspective. The start of injection tends to advance with increasing speed and load, while the boost pressure increases. Meanwhile, the EGR ratio generally decreases with the amount of fuel injected. Since biodiesel has a lower

energy content than diesel, the ECM assumes a higher load, meaning that with higher biodiesel content, the main injection timing will advance, the boost pressure will increase, and the EGR ratio will decrease, albeit by rather small increments.

Table 3.3: Summary of test conditions for conventional combustion study

	B0	B20	B50	B100
1000 rpm, 3 bar bmep	1	1,2	1,2,3	1,2,3
1000 rpm, 5 bar bmep	1	1,2	1,2,4	1,2,4
1500 rpm, 3 bar bmep	1	1,2	1,2,3	1,2,3
1500 rpm, 5 bar bmep	1	1,2	1,2,4	1,2,4
2000 rpm, 3 bar bmep	1	1,2	1,2,3	1,2,3
1: ECM default settings				
2: delayed injection timings at default EGR ratio				
3: advanced injection timings at an increased EGR ratio				
4: increased EGR ratio at default timings				

3.5.3 Low Temperature Combustion Study Operating Conditions

For the studies aimed to achieve low temperature combustion, tests were again run at various speed and load conditions, as indicated in Table 3.4. The given load conditions in bar bmep correspond to the engine load with no EGR. Note that, instead of adjusting the fueling rate to achieve constant load as done in the conventional combustion study, the fueling rate was held constant, and the brake torque was recorded in each case. Therefore, the engine was brought to the designated speed and load with the EGR system disabled. At this point, the fuel flow rate and engine speed were held constant as the EGR ratio was increased incrementally. For each speed and load combination, the EGR ratio was generally varied from no EGR to high levels where combustion efficiency began to deteriorate (observed by a substantial rise in CO

emissions). This maximum level varied based on engine operating condition, which is why the range of measurement points appears arbitrary. The EGR was then set to a level just below the point of combustion deterioration, and injection strategies were altered with emphasis on reducing soot and maintaining reasonable power output. More detailed operating conditions are included in Appendix B for reference.

Table 3.4: Summary of test conditions for low temperature combustion study

	engine load without EGR (bar bmep)			
	2	3	5	7
1000 rpm	1	1,2	1,2	1,2
1500 rpm			1,2	
2000 rpm			1,2	
1: Vary EGR ratio to point of combustion deterioration				
2: Alter injection strategy with high EGR				

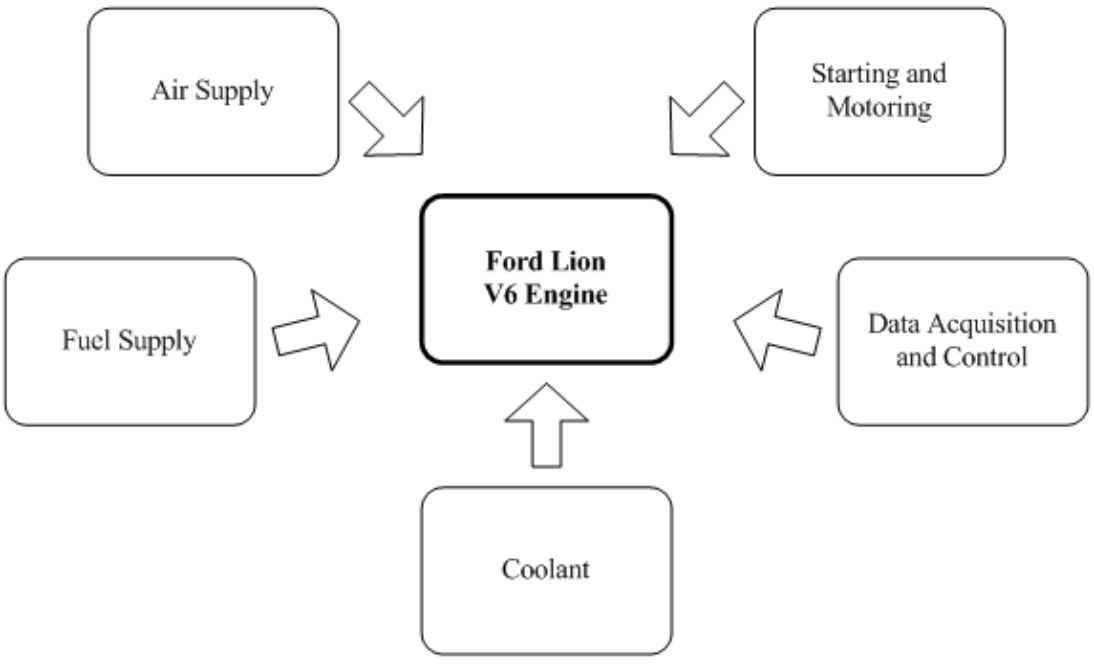


Figure 3.1: Ford Lion V6 engine subsystems [45]

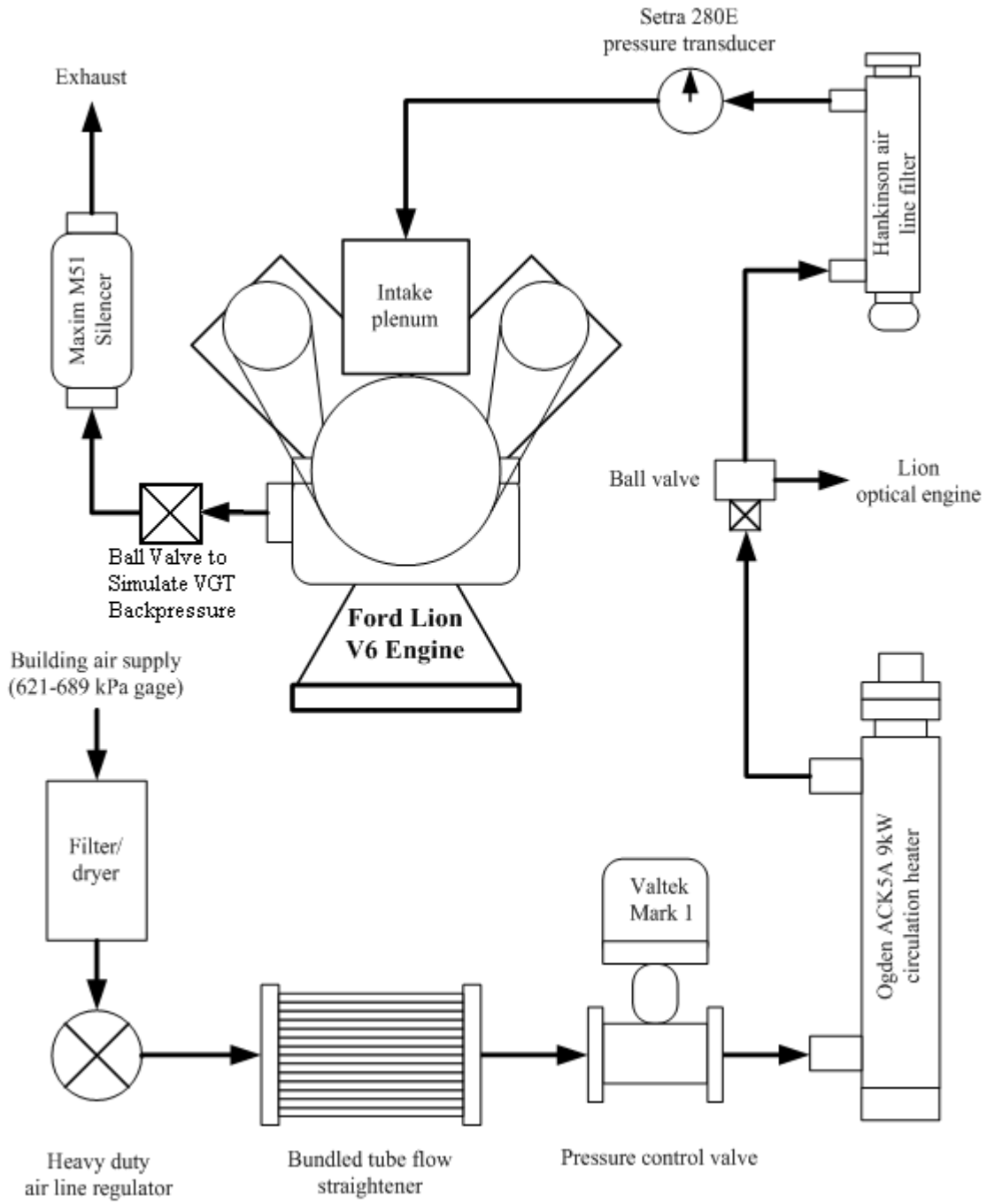


Figure 3.2: Ford Lion V6 engine air supply and exhaust (adapted from [45])

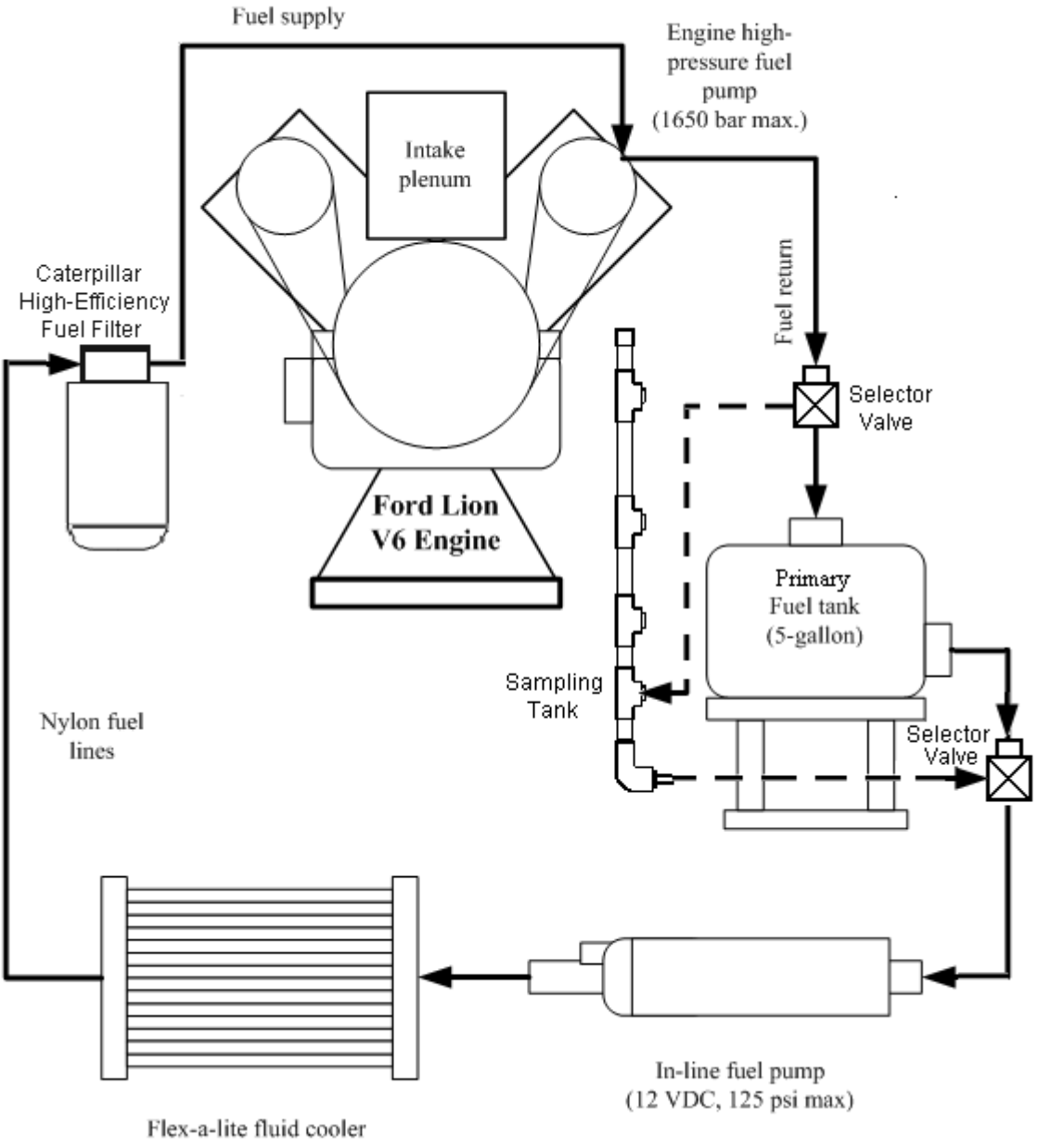


Figure 3.3: Ford Lion V6 engine fuel supply system (adapted from [45])

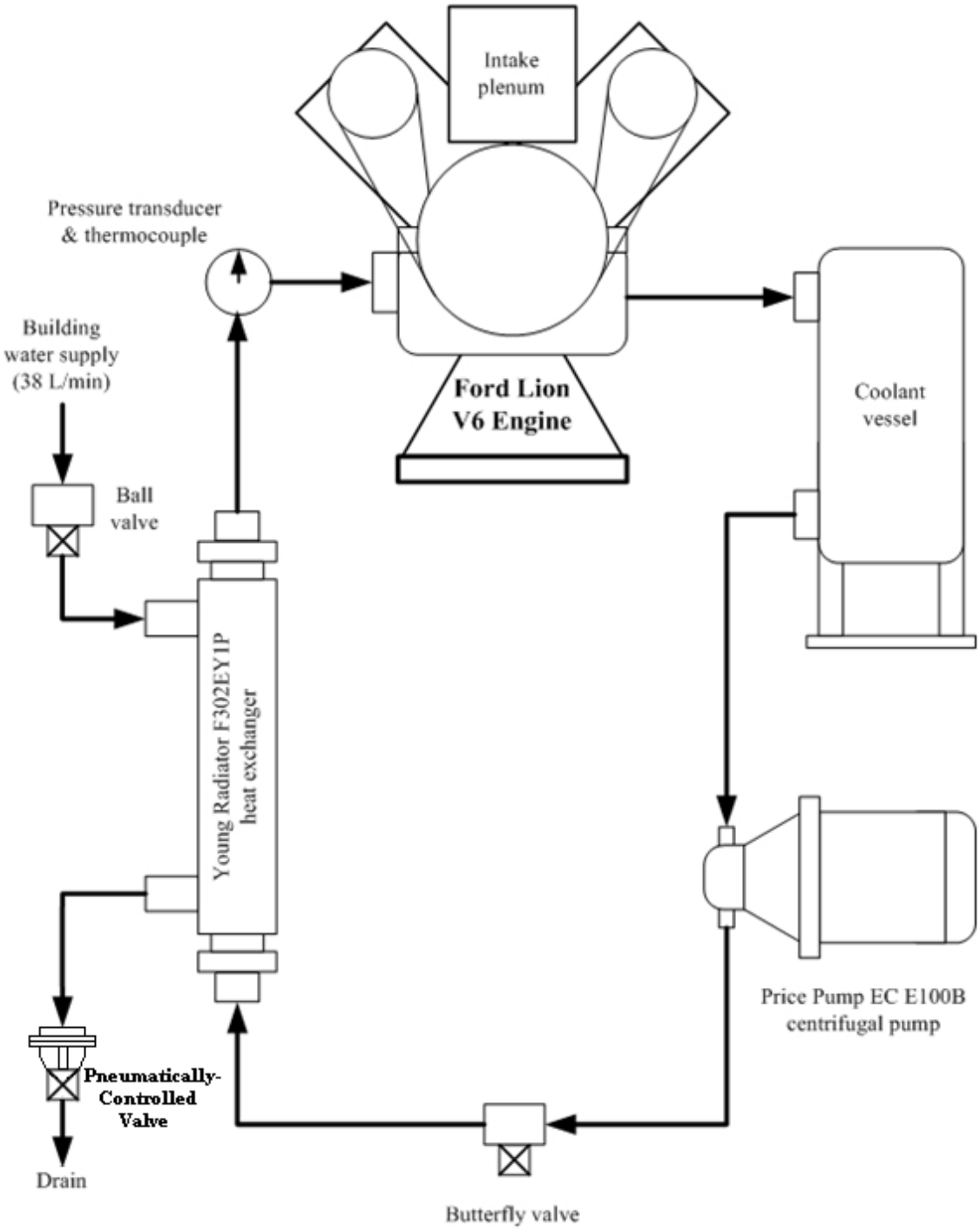


Figure 3.4: Ford Lion V6 engine coolant system (adapted from [45])

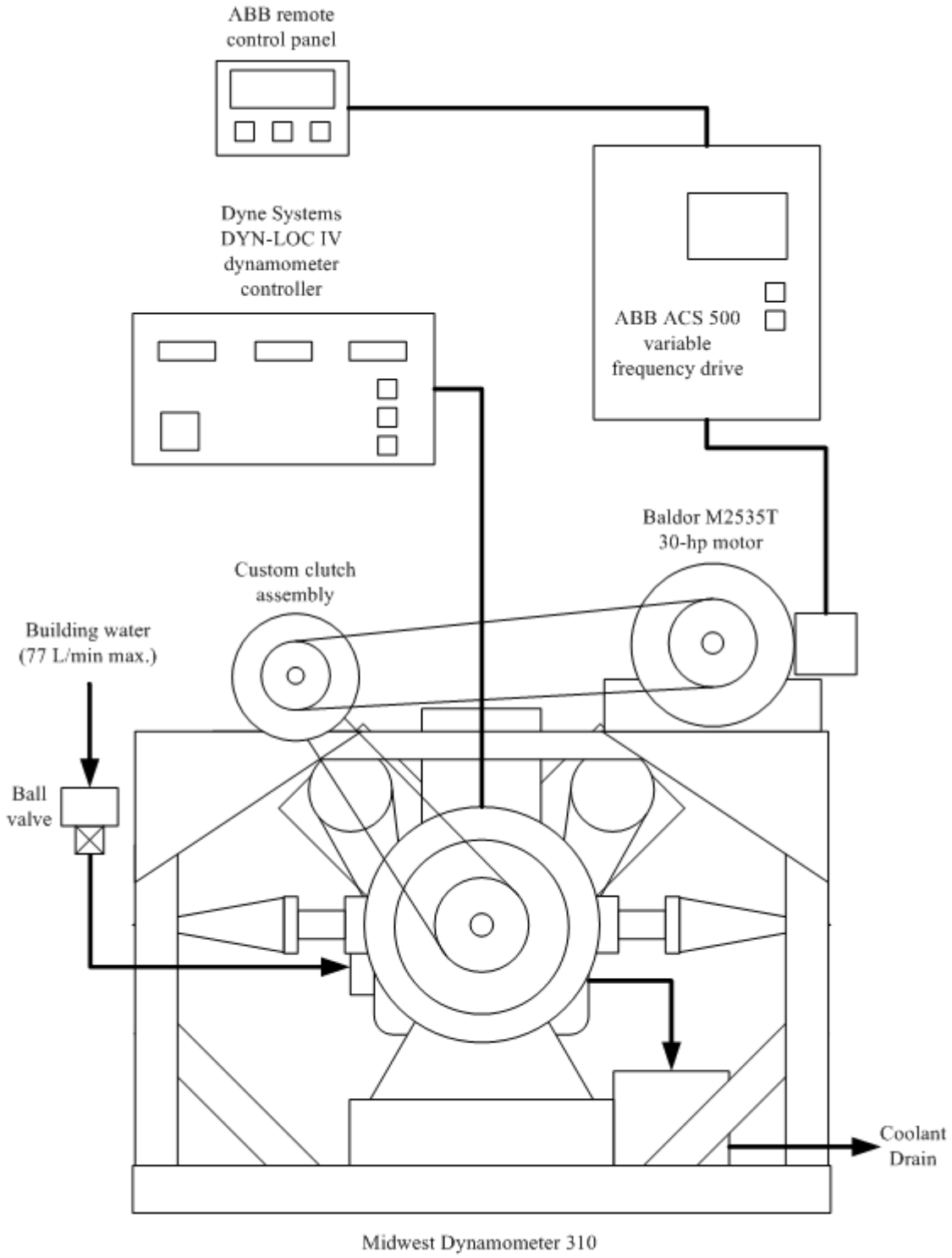


Figure 3.5: Ford Lion V6 engine starting, motoring, and power absorbing system [45]

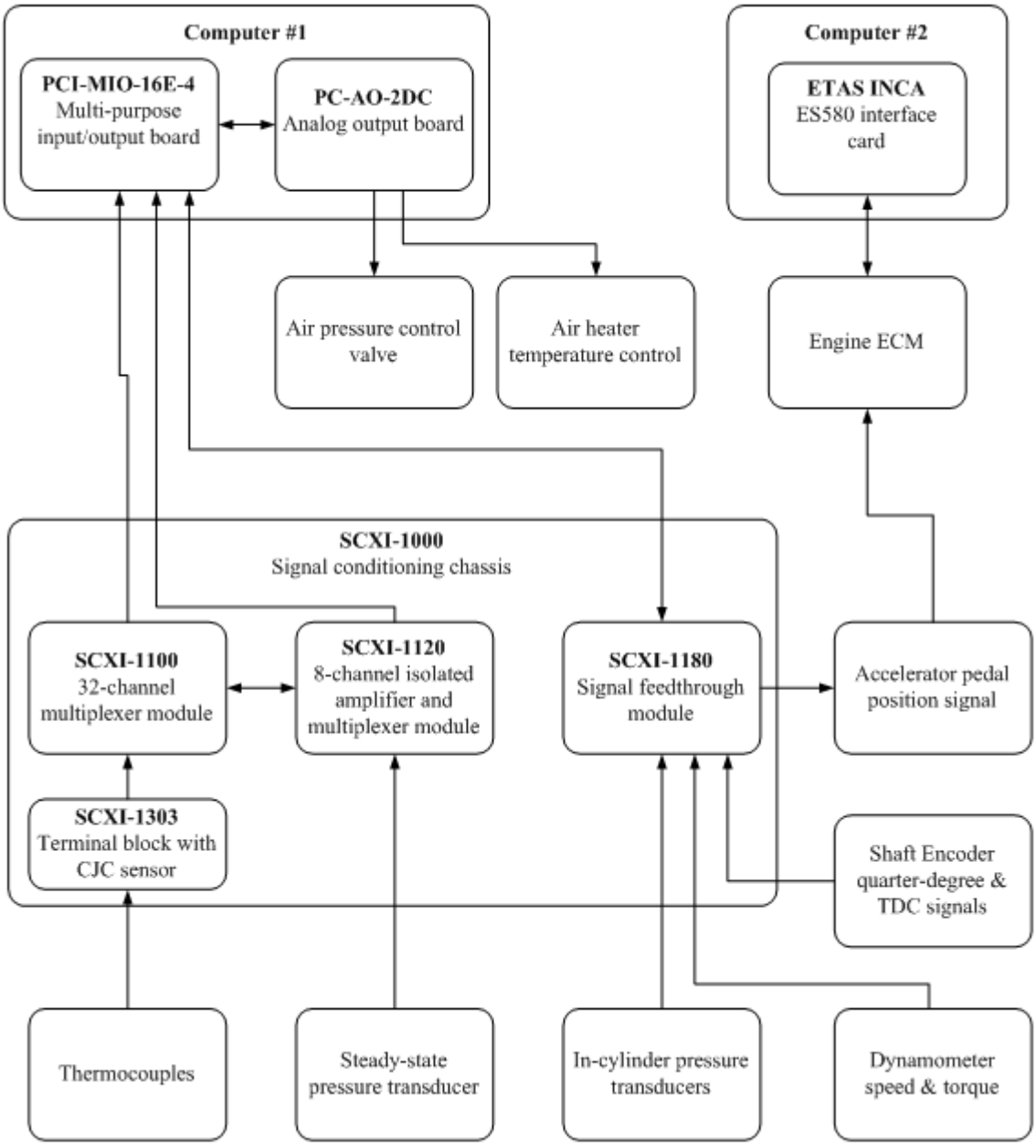


Figure 3.6: Ford Lion V6 engine data acquisition and control system [45]

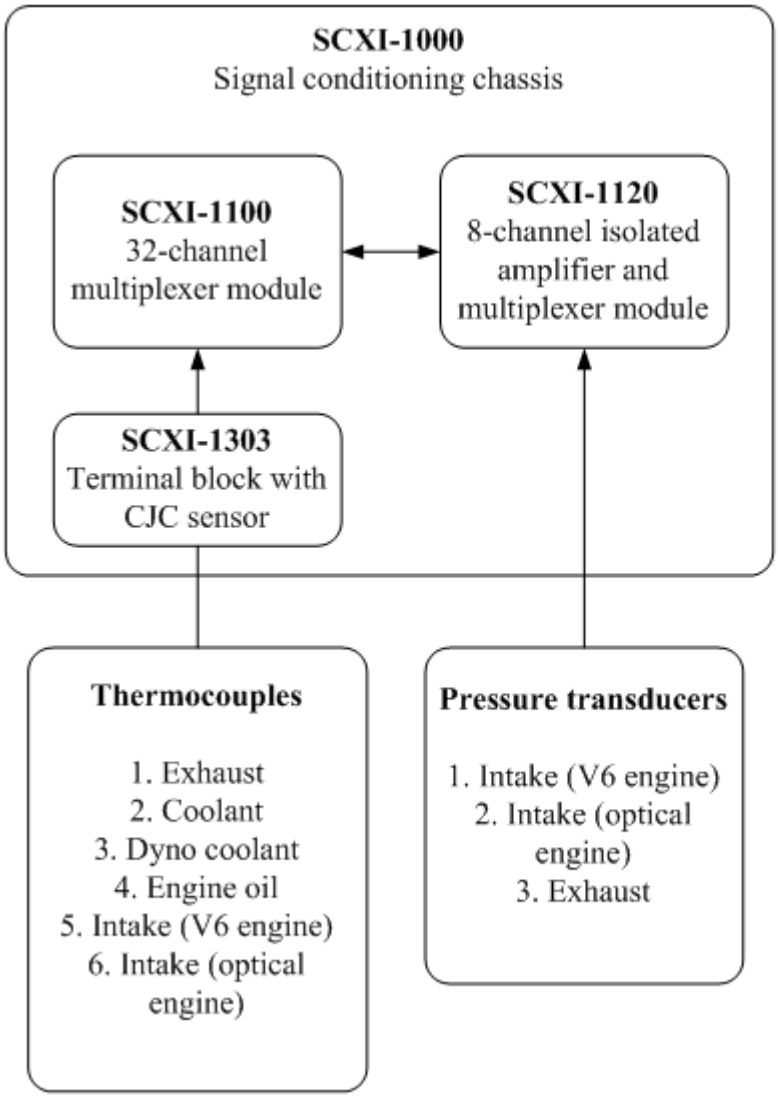


Figure 3.7: Wiring of thermocouples and pressure transducers [45]

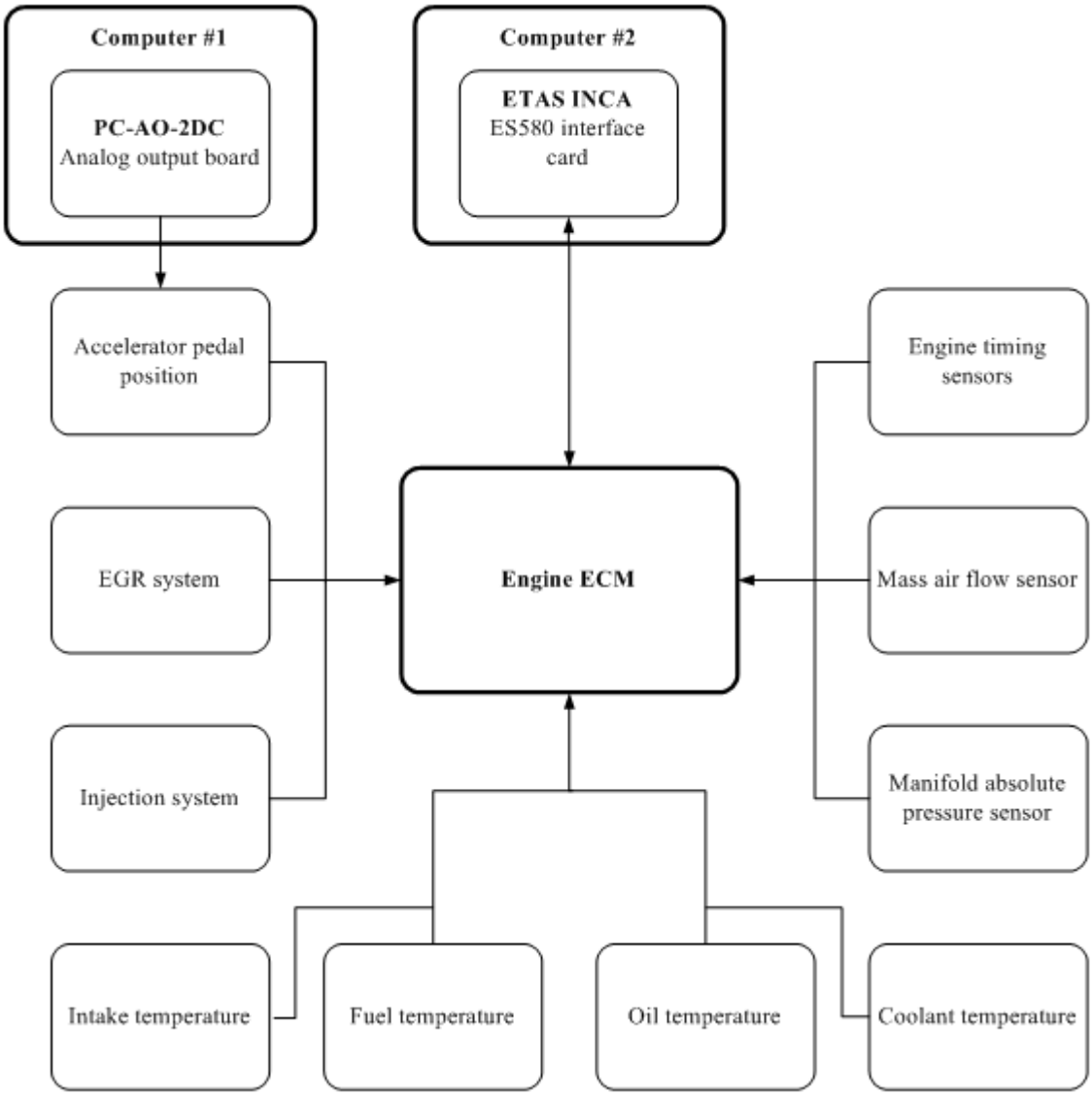


Figure 3.8: Ford Lion V6 engine ECM control and management [45]

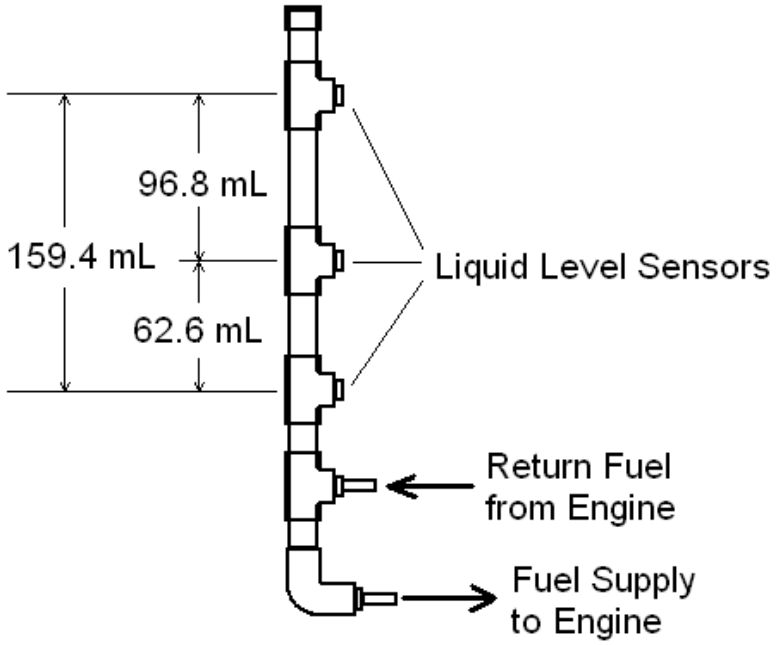


Figure 3.9: Schematic of fuel consumption sampling tank

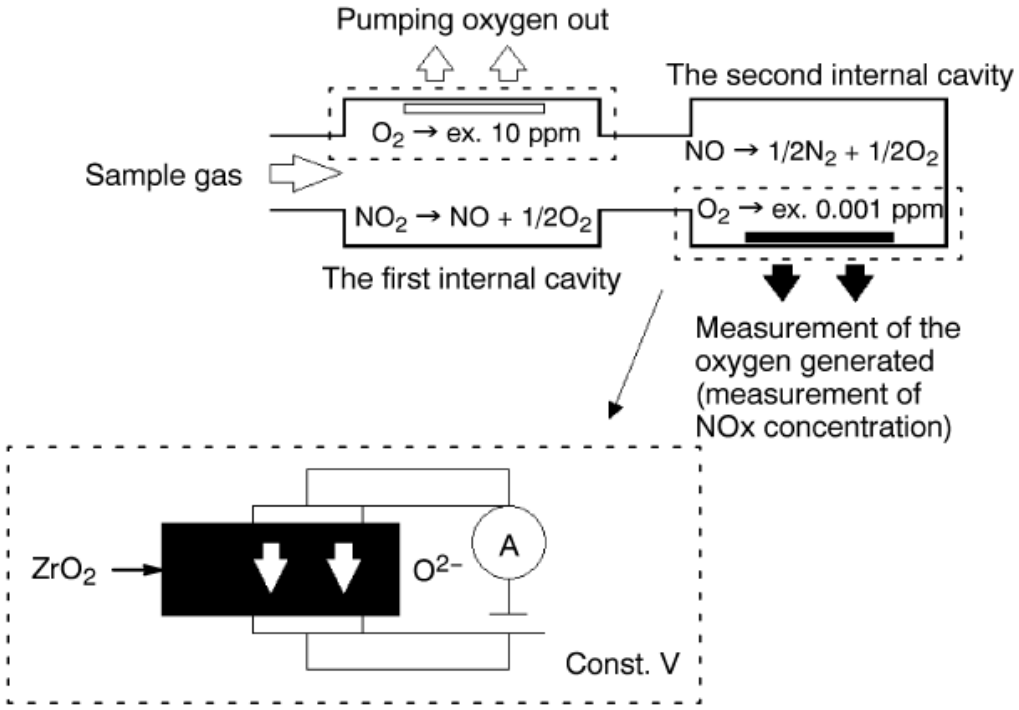


Figure 3.10: Principle of zirconia sensor for NOx measurement [47]

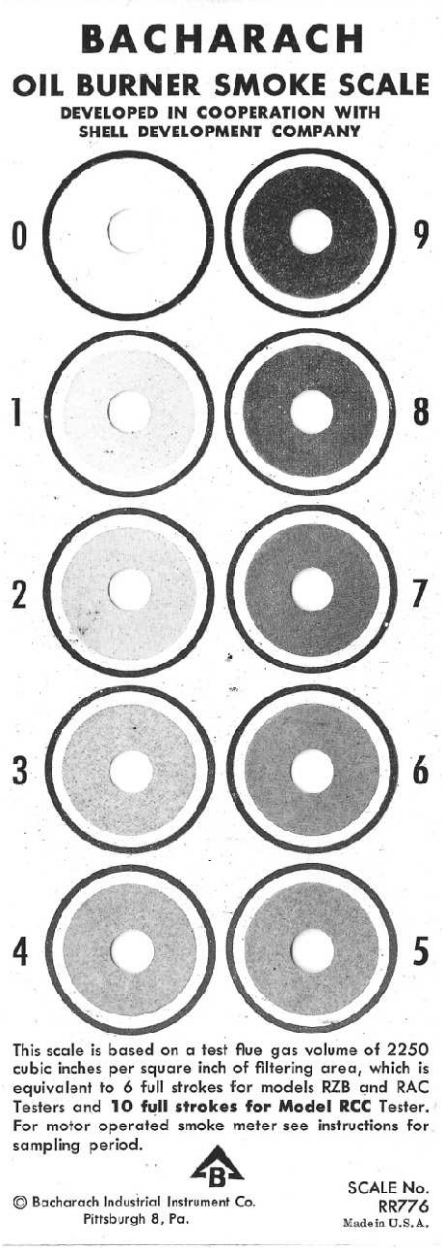


Figure 3.11: Scan of Bacharach smoke scale used to relate average pixel value and paper blackening

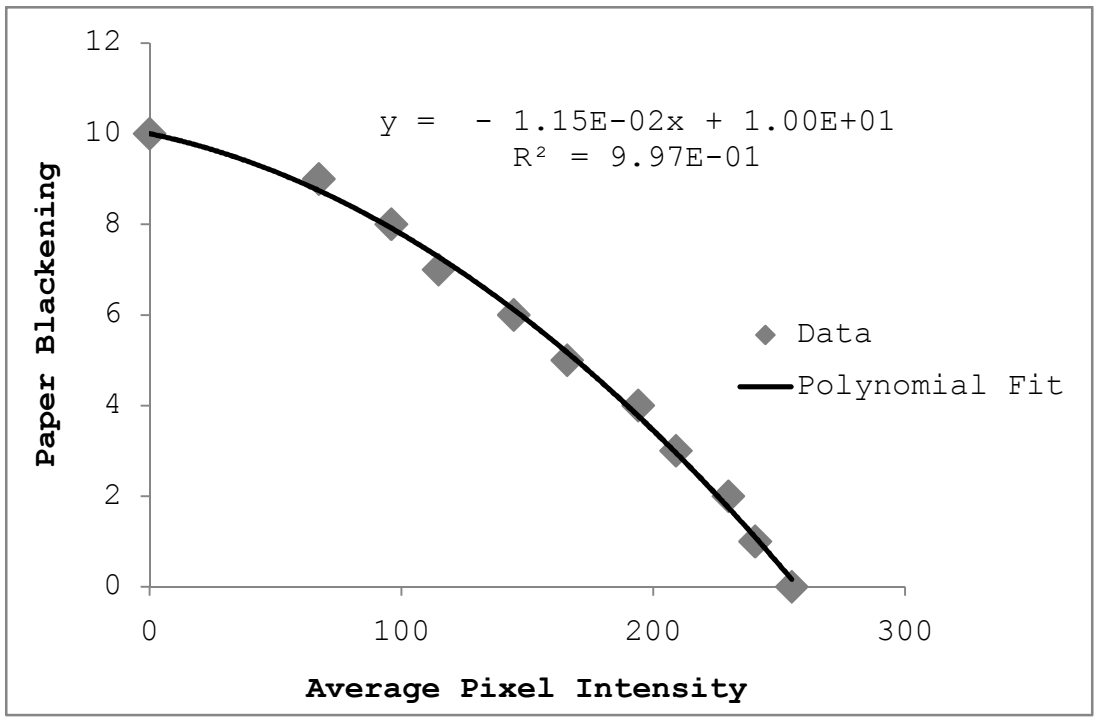


Figure 3.12: Polynomial fit of paper blackening versus average pixel intensity

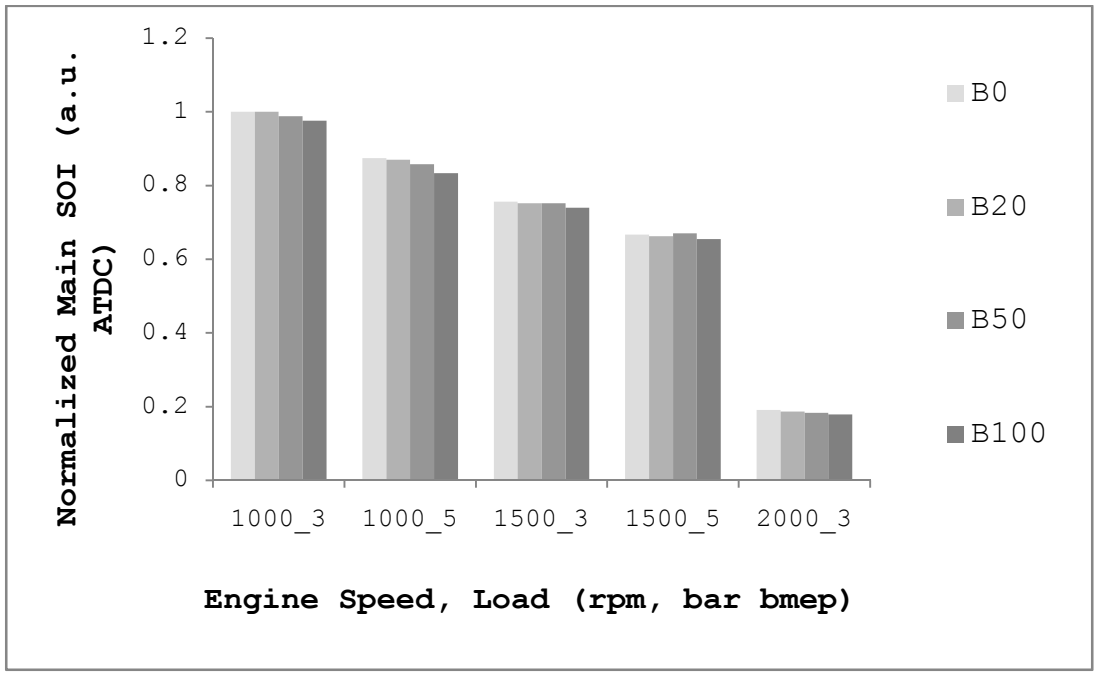


Figure 3.13: Trends in main injection timing for the cases studied

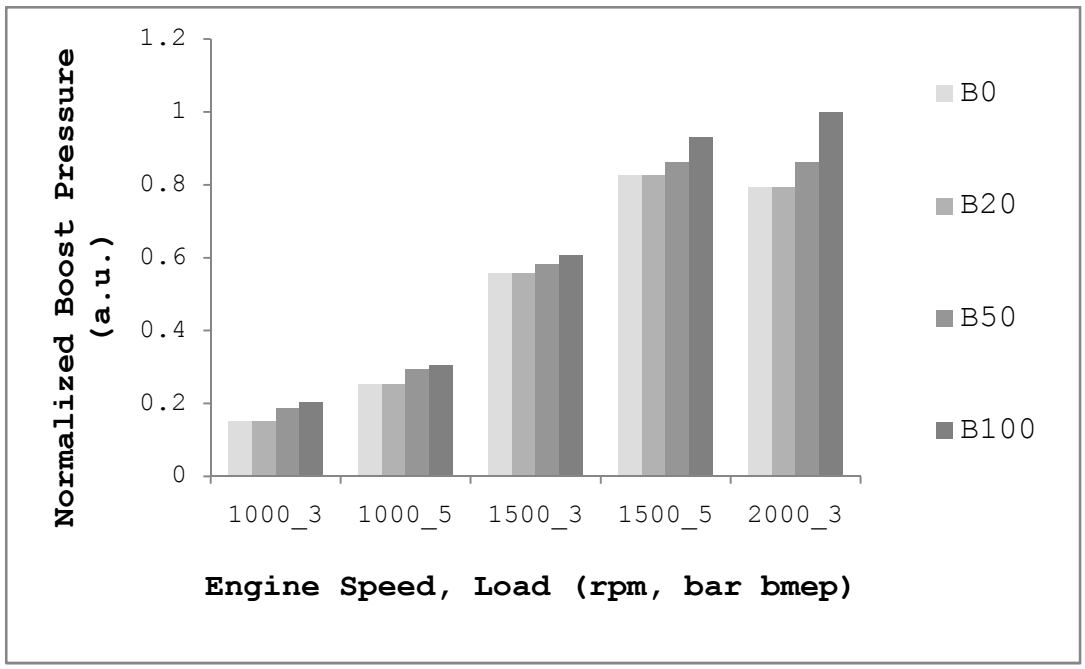


Figure 3.14: Trends in boost pressure for the cases studied

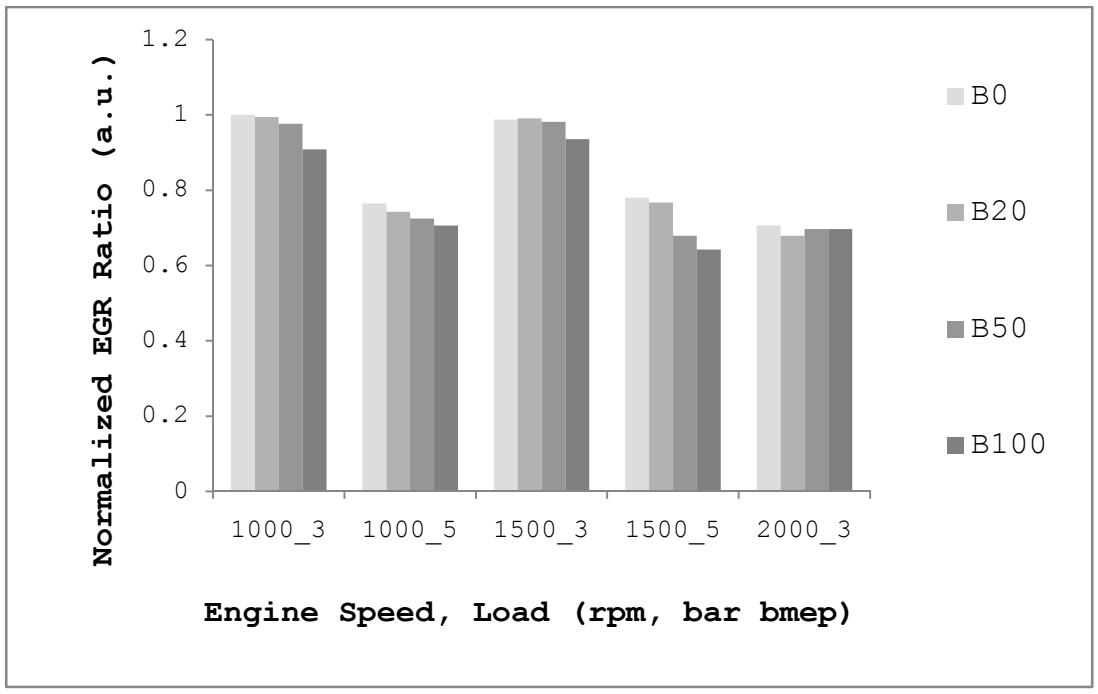


Figure 3.15: Trends in EGR ratio for the cases studied

Chapter 4:
Experimental Results and Discussion

4.1 Conventional Combustion Study

4.1.1 Overall Trends in NOx Emissions for Different Speed and Load Conditions

Figure 4.1 shows the overall trends in NOx emissions for different fuel blends and different speed and load conditions for the engine operating with its default ECM settings. At low speed and light load, increased biodiesel content has relatively little effect on NOx for this engine at its default operating conditions. A possible explanation is that in these cases, the EGR ratio is near its maximum level and the amount of fuel is small, so that NOx emissions are kept minimal due to a rather low combustion temperature, regardless of fuel type. At moderate load, the increase in NOx with biodiesel content becomes notable, as much as a 50% increase over that of diesel. The case of 2000 rpm, 3 bar bmep is seen to have significantly higher NOx than the other cases at 3 bar bmep. This is due to some changes in ECM parameters, specifically, earlier injection timings and a lower EGR ratio.

4.1.2 In-Cylinder Pressure and Apparent Heat Release Rate

Figure 4.2 is typical of the in-cylinder pressure and calculated heat release rate curves for the different fuels. From the heat release rate plot, the pre-injection seems to ignite around -10° ATDC. With higher biodiesel content, the amount of energy released during the pre-injection is somewhat lower. The pre-injection duration is essentially the same for the different fuels at a given speed and load, so approximately the same volume of fuel should be injected. Biodiesel is about 5% more dense than diesel, but its lower heating value is about 12% less than that of diesel, explaining the reduction in energy released. Following the pre-injection heat release, the main injection occurs. As the injected fuel vaporizes, there is a slight dip into negative territory

for the heat release rate, occurring around 5° ATDC. Shortly thereafter, around 7° ATDC, the heat release rate turns positive as the fuel energy is released. Based on the heat release rate plot, there appears to be premixed-dominated combustion with mixing-controlled combustion at this engine condition. There is relatively little difference between fuels. However, B100 is seen to ignite slightly ahead of the other fuels, possibly contributing to its higher NOx emissions. This earlier ignition may be a result of biodiesel's high cetane number, or possibly a higher intake oxygen concentration due to the lower EGR ratio specified for this case. With B0, B20, and B50, it is interesting to note that for very similar pressure and heat release rate curves, notable differences in NOx can be seen. As discussed in the literature review, there have been numerous studies aimed at explaining this type of phenomenon. Speculations will not be made here, as this type of detailed work is better performed on single-cylinder or optical engines with more precise control and instrumentation.

The influence of injection timing on the in-cylinder pressure and apparent heat release rate is shown in Figures 4.3 and 4.4. These particular data correspond to B20 run at 1000 rpm and 5 bar bmep. Similar data were obtained for each fuel blend at each engine operating condition, but the trends were mostly the same, so only a representative case was chosen to be included here. Each curve on the plot represents a different injection timing relative to the ECM default injection timing. A curve is also included for B0 for comparison. At different injection timings, the in-cylinder pressure is shifted one way or the other on the diagram, as would be expected. With later injection timings, the relative shift seems to become more significant, and there may be slightly more mixing time prior to combustion, resulting in a higher peak heat release rate as seen in Figure 4.4.

4.1.3 Light-Load Optimization

An example of light-load optimization for B100 is shown in Figures 4.5 through 4.7. These particular results correspond to 1500 rpm & 3 bar bmep. Similar results were found for 1000 rpm and 2000 rpm at 3 bar bmep, so only a representative case is shown here. In these figures, shaded markers represent the ECM's default settings for that fuel at the given speed and load. Injection timings were advanced and retarded around the ECM's default setting, as represented by the horizontal axis in each figure. This was done at the default EGR ratio (using the default MAF setpoint) and at an increased EGR ratio obtained by adjusting the default MAF setpoint by a factor of 12.6/14.6 (the stoichiometric air-fuel ratio of biodiesel divided by that of diesel; an addition of about 6% EGR as estimated by the ECM). Note in Figure 4.7 that the fuel consumption results for biodiesel has been corrected by a factor of 37.3/42.5 (the lower heating value of biodiesel divided by the lower heating value of diesel) to obtain fuel consumption in units of grams diesel equivalent per kilowatt-hour. Even after corrected, the fuel consumption for biodiesel is seen to be slightly higher than diesel at default ECM conditions. However, advancing the injection timing by 2 to 4 CAD is seen to result in equal or lower bsfc compared with diesel at the default ECM conditions. Since the case with default ECM conditions is similar to diesel in terms of NOx, correcting the MAF setpoint is sufficient to bring NOx emissions below that of diesel with essentially no penalty to fuel consumption. Additionally, by advancing the injection timing between two and four degrees, a savings in fuel consumption of about 3% can be realized with NOx emissions below that of diesel at the default ECM configurations. For the advanced injection cases, the soot increases somewhat, likely due to injection into a hotter environment, but it is still well below that of diesel. Also notice that a significant penalty to fuel consumption is required to decrease NOx emissions simply with a delay in injection timing.

Since the ECM already uses late injections, fuel efficiency begins to drop off quite rapidly with further retardations due to poor combustion phasing. To reduce NOx emissions to the level of diesel with late injection timings alone, the penalty to fuel consumption, averaged over all cases studied, is 1.9% for B20, 3.4% for B50, and 4.6% for B100. By comparison, increasing the EGR to account for the lower stoichiometric air-fuel ratio of biodiesel and advancing the injection timing allows for a reduction of NOx emissions along with better combustion phasing, producing better fuel efficiency.

Results for B50 were similar to the previously described results for B100 at light load conditions. Figures 4.8 through 4.10 show the NOx, soot, and bsfc results for 1500 rpm & 3 bar bmep. Again, results for 1000 and 2000 rpm were similar and are not shown here to avoid redundancy. The increased EGR ratio in this case was obtained by adjusting the MAF setpoint value by a factor of 13.6/14.6 (the stoichiometric air-fuel ratio of B50 divided by that of diesel). The fuel consumption data in Figure 4.10 have been adjusted as done for B100, but in this case, the ratio of heating values is 39.9/42.5. Looking at these results together, the conclusion is much the same as it was for B100. A slight increase in EGR coupled with an advance in injection timing is beneficial in terms of reducing NOx and fuel consumption with similar levels of soot.

4.1.4 Moderate Load Optimization: EGR Effects

For cases with moderate load, a closer look was taken at the EGR and air-fuel ratios. The air-fuel ratio was calculated from measured fresh air flow rate and fuel flow rate. For all fuels, the calculated air-fuel ratio is essentially the same at a given speed and load since this is controlled through ECM by adjusting the positions of the EGR valves. However, the stoichiometric air-fuel ratio for B100 is lower than that of diesel, so at the same air-fuel ratio, the

equivalence ratio is lower. Note that the equivalence ratio and EGR ratio are related at a given speed and load since the addition of EGR displaces some of the fresh air flow, resulting in a higher equivalence ratio.

To investigate the effects of different EGR ratios on NOx emissions for B50 and B100, the MAF setpoint in the ECM was adjusted to different values, resulting in points of different EGR ratio and equivalence ratio. Only the ECM default case was run for B20 since the change in stoichiometric air-fuel ratio from B0 is relatively small. Likewise, for B0, only the default ECM setting was run, as the ECM was designed and optimized for use with this fuel. Figure 4.11 shows the normalized brake-specific NOx emissions versus equivalence ratio. The shaded markers represent the ECM's default settings, while the hollow markers represent the points obtained by changing the MAF setpoint. With the ECM's default settings, B100 operates at the leftmost point in Figure 4.11, a fair amount leaner than B0 and B20. Meanwhile, for B50, the ECM default operating point is the center point, again leaner than the B0 and B20. This can be considered another ECM calibration effect for engines equipped with this type of EGR system. Since biodiesel has oxygen within the fuel molecules, its stoichiometric air-fuel ratio is lower, and a diesel engine designed to run at a certain air-fuel ratio will run relatively leaner when fueled with biodiesel.

The results in Figure 4.11 show a clear trend of lower NOx emissions for equivalence ratios closer to stoichiometric. Recall that to change the equivalence ratio for this engine, the EGR ratio must be adjusted, so the reduction in NOx is a combination of these factors. With the ECM's default settings, there is a substantial increase in brake-specific NOx emissions for fuels of high biodiesel content. This can, to some extent, be considered a result of the engine being optimized for diesel and not biodiesel, an ECM calibration effect. In fact, for similar

equivalence ratios, NOx emissions are seen to be quite similar for the different fuels. Meanwhile, biodiesel still produces less soot than diesel, as seen in Figure 4.12. Therefore, adjusting the ECM's MAF setpoint tables based on stoichiometric air-fuel ratio appears to be an effective way of eliminating the problematic increase in NOx normally seen when running biodiesel in this engine designed for diesel. For engines equipped with this type of EGR system, the mass flow rate of fresh air should be considered a useful parameter for optimizing the engine to run on biodiesel.

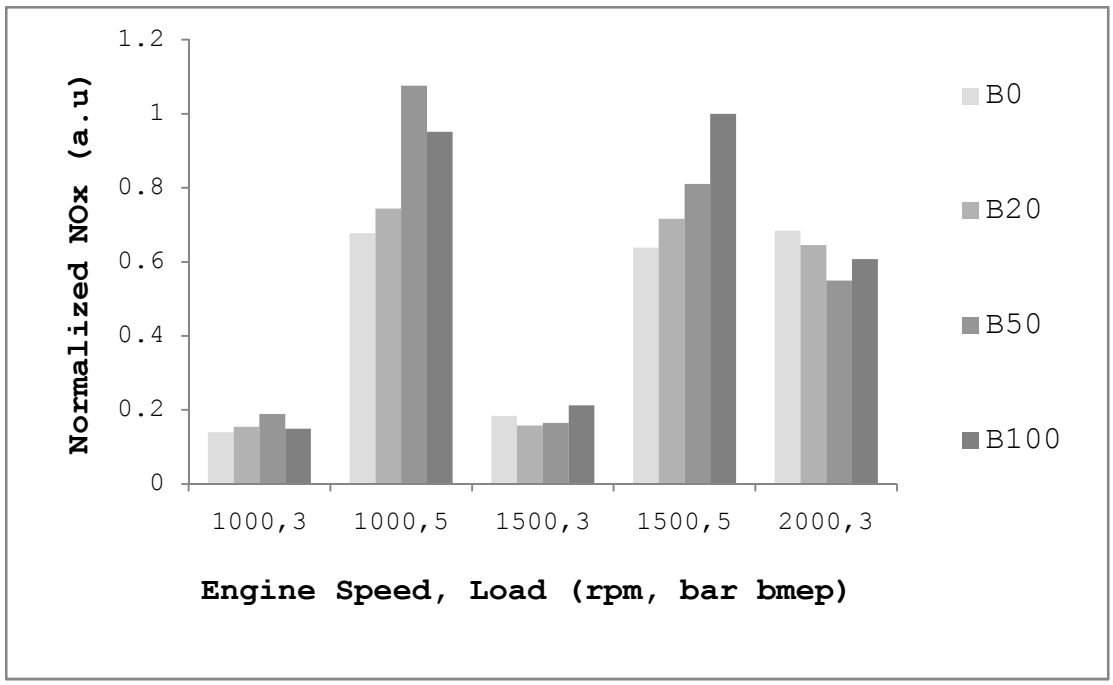


Figure 4.1: NOx trends for different biodiesel blends at default engine operating conditions

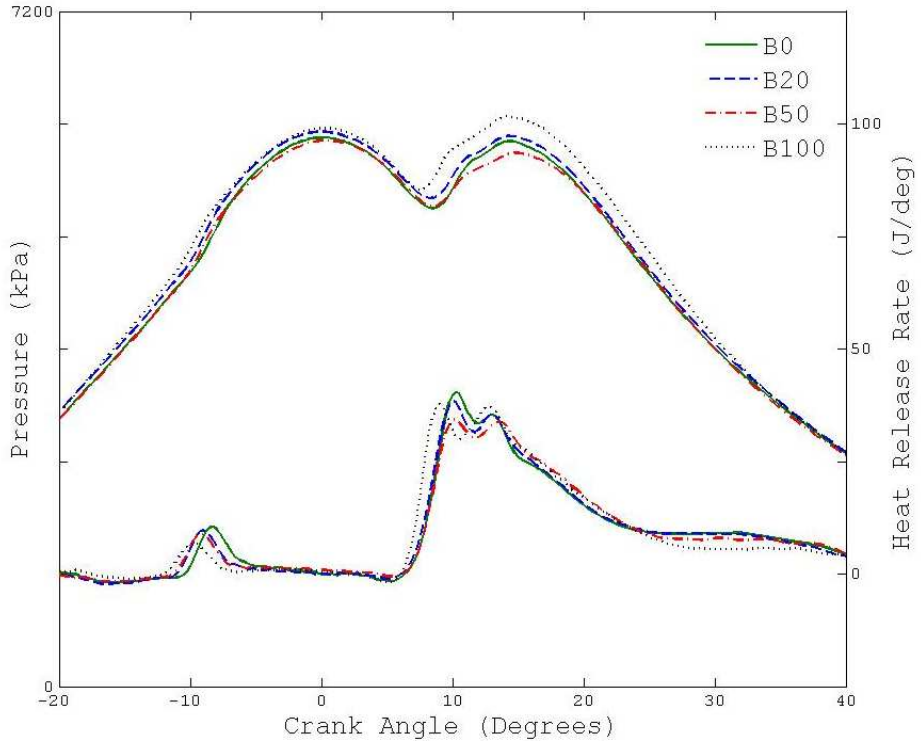


Figure 4.2: Influence of fuel type on pressure and calculated heat release rate at 1500 rpm, 5 bar bmep

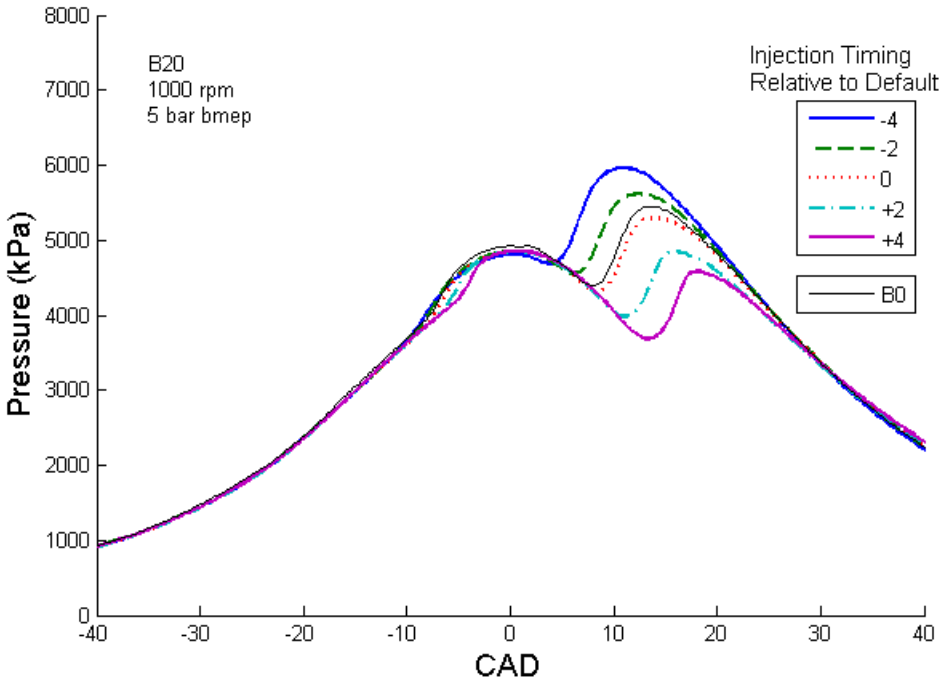


Figure 4.3: Effect of injection timing on in-cylinder pressure

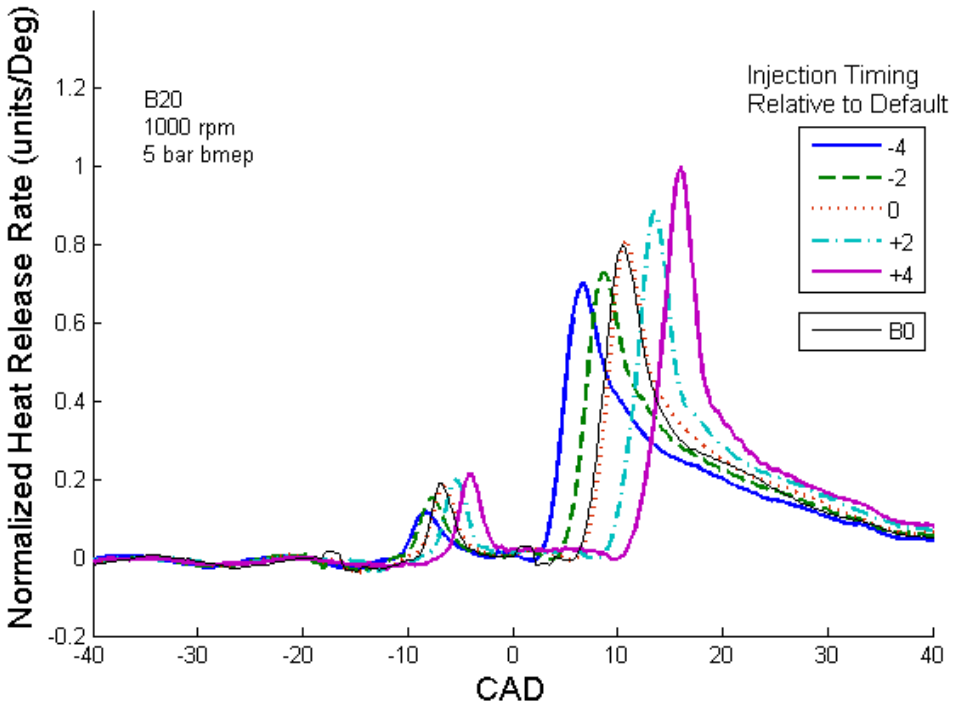


Figure 4.4: Effect of injection timing on apparent heat release rate

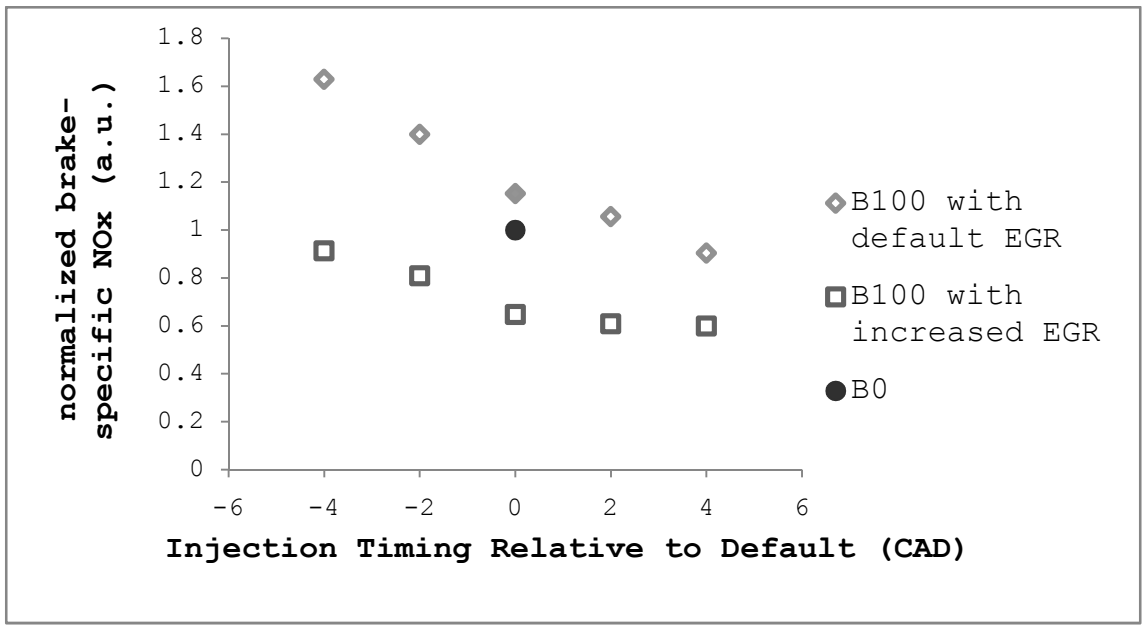


Figure 4.5: Normalized brake-specific NOx emissions for B100 at 1500 rpm, 3 bar bmep with different EGR ratios and injection timings

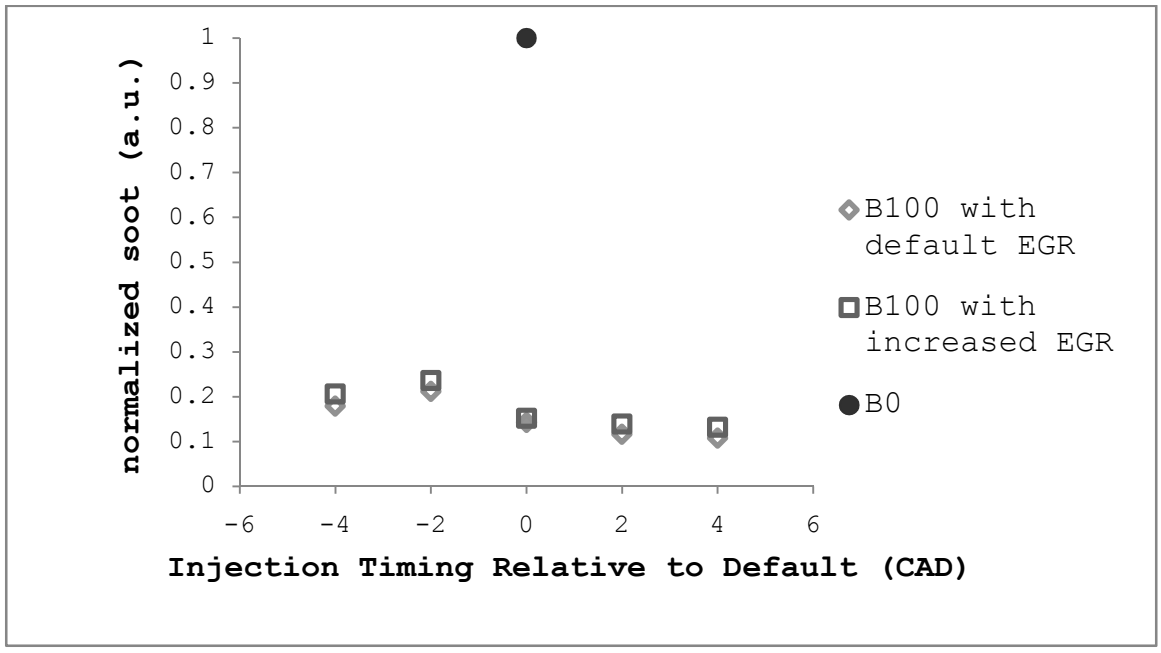


Figure 4.6: Relative soot concentrations for B100 at 1500 rpm, 3 bar bmep with different EGR ratios and injection timings

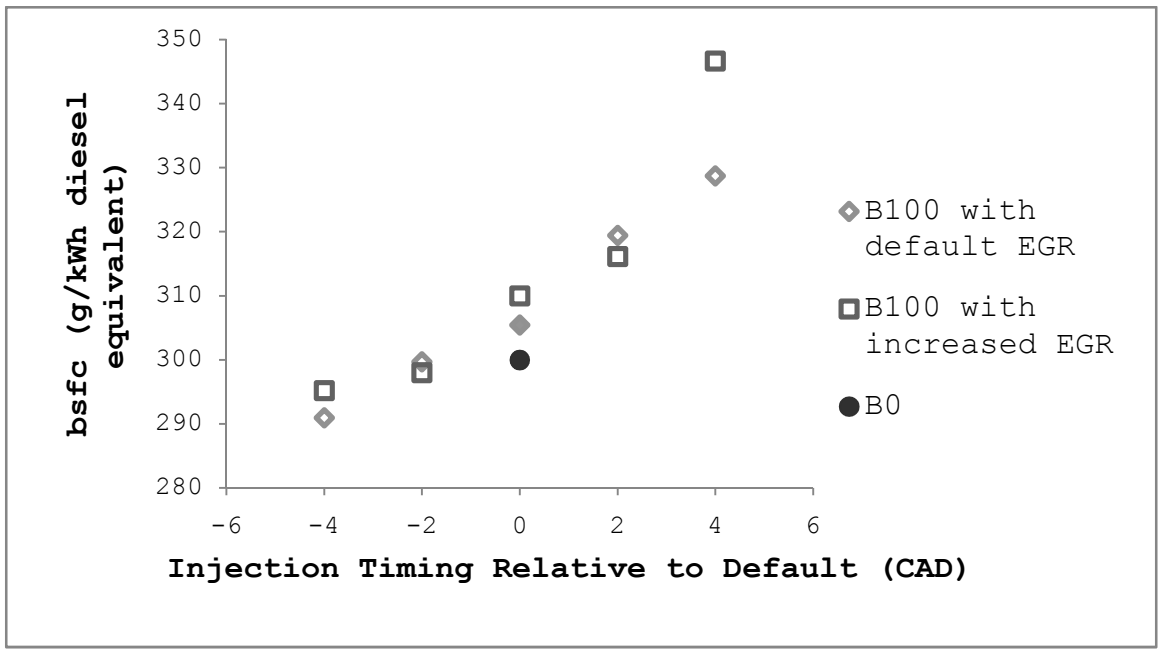


Figure 4.7: Brake-specific fuel consumption for B100 at 1500 rpm, 3 bar bmep with different EGR ratios and injection timings (corrected to account for the difference in heating value)

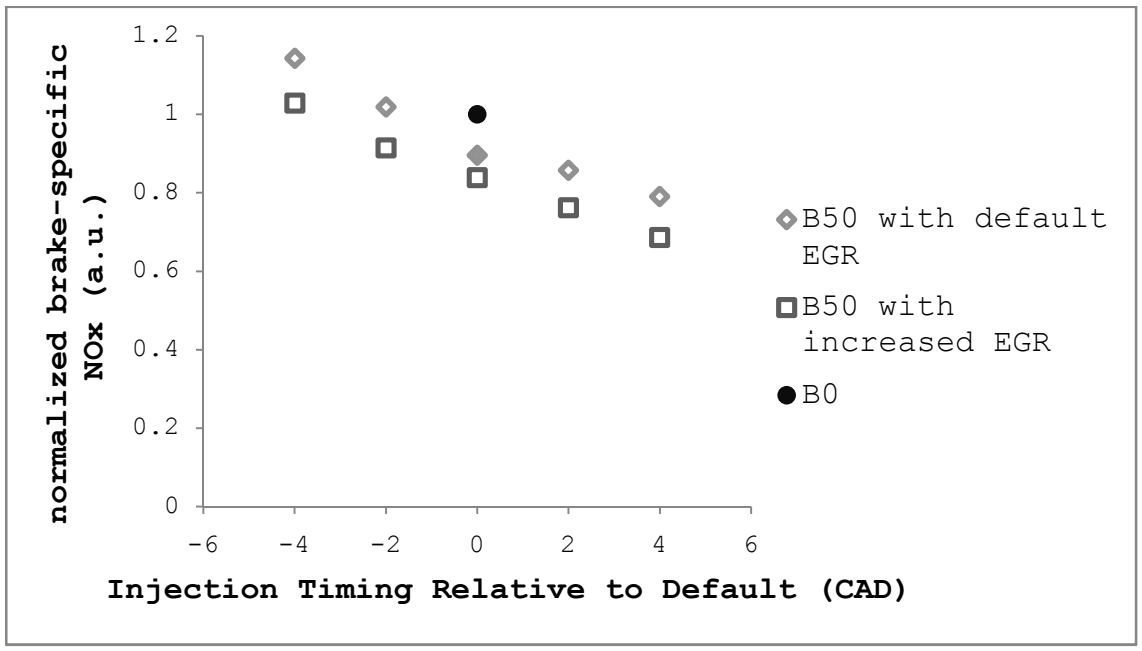


Figure 4.8: Normalized brake-specific NOx emissions for B50 at 1500 rpm, 3 bar bmep with different EGR ratios and injection timings

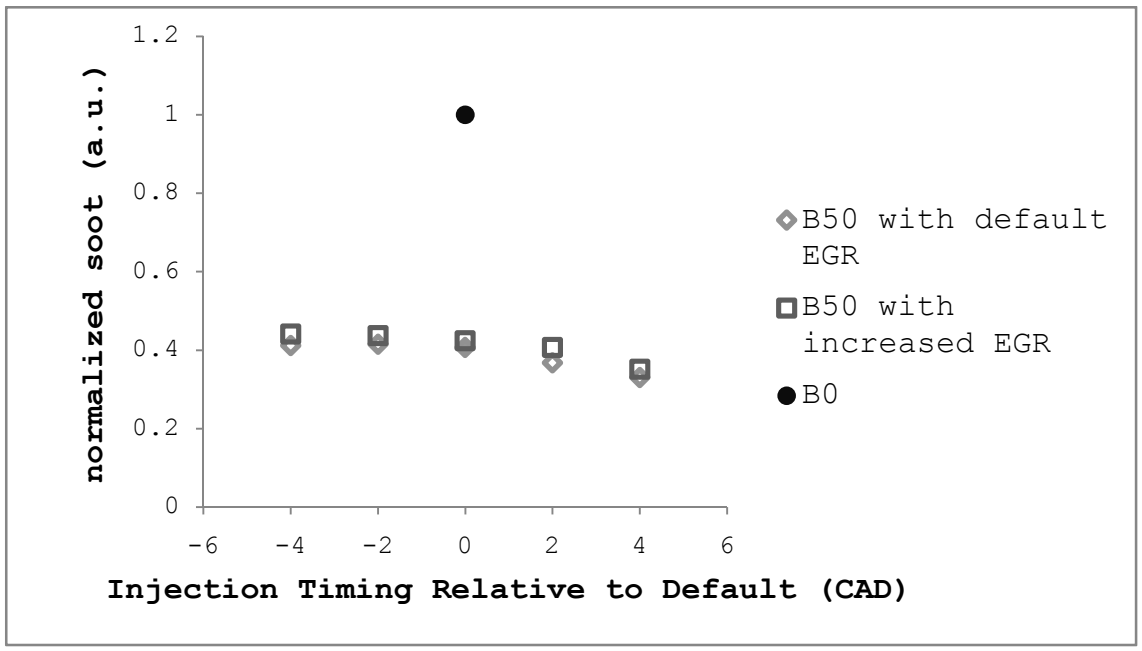


Figure 4.9: Relative soot concentrations for B50 at 1500 rpm, 3 bar bmep with different EGR ratios and injection timings

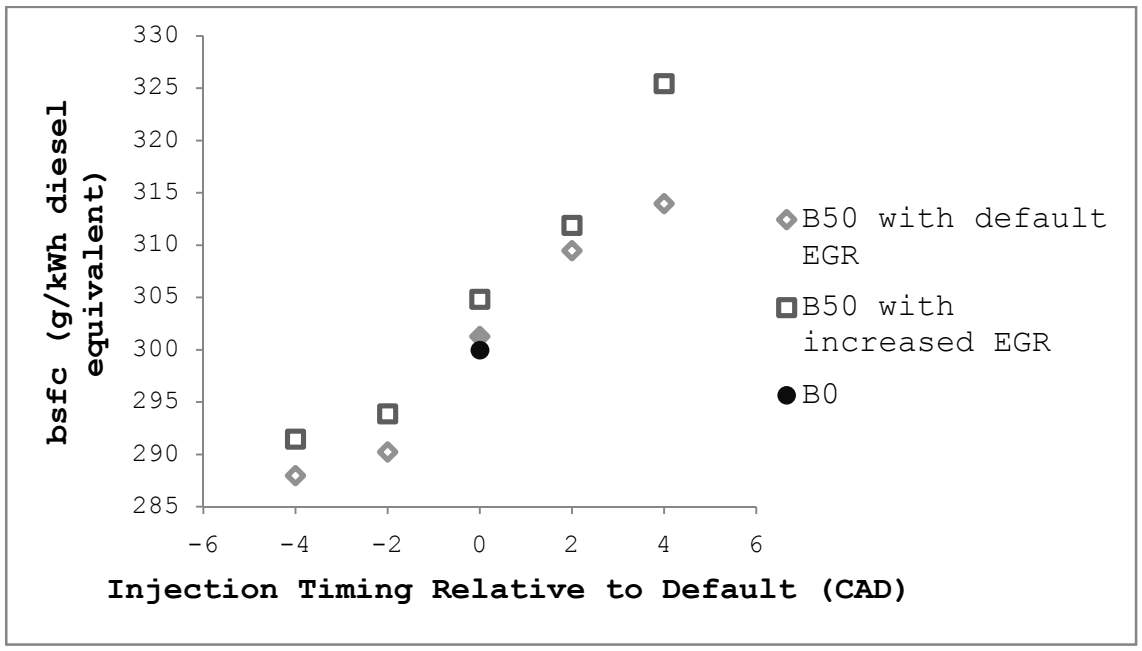


Figure 4.10: Brake-specific fuel consumption for B50 at 1500 rpm, 3 bar bmep with different EGR ratios and injection timings (corrected to account for the difference in heating value)

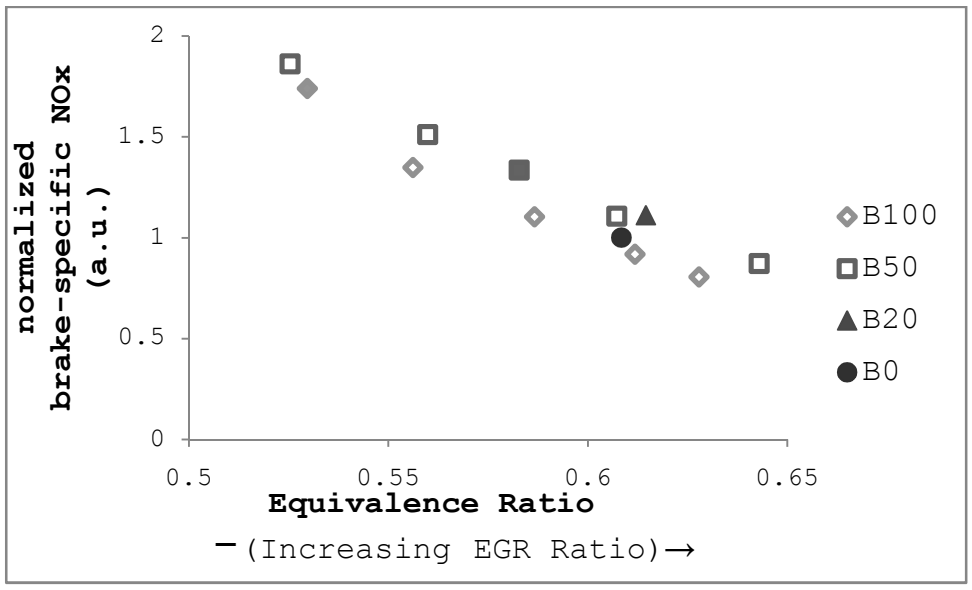


Figure 4.11: Effect of air-fuel ratio adjustment on NOx emissions at 1500 rpm, 5 bar bmep

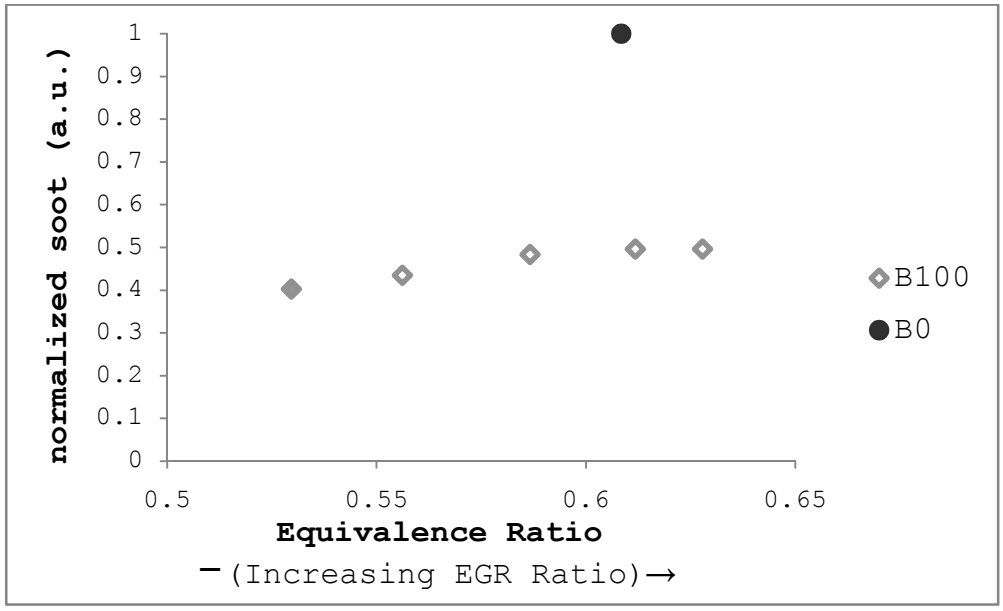


Figure 4.12: Relative soot concentrations for biodiesel and diesel at 1500 rpm, 5 bar bmep

4.2 Low Temperature Combustion Study

4.2.1 In-Cylinder Pressure and Apparent Heat Release Rate

To gain some insight on the type of combustion resulting in low emissions, in-cylinder pressure and apparent heat release rate plots are shown for all results (see Figures 4.13 through 4.32). Not every figure will be explained here, but the general ideas will be covered. Beginning with Figures 4.13 and 4.14, for 2 bar bmep, it can be seen that lower intake oxygen (higher EGR) results in later heat release. Since the injection timing is held constant in these cases, this means a longer ignition delay, allowing more time for more mixing prior to the start of combustion. However, all heat release rate curves here appear to indicate premixed-dominated combustion. A slight difference is that for high EGR, the initial rise in heat release rate seems to occur more gradually. The heat release rate then generally achieves a higher peak and finally drops off more sharply. Similar trends are seen for 3 bar bmep using the default injection strategy. However the soot continues to increase with EGR ratio and does not drop off as it does for 2 bar bmep. This observation holds true for the remainder of the speed and load conditions tested. A possible explanation is that due to the higher amount of fuel injected, diffusion combustion plays a larger role, allowing for more soot formation. By contrast, for the 2 bar bmep case, low temperature combustion appears to have been reached for the case with high EGR. Figures 4.17 and 4.18 show some of the attempts to achieve low temperature combustion at 3 bar bmep. The early injection resulted in higher soot while the later injection resulted in lower soot. However, by delaying the injection to achieve lower soot, the combustion phasing is later than optimum, resulting in poor fuel efficiency. By contrast, injecting less fuel during the pre-injection seems to allow for lower temperature during the main injection and less soot without hurting combustion phasing drastically.

For the remainder of the cases (1000, 1500, and 2000 rpm at 5 bar bmep and 1000 rpm at 7 bar bmep) with the default injection strategy, diffusion combustion appears to become more apparent. For 1000 and 1500 rpm at 5 bar bmep, the increase in EGR seems to have minimal effect on the heat release rate. Meanwhile, for 2000 rpm at 5 bar bmep, increasing the EGR appears to cause a transition from premixed-dominated with mixing-controlled combustion to mixing-controlled dominated combustion with premixed combustion. In any case, the injection scheme was modified by reducing the fraction of fuel injected during the pre-injection and shifting the injection timing later in the cycle, both meant to provide for lower in-cylinder temperatures. As seen in Figures 4.22, 4.28, and 4.32, this results in a premixed-dominated combustion, occurring later in the cycle.

4.2.2 Ignition Delay Trends

Analysis of the heat release rate plots can be used to obtain the crank angle at the start of combustion. Though a couple different definitions are used, the start of combustion here will be defined as the location where minimum heat release occurs prior to positive heat release after fuel injection. In diesel engines, the heat release rate generally dips after fuel injection, reflecting the energy utilized in vaporizing the fuel. Once the combustion chemistry releases enough energy to overcome the energy losses, the heat release rate will reach a minimum. Thus, the point of minimum heat release rate is a good indicator that combustion chemistry has commenced. The heat release rate data were analyzed in this way, and knowing the start of injection from the ECM, the ignition delay was calculated. Figure 4.33 shows the ignition delay results for the range of cases studied. Two values are shown for the default injection strategy, a minimum ignition delay corresponding to the case with no EGR, and a maximum ignition delay

corresponding to a case with high EGR. The ignition delay for the modified injection case resulting in low temperature combustion is also shown. The ignition delay for low temperature combustion is typically on the higher end of the range of values for a given speed and load, and in some instances, it is higher. Not too much can be inferred from these results, but it makes sense that low temperature combustion should have rather long ignition delays due to the high rates of EGR generally required for the reduction in NOx emissions. To be clear, a long ignition delay in itself does not indicate low temperature combustion, as several of the conventional combustion cases exhibited ignition delays of comparable length to the low temperature combustion case for the particular speed and load.

4.2.3 Cycle-to-Cycle Variation

Each in-cylinder pressure curve plotted in previous sections is an ensemble average of 30 cycles of data for that operating condition. While this removes pressure fluctuation and noise, it also obscures some important information. For low temperature combustion in particular, cycle-to-cycle variation is often a concern because of the high rates of EGR generally employed. Depending on the inlet air system design, the recirculated exhaust gases may not mix evenly from cycle to cycle. As described in previous sections, the rate of EGR tends to affect the ignition delay and combustion phasing, so uneven EGR from cycle to cycle can cause variations in the combustion timing, resulting in uneven engine operation. In fact, cylinder-to-cylinder variation is another potential problem with high rates of EGR, as the geometry of the intake manifold may cause certain cylinders to receive more or less than the desired amount of EGR. Only one in-cylinder pressure transducer was available for this study, so cylinder-to-cylinder variations cannot be accounted for.

To qualitatively look at cycle-to-cycle variation, ten random individual cycles were plotted both for the case of no EGR and for the low temperature combustion obtained through modified injection strategies. Figures 4.34 and 4.35 show the results for the case of 2 bar nominal bmep, while Figures 4.36 and 4.37 show the results for the case of 7 bar nominal bmep. In both cases, the low temperature combustion scheme is seen to result in more cycle-to-cycle variation, particularly in the point at which in-cylinder pressure begins to rise again after top dead center. For the 2 bar nominal bmep case, the difference here translates into a shift in the overall pressure curve. Meanwhile, for the 7 bar nominal bmep case, the differences here seem to be balanced somewhat by different rates of pressure rise, leaving the second peak of in-cylinder pressure relatively stable. Qualitatively, the engine sounded stable at all points included in this study. Conditions which caused the engine to operate in a noticeably uneven manner were deemed undesirable and discarded.

4.2.4 Emissions and Fuel Consumption Trends versus EGR Ratio

Figures 4.38 through 4.41 show the emissions and fuel consumption trends obtained for the various speed and load conditions with the ECM default injection settings and different rates of EGR. As described in the experimental methodology, the mass-based EGR ratio was calculated based on the CO_2 content of the mixed intake air and exhaust. All emissions measurements have been normalized based on the highest data point obtained. Fuel consumption measurements have been adjusted to show the g/kWh measurement expected if biodiesel had the same heating value as diesel, which allows for better comparison to previous results.

Brake-specific NOx emissions, as seen in Figure 4.38, initially decrease quite sharply with increasing EGR ratio, but the slope continually becomes shallower until at higher EGR

ratios, the decrease in NOx for a given increase in EGR is minimal. The different speed and load conditions seem to follow a similar curve, showing similar dependence of NOx on EGR.

Soot emissions do not follow such a clear trend, as seen in Figure 4.39. At one condition (1000 rpm & 2 bar bmep), the soot was found to increase slightly with EGR at first, before dropping back down in what is thought to correspond to achievement of low temperature combustion. For all other cases, the soot was seen to only increase with EGR ratio, though at different rates. Tests run at higher load conditions typically showed higher soot levels at a given EGR ratio. It should be noted that these soot results are filter smoke number data normalized based on the highest measurement. Therefore, the flow rate of exhaust gases and the power output of the engine are not considered. If mass-based soot measurements were taken, brake-specific soot emissions could be calculated, which might provide better insight.

Fuel consumption is seen to increase gradually with increasing EGR up to a certain level, as seen in Figure 4.40. Beyond this level, further increase in EGR is seen to increase fuel consumption more significantly. This occurs somewhere around 40 or 50%, depending on engine operating conditions. Fuel consumption is seen to be highest for low-load conditions and decrease with increasing load as friction losses become a smaller portion of the overall energy released.

Brake-specific CO emissions are quite small with low EGR, as seen in Figure 4.41. At a certain point, corresponding approximately to the previously mentioned increase in fuel consumption, CO emissions are seen to increase quite rapidly. This relationship is expected, as presence of significant CO emissions is indicative of incomplete combustion. This illustrates how CO emissions, though normally minimal in a modern diesel engine, especially when fueled with biodiesel, can become problematic at high rates of EGR.

4.2.5 Modification to Injection Scheme

As discussed in the literature review, NOx and soot have been the most problematic emissions for typical diesel engines due to a tradeoff between the two; strategies that decrease one pollutant typically increase the other. Indeed, this phenomenon was seen in the previously-described results. When using the default injection settings, the only case where this did not hold was 1000 rpm & 2 bar bmep, where the simultaneous reduction of NOx and soot consistent with low temperature combustion was seen (see Figure 4.42). For the remainder of the operating conditions, further work clearly needs to be done to achieve simultaneous reduction of NOx and soot. For this reason, cases were run with injection strategies focused on providing lower in-cylinder temperature during the main injection. The amount of fuel injected during the pre-injection was considered in addition to different injection timings.

Figures 4.42 through 4.47 illustrate the soot-NOx tradeoff at different engine speed and load conditions and the efforts made to simultaneously reduce both emissions. As previously mentioned, at 1000 rpm & 2 bar bmep, simultaneous reduction of NOx and soot was seen by operating with a high level of EGR. Initially, the soot increases slightly as NOx decreases, but it eventually drops by about 40% to a level below the case with no EGR. This eventual drop in soot is never realized for the remainder of speed and load conditions with the default injection settings, as seen in Figures 4.43 through 4.47. At 3 bar bmep, as seen in Figure 4.43, the influence of injection timing was first observed by advancing and retarding the start of injection by 2.5 degrees with EGR held constant around 50%. The early injection was found to produce more soot, while the late injection produced significantly less. On the downside, the late injection resulted in poor combustion phasing, ultimately hurting fuel efficiency. On the other

hand, reducing the pre-injection to a minimum produced a similar reduction in soot, but with better combustion phasing, resulting in better fuel efficiency. It is worth noting that during these tests, changes to the injection scheme were seen to have only small effects on NOx emissions, as this pollutant was kept minimal due to high levels of EGR. This held true for all speed and load conditions tested. However, as discussed in the conventional combustion study, injection timing does generally affect NOx emissions.

For the remaining speed and load conditions, reduction of soot using only a smaller pre-injection was found to be inadequate. A combination of small pre-injection and later injection timings had to be utilized. The cases run at 5 bar bmep with different engine speed (1000, 1500, and 2000 rpm) all produced similar results, as seen in Figures 4.44, 4.46, and 4.47. Note that in these cases, the soot was still slightly higher in terms of filter smoke number than the case with no EGR. However, given that the exhaust flow rate was reduced by 35 to 40% through the use of high EGR, results in terms of overall soot mass would be more favorable. The same goes for the case of 1000 rpm & 7 bar bmep (Figure 4.45). At this operating condition, cases of high EGR with the default injection strategy were avoided because very high levels of soot were observed.

As discussed in the explanation of in-cylinder pressure and apparent heat release rate data above, the combustion phasing was generally later than desirable for the low-emission cases with modified injection strategies. This came from a need to delay injection timings and inject into a cooler in-cylinder temperature to reduce the amount of soot emitted by the engine. The effect on fuel consumption varied in magnitude from case to case, but there was a general increase in fuel consumption associated with the reduction in emissions. Figure 4.48 illustrates this point, showing the best-case fuel consumption achieved with the default injection strategy (obtained

using no EGR), the worst-case fuel consumption achieved with the default injection strategy (obtained by using a high EGR ratio), and the fuel consumption achieved for the low-emission case with modified injection strategy. In select cases, the fuel consumption for the cases with modified injection strategy were at similar or lower levels compared with the fuel consumption for the high EGR cases (1000 rpm & 3 bar bmep, 2000 rpm & 5 bar bmep). The remainder of the cases saw slight increases in fuel consumption over the high EGR default injection cases. The trends in fuel consumption across speed and load conditions for the low-emission cases appear similar to the default cases, just offset to higher values.

Ultimately, the data explained above indicate that for biodiesel, control of NOx to very low levels can be accomplished through high rates of EGR. However, an increase in fuel consumption generally accompanies this increase in EGR. With the NOx under control, reduction of soot is another obstacle. In this study, soot was controlled by adjusting pre-injection quantity and injection timing for each case. Combustion phasing suffered in many cases as a result of these adjustments. For most cases, this meant another small increase in fuel consumption, though some cases were achieved with similar or slightly lower fuel consumption. Overall, though, a tradeoff between soot and fuel consumption was seen when adjusting these injection parameters under constant EGR.

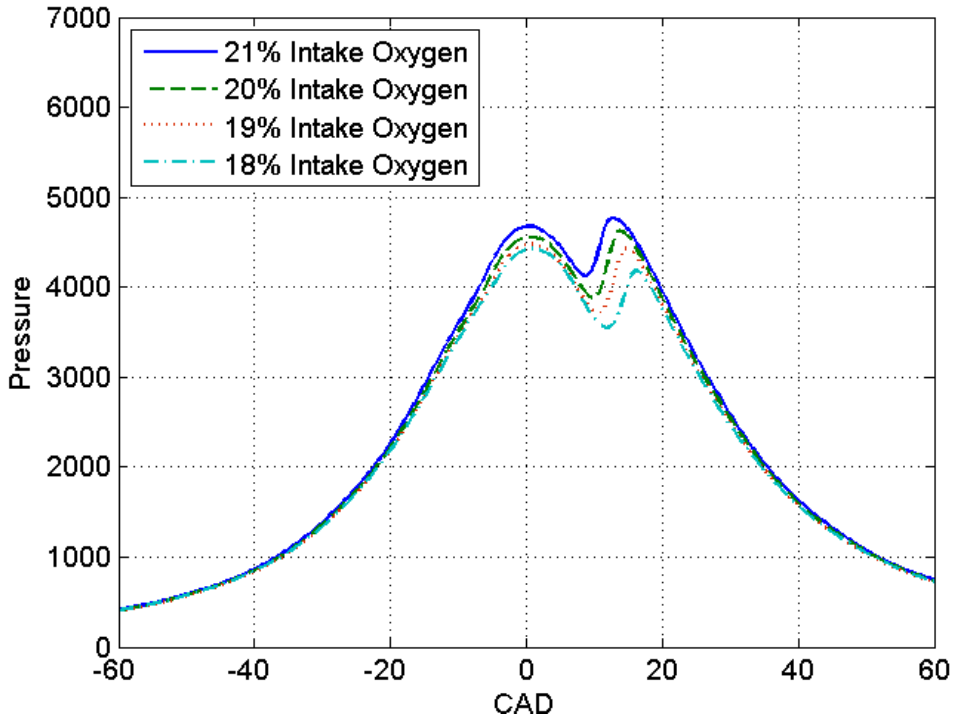


Figure 4.13: In-cylinder pressure versus crank angle for 1000 rpm & 2 bar initial bmep using default injection strategy

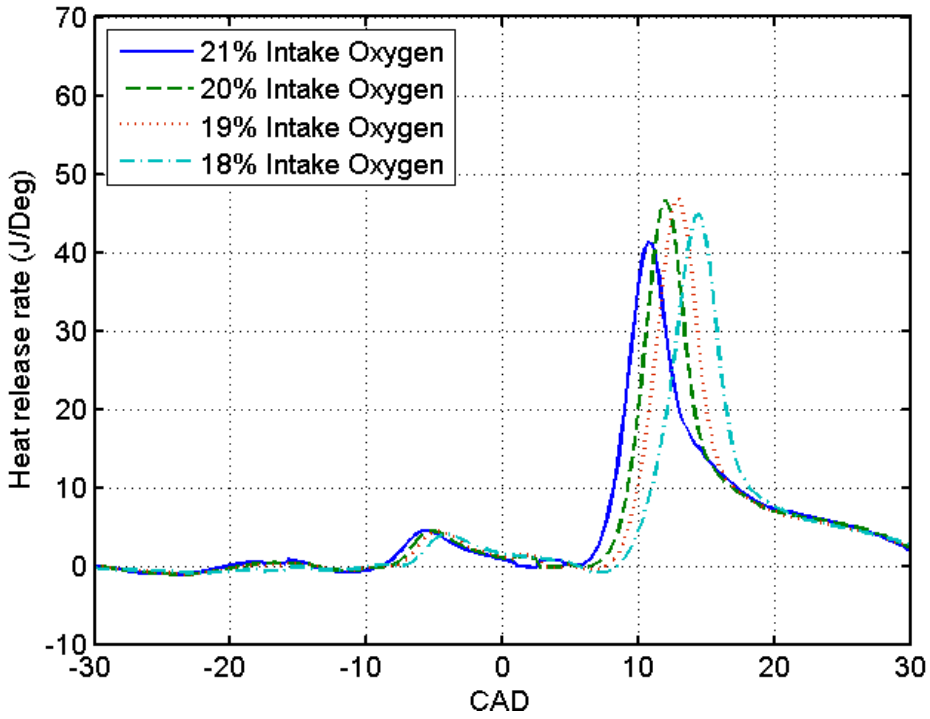


Figure 4.14: Apparent heat release rate versus crank angle for 1000 rpm & 2 bar initial bmep using default injection strategy

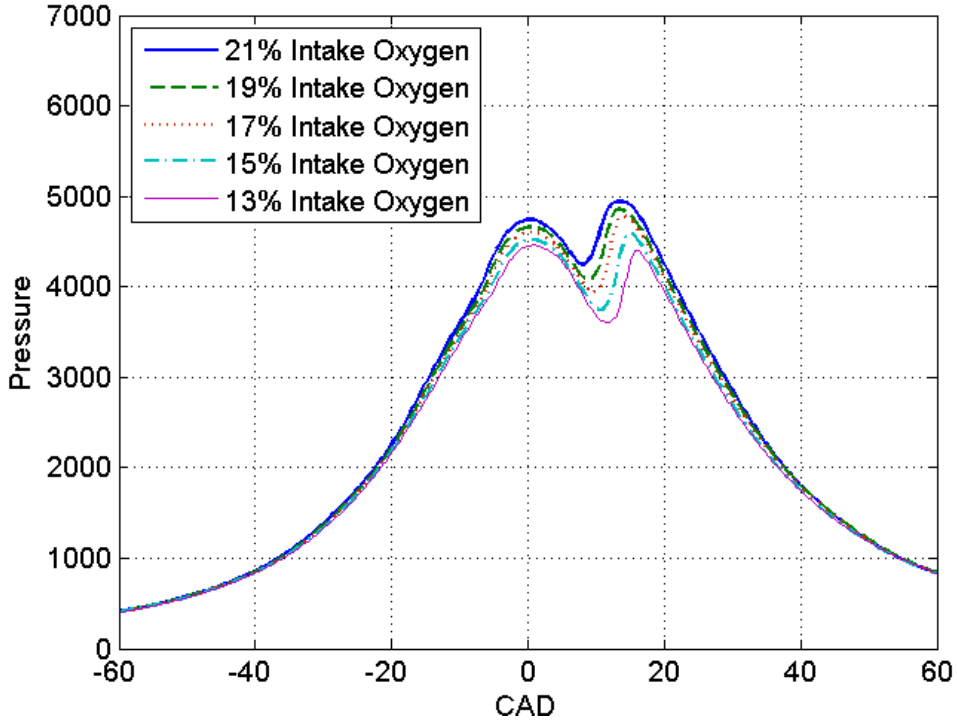


Figure 4.15: In-cylinder pressure versus crank angle for 1000 rpm & 3 bar initial bmep using default injection strategy

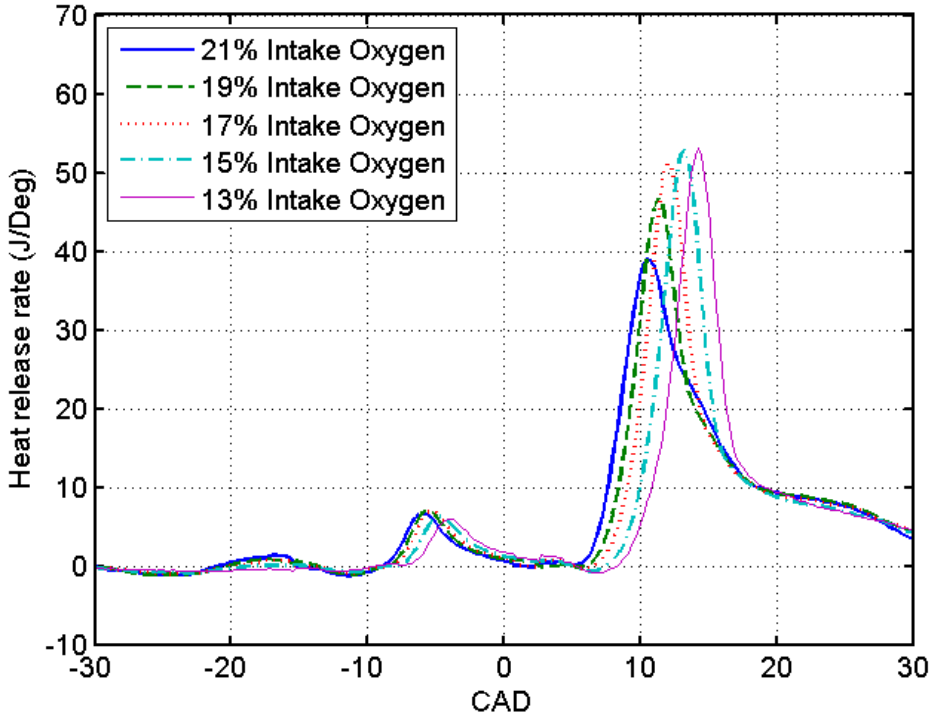


Figure 4.16: Apparent heat release rate versus crank angle for 1000 rpm & 3 bar initial bmep using default injection strategy

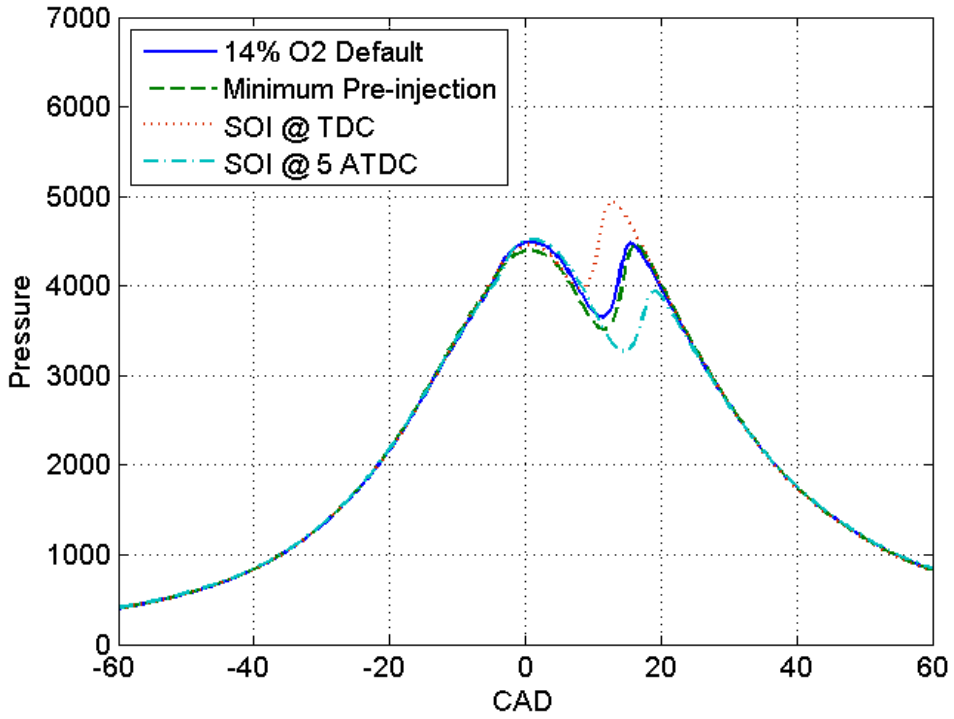


Figure 4.17: In-cylinder pressure versus crank angle for 1000 rpm & 3 bar initial bmep using modified injection strategy

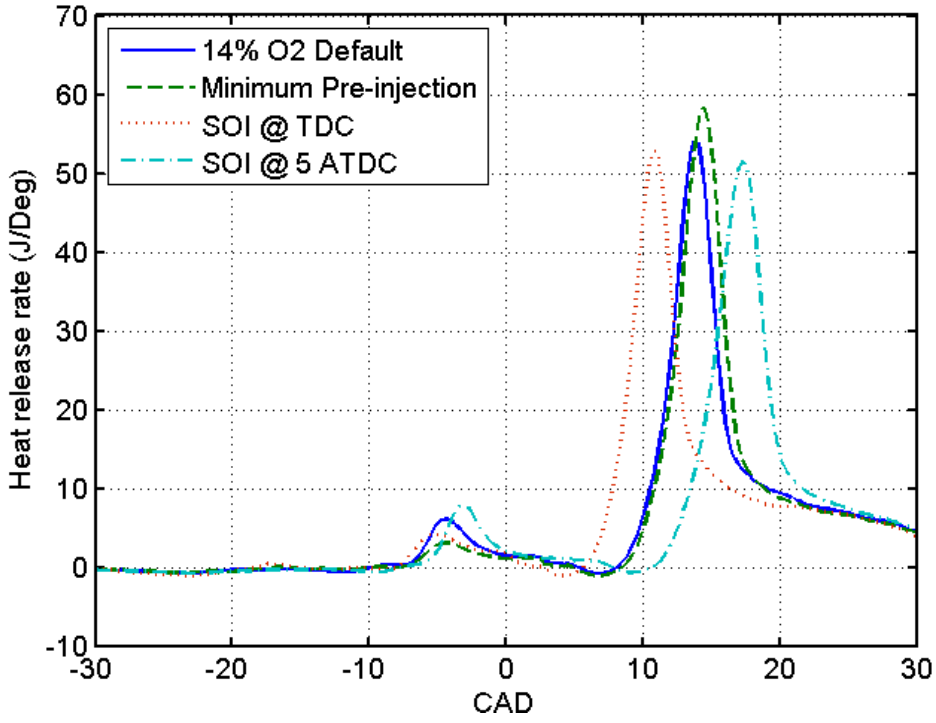


Figure 4.18: Apparent heat release rate versus crank angle for 1000 rpm & 3 bar initial bmep using modified injection strategy

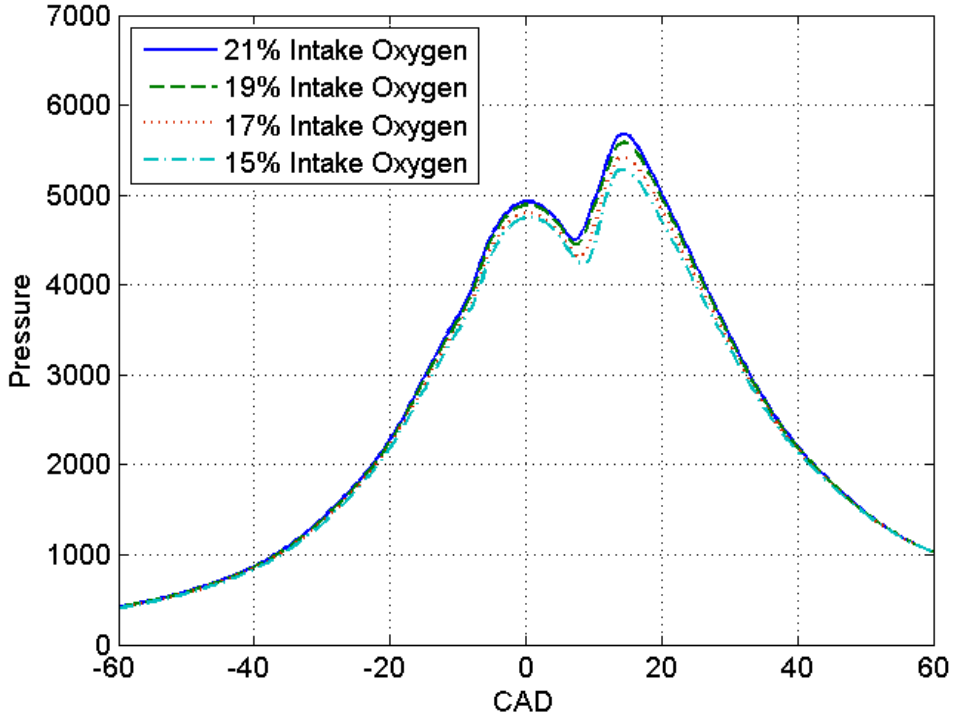


Figure 4.19: In-cylinder pressure versus crank angle for 1000 rpm & 5 bar initial bmep using default injection strategy

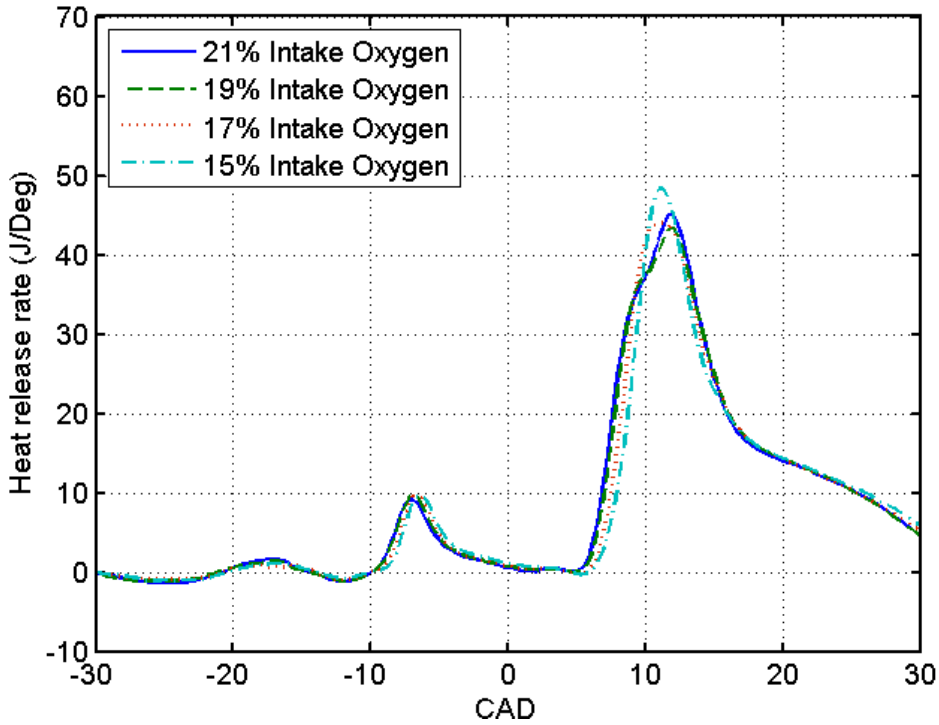


Figure 4.20: Apparent heat release rate versus crank angle for 1000 rpm & 5 bar initial bmep using default injection strategy

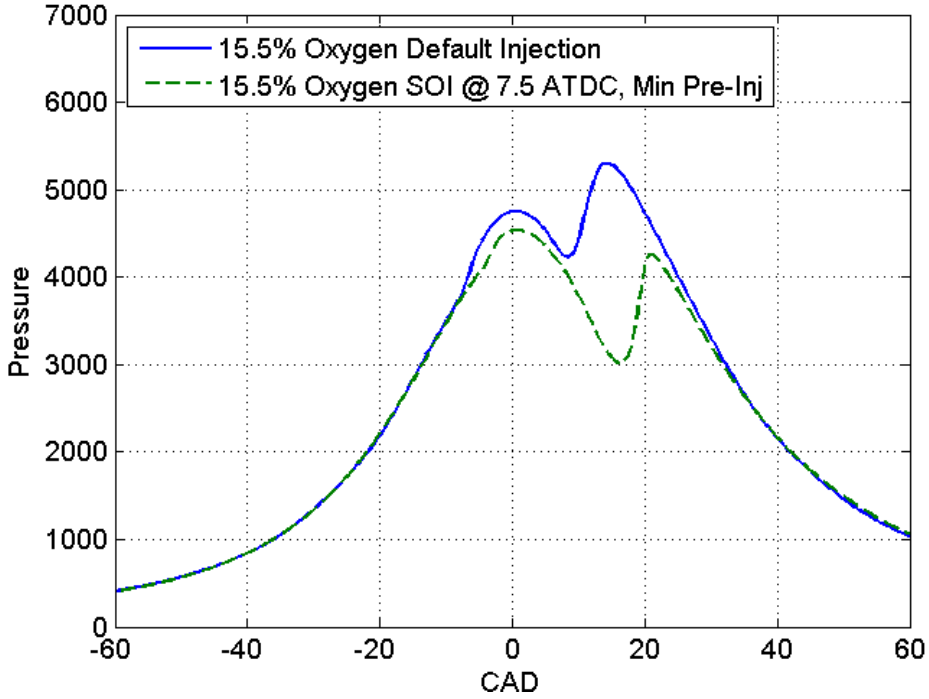


Figure 4.21: In-cylinder pressure versus crank angle for 1000 rpm & 5 bar initial bmep using modified injection strategy

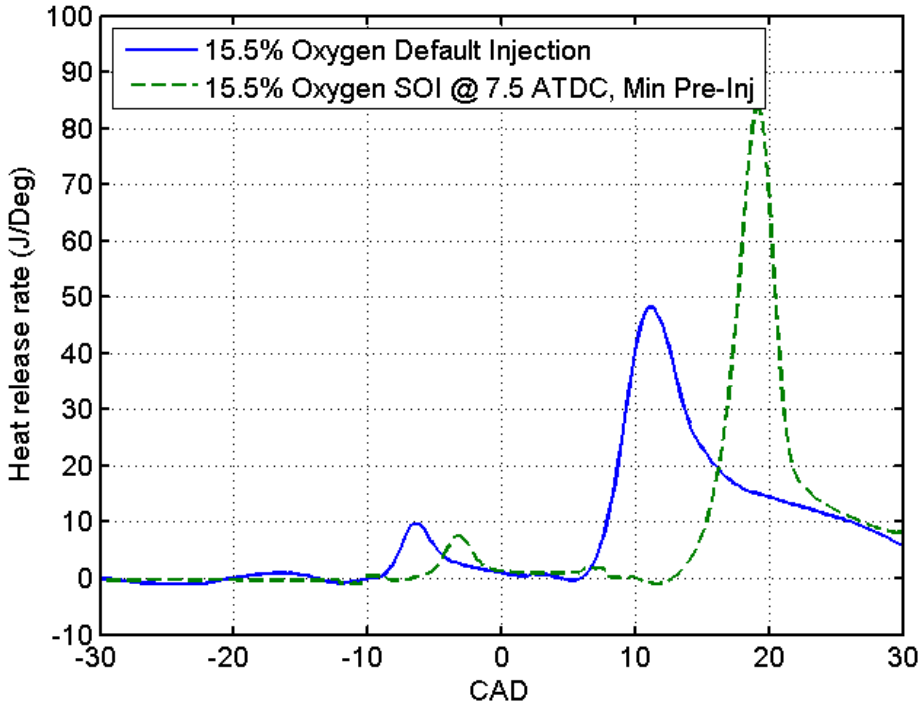


Figure 4.22: Apparent heat release rate versus crank angle for 1000 rpm & 5 bar initial bmep using modified injection strategy

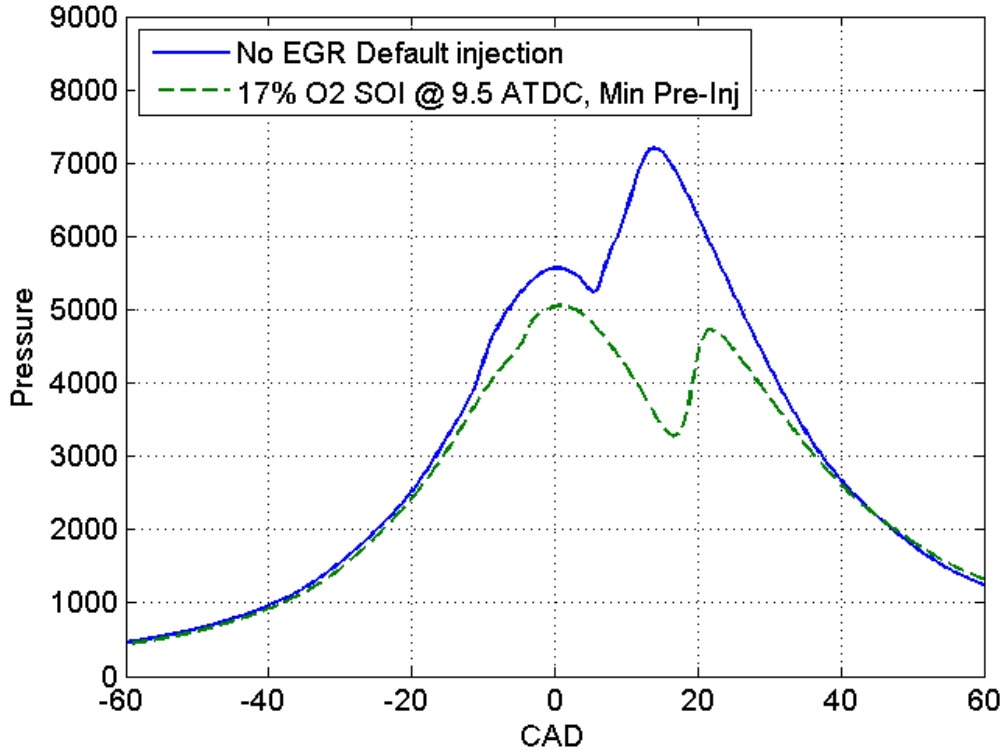


Figure 4.23: In-cylinder pressure versus crank angle for 1000 rpm & 7 bar initial bmep

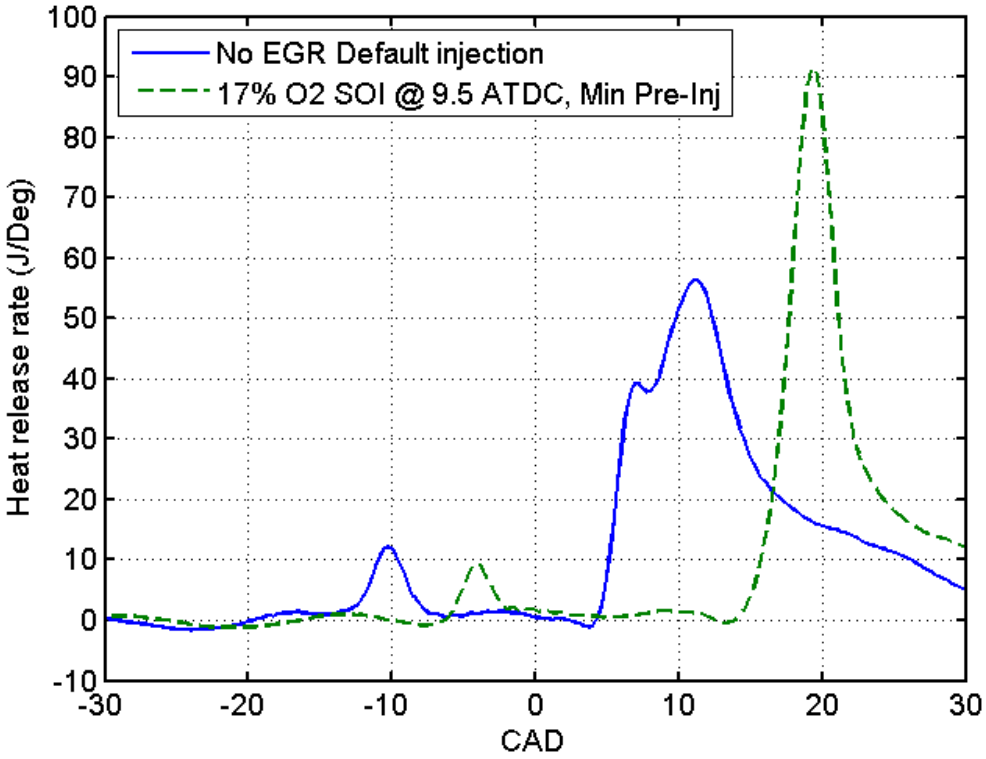


Figure 4.24: Apparent heat release rate versus crank angle for 1000 rpm & 7 bar initial bmep

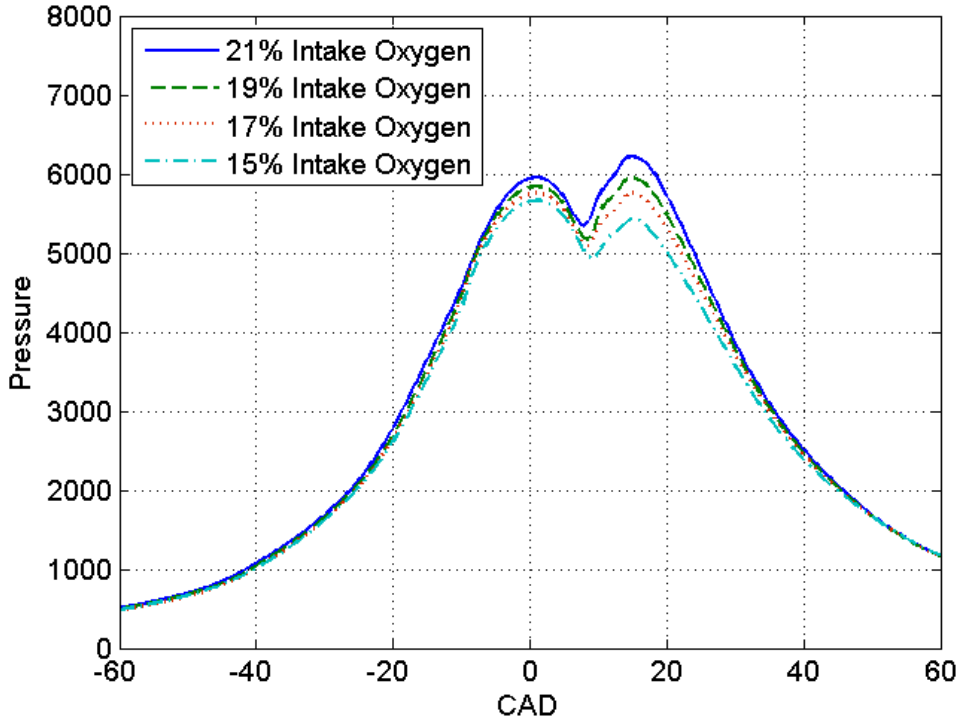


Figure 4.25: In-cylinder pressure versus crank angle for 1500 rpm & 5 bar initial bmep using default injection strategy

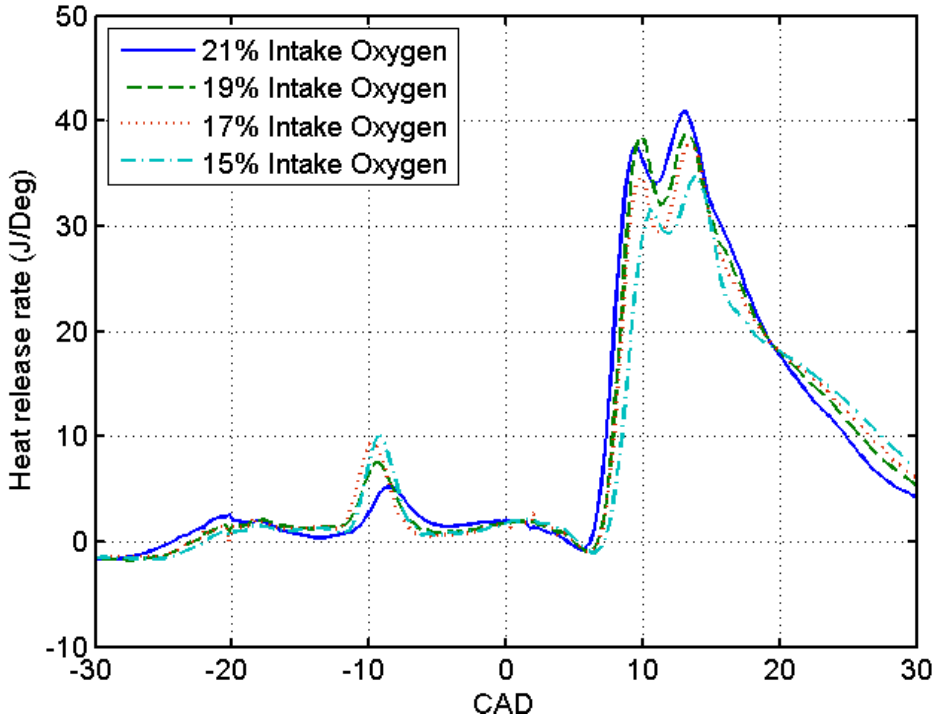


Figure 4.26: Apparent heat release rate versus crank angle for 1500 rpm & 5 bar initial bmep using default injection strategy

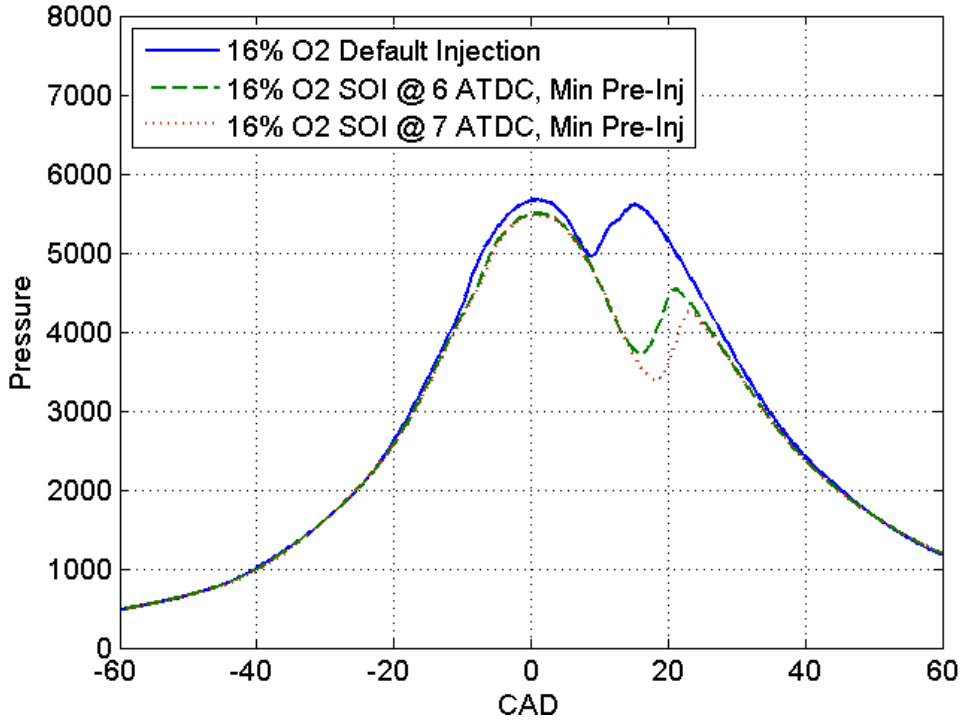


Figure 4.27: In-cylinder pressure versus crank angle for 1500 rpm & 5 bar initial bmep using modified injection strategy

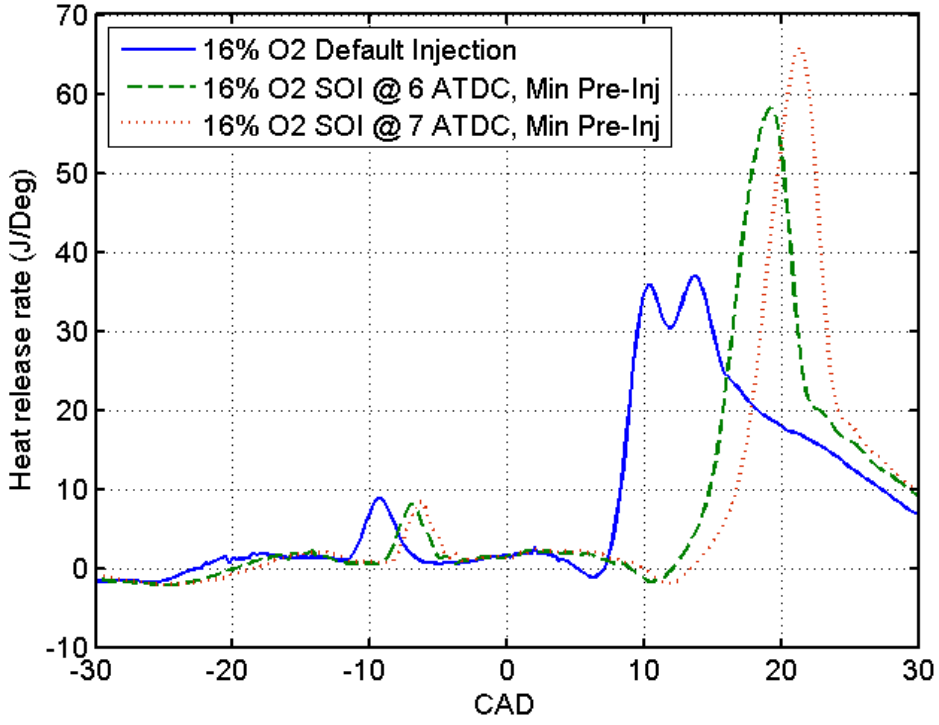


Figure 4.28: Apparent heat release rate versus crank angle for 1500 rpm & 5 bar initial bmep using modified injection strategy

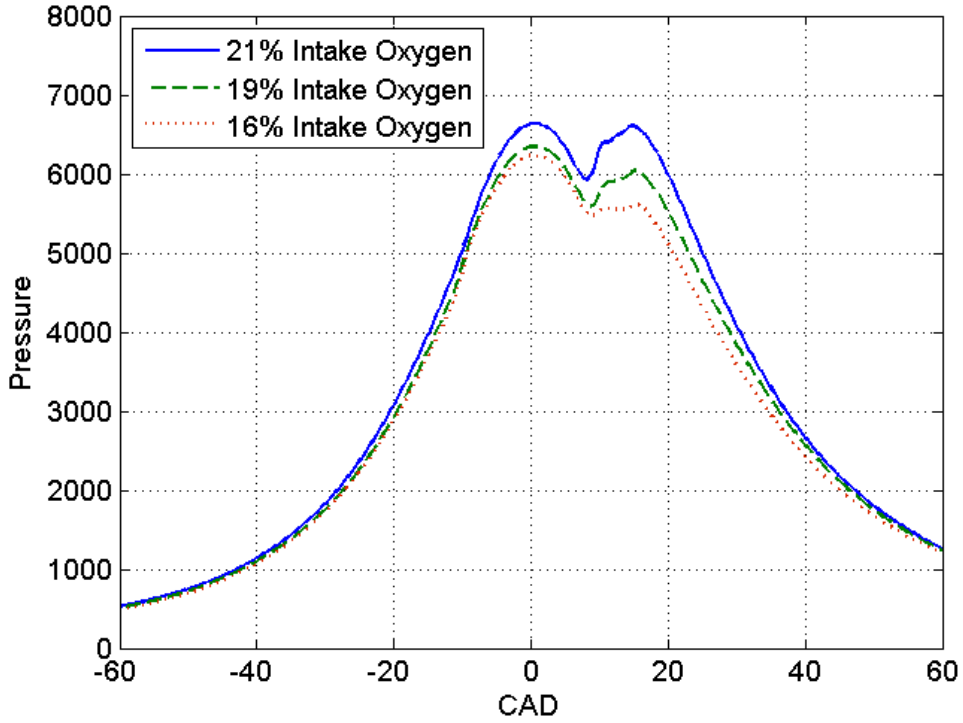


Figure 4.29: In-cylinder pressure versus crank angle for 2000 rpm & 5 bar initial bmep using default injection strategy

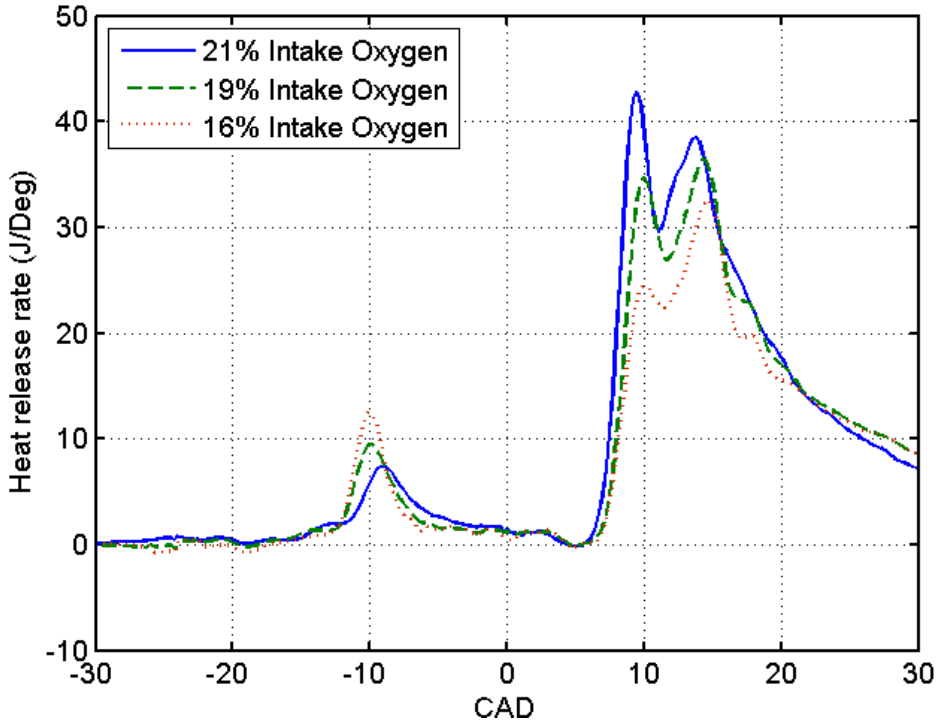


Figure 4.30: Apparent heat release rate versus crank angle for 2000 rpm & 5 bar initial bmep using default injection strategy

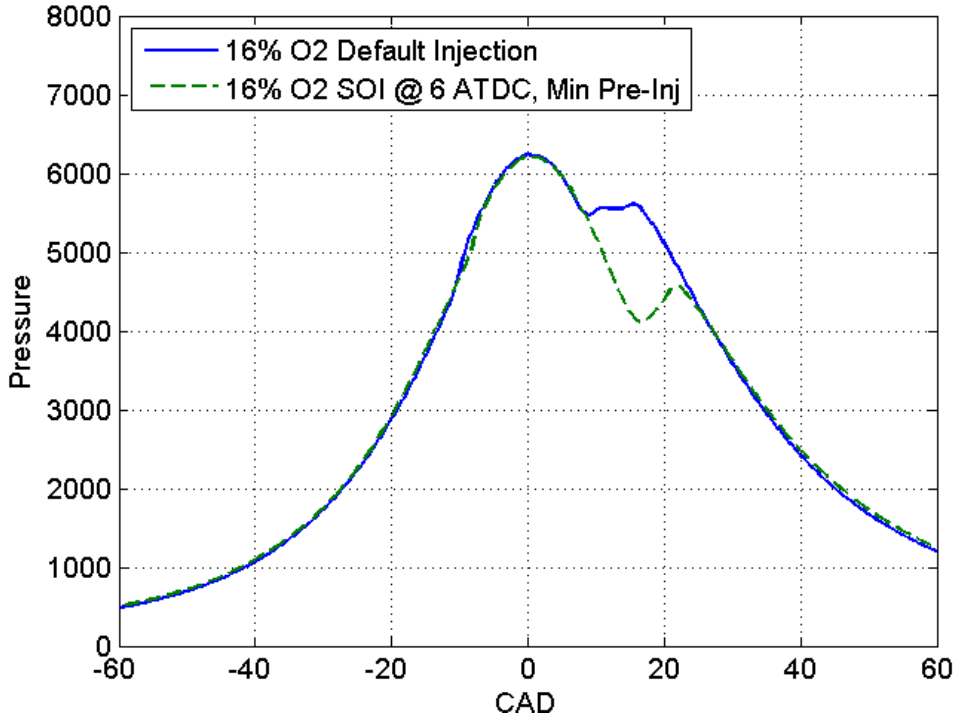


Figure 4.31: In-cylinder pressure versus crank angle for 2000 rpm & 5 bar initial bmep using modified injection strategy

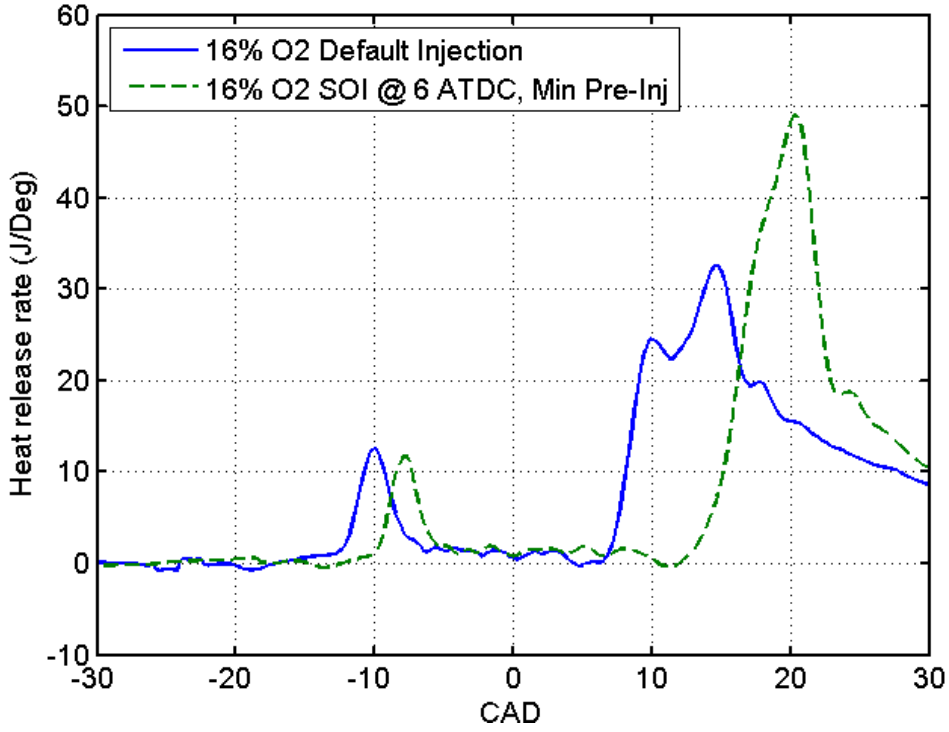


Figure 4.32: Apparent heat release rate versus crank angle for 2000 rpm & 5 bar initial bmep using modified injection strategy

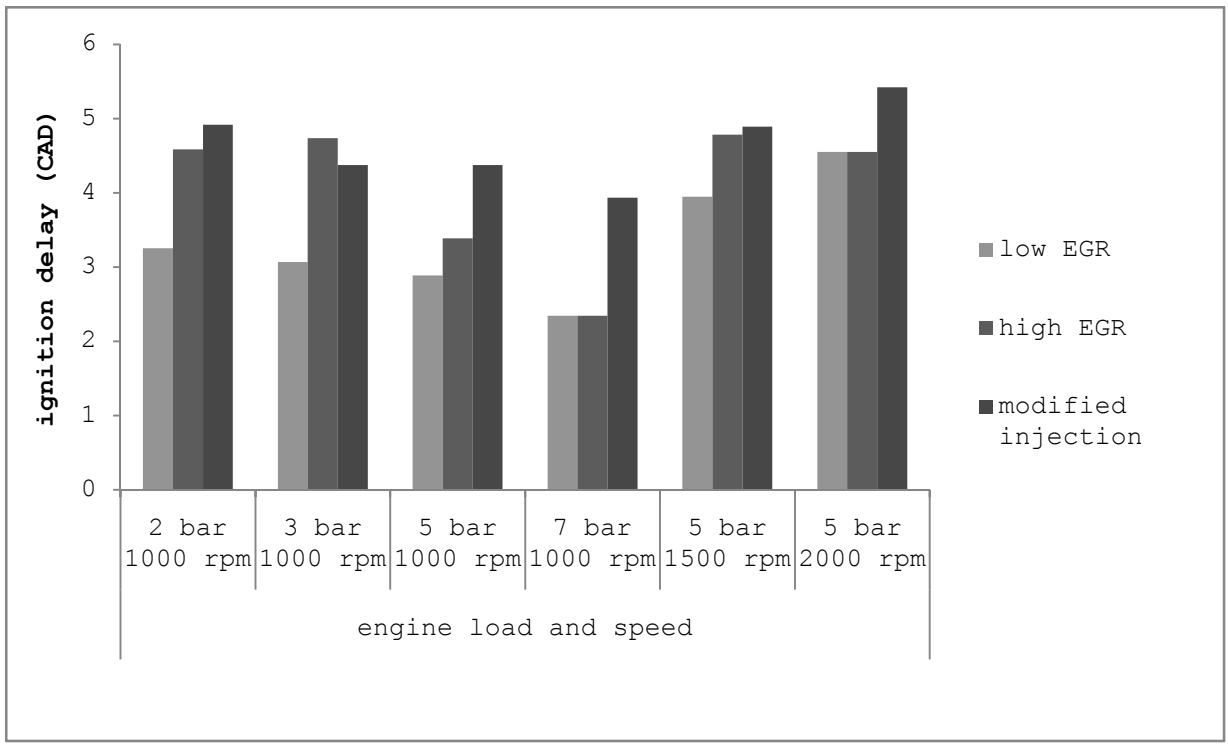


Figure 4.33: Ignition delay trends for the range of cases studied

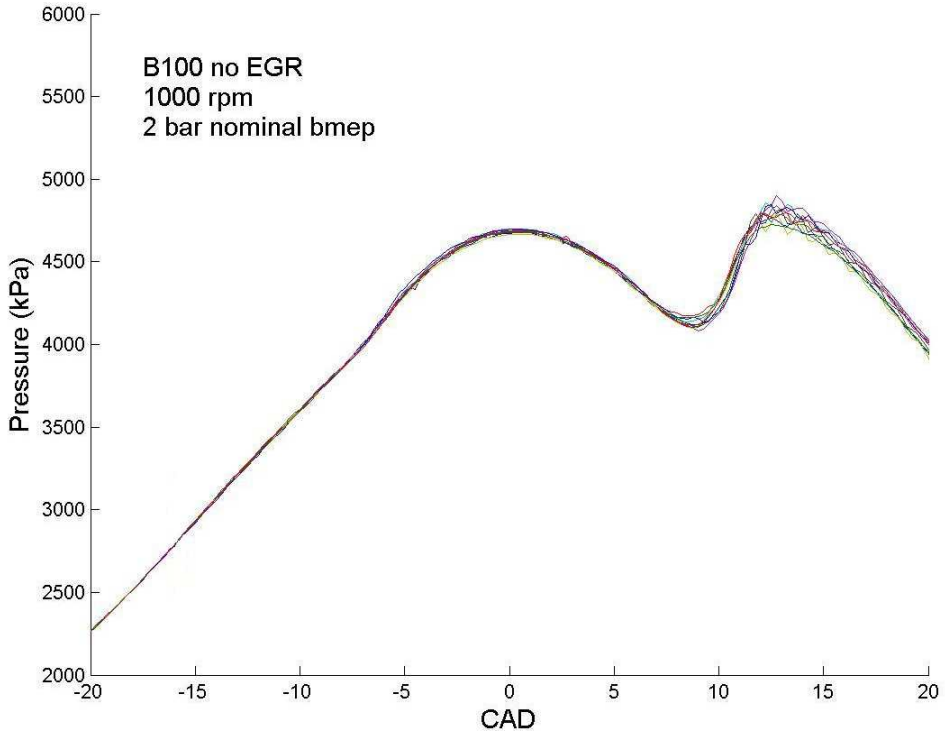


Figure 4.34: In-cylinder pressure data of ten individual cycles for qualitative analysis of cycle-to-cycle variation (default injection strategy with no EGR at 1000 rpm & 2 bar nominal bmep)

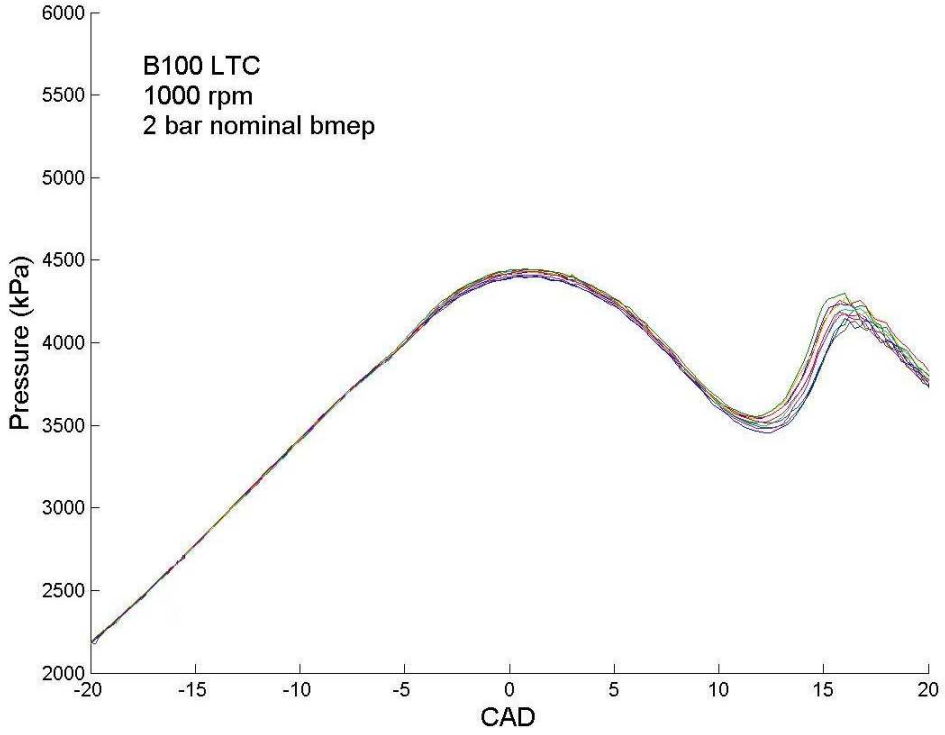


Figure 4.35: In-cylinder pressure data of ten individual cycles for qualitative analysis of cycle-to-cycle variation (modified injection strategy at 1000 rpm & 2 bar nominal bmep)

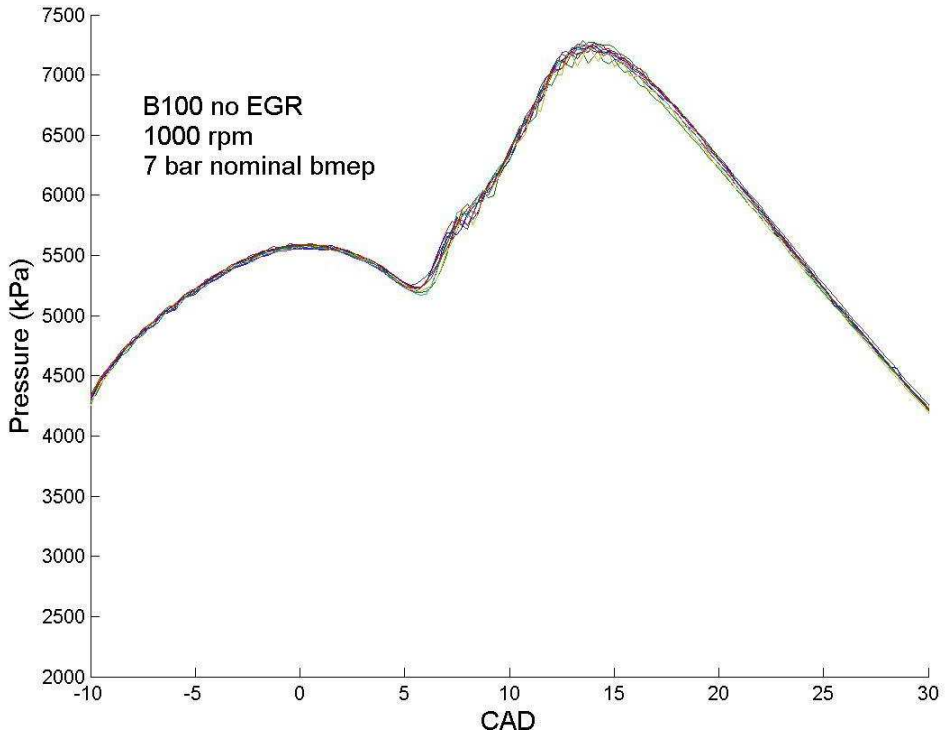


Figure 4.36: In-cylinder pressure data of ten individual cycles for qualitative analysis of cycle-to-cycle variation (default injection strategy with no EGR at 1000 rpm & 7 bar nominal bmep)

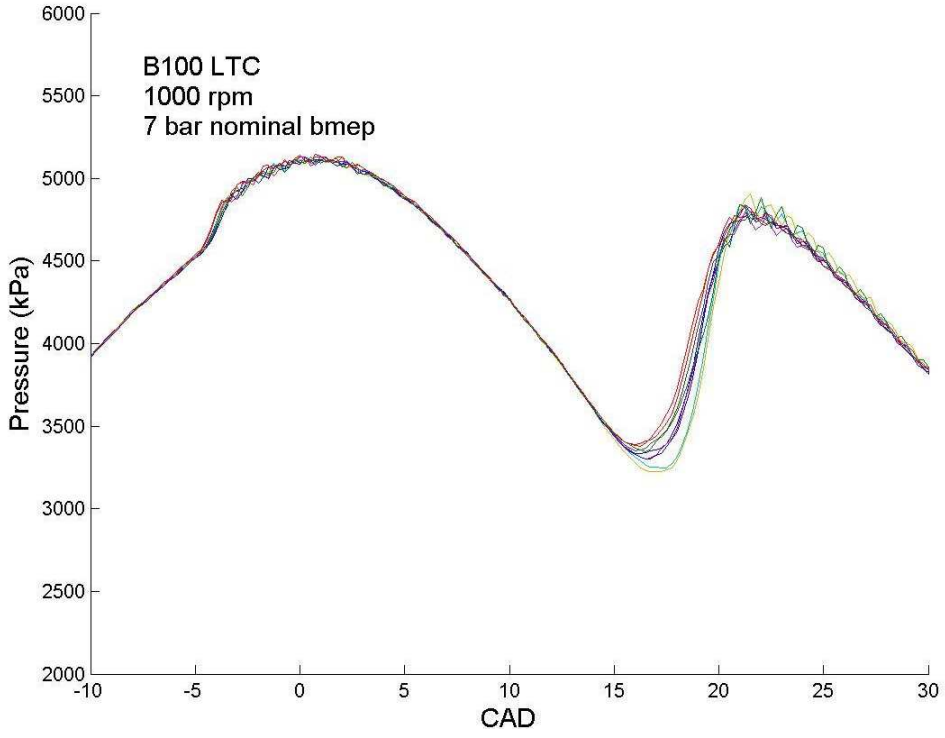


Figure 4.37: In-cylinder pressure data of ten individual cycles for qualitative analysis of cycle-to-cycle variation (modified injection strategy at 1000 rpm & 7 bar nominal bmep)

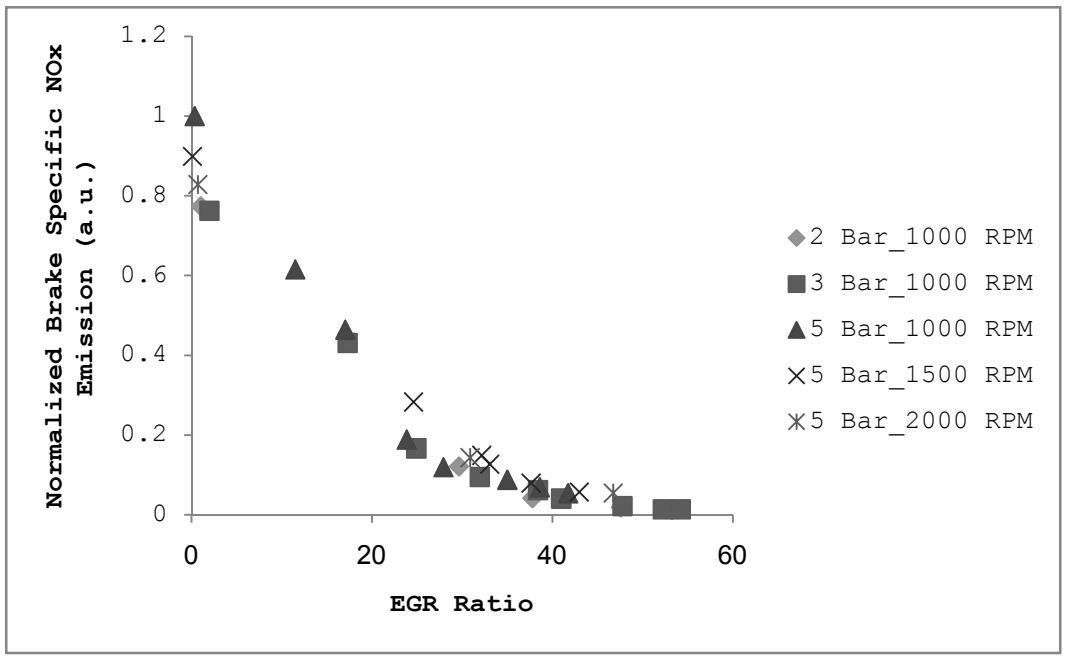


Figure 4.38: Normalized brake-specific NOx emissions versus EGR ratio for default injection strategy

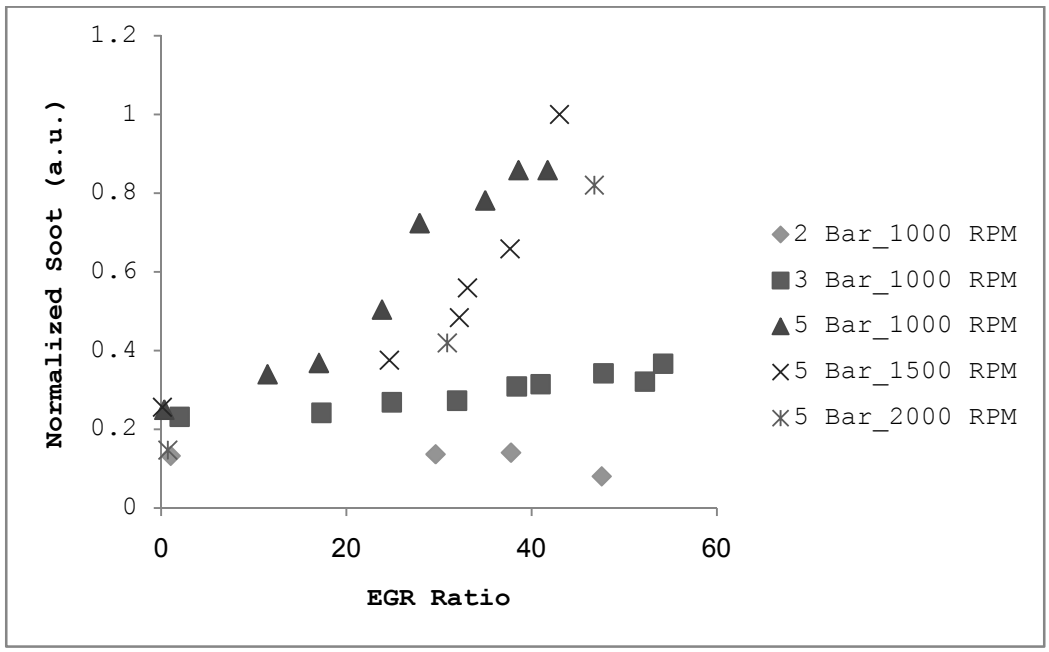


Figure 4.39: Normalized soot versus EGR ratio for default injection strategy

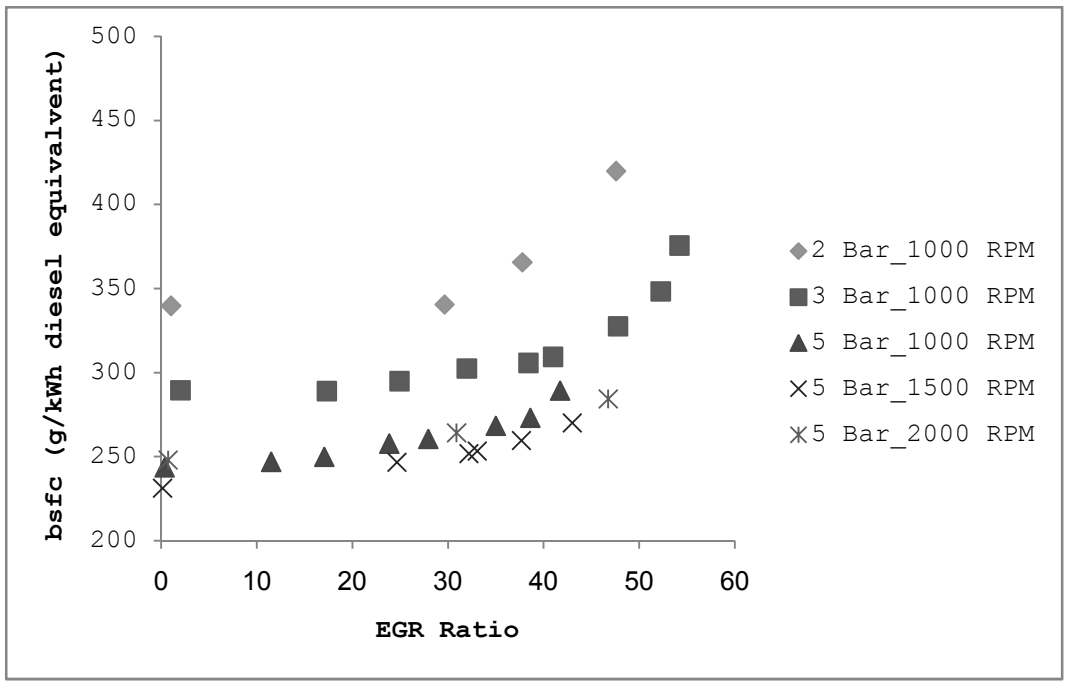


Figure 4.40: Brake-specific fuel consumption versus EGR ratio for default injection strategy

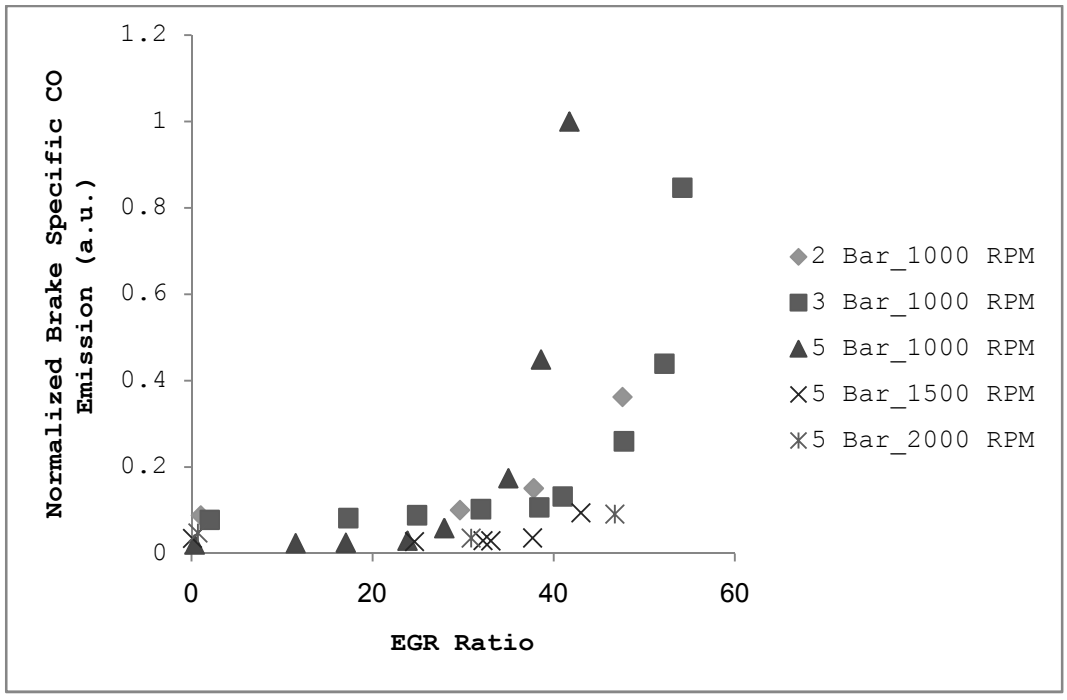


Figure 4.41: Normalized brake-specific CO emissions versus EGR ratio for default injection strategy

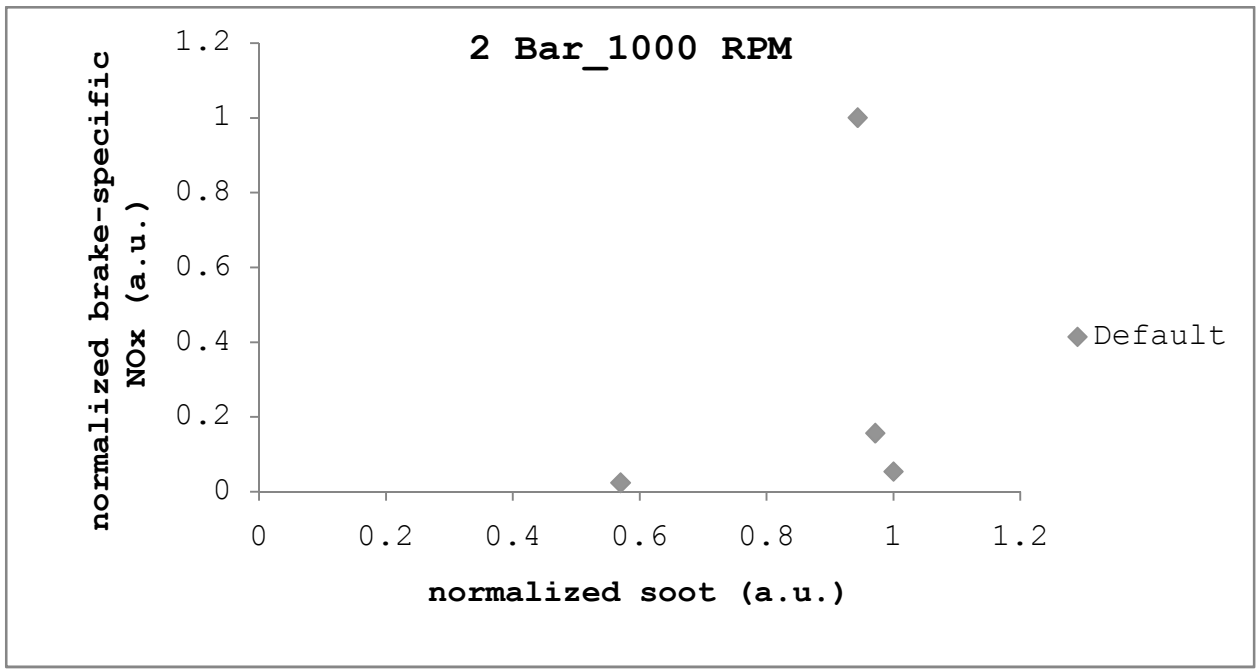


Figure 4.42: Soot-NOx tradeoff for 1000 rpm & 2 bar bmep

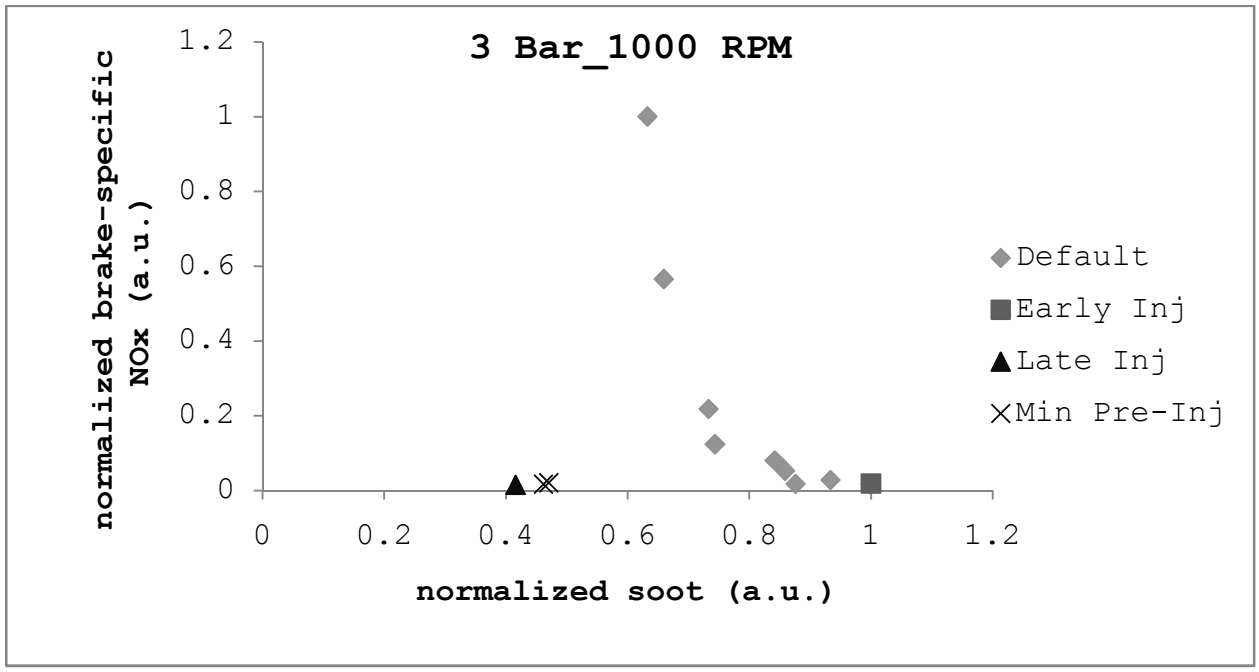


Figure 4.43: Soot-NOx tradeoff for 1000 rpm & 3 bar bmep

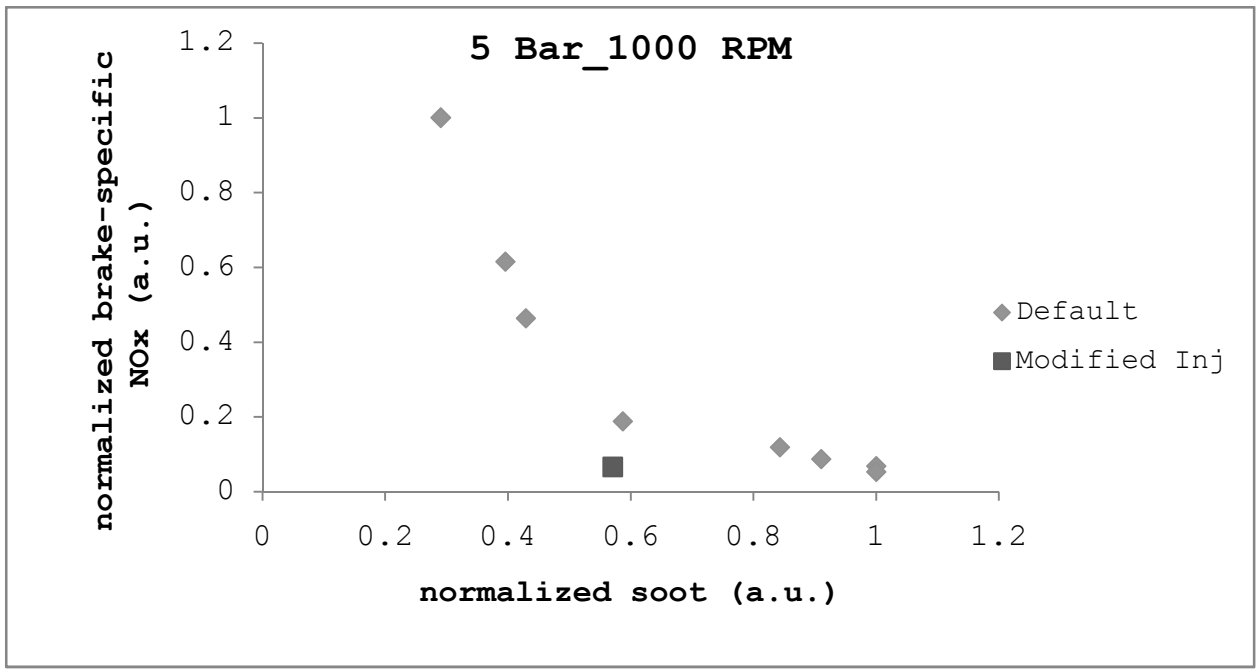


Figure 4.44: Soot-NOx tradeoff for 1000 rpm & 5 bar bmep

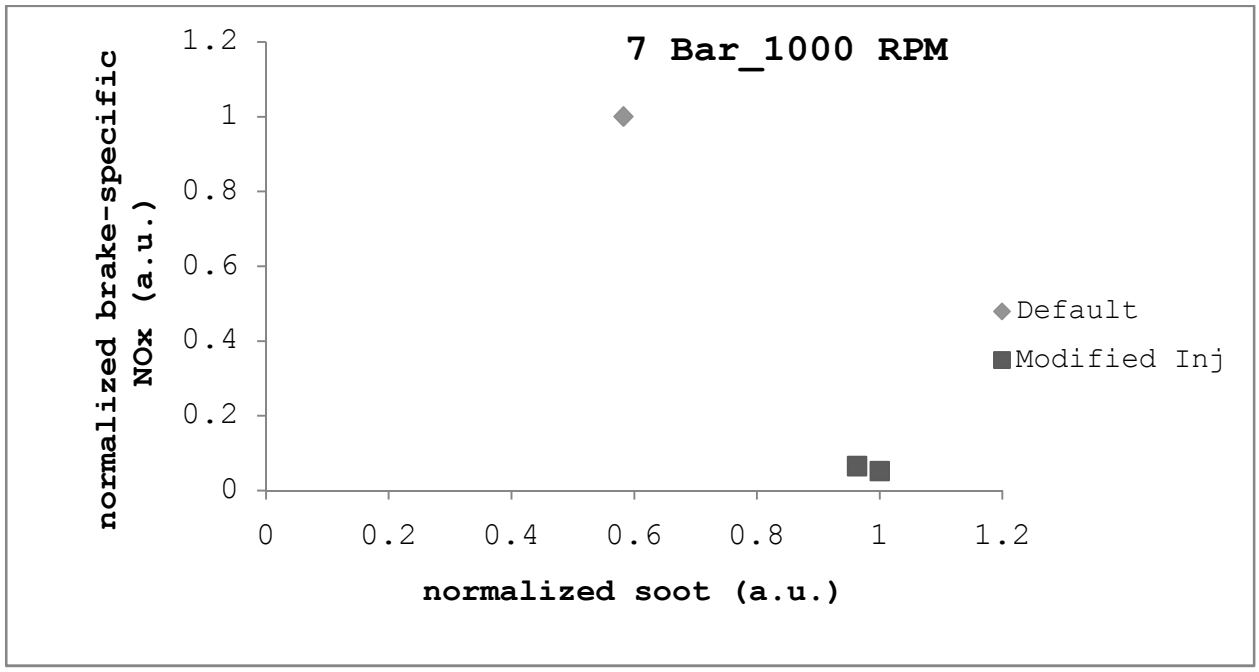


Figure 4.45: Soot-NOx tradeoff for 1000 rpm & 7 bar bmep

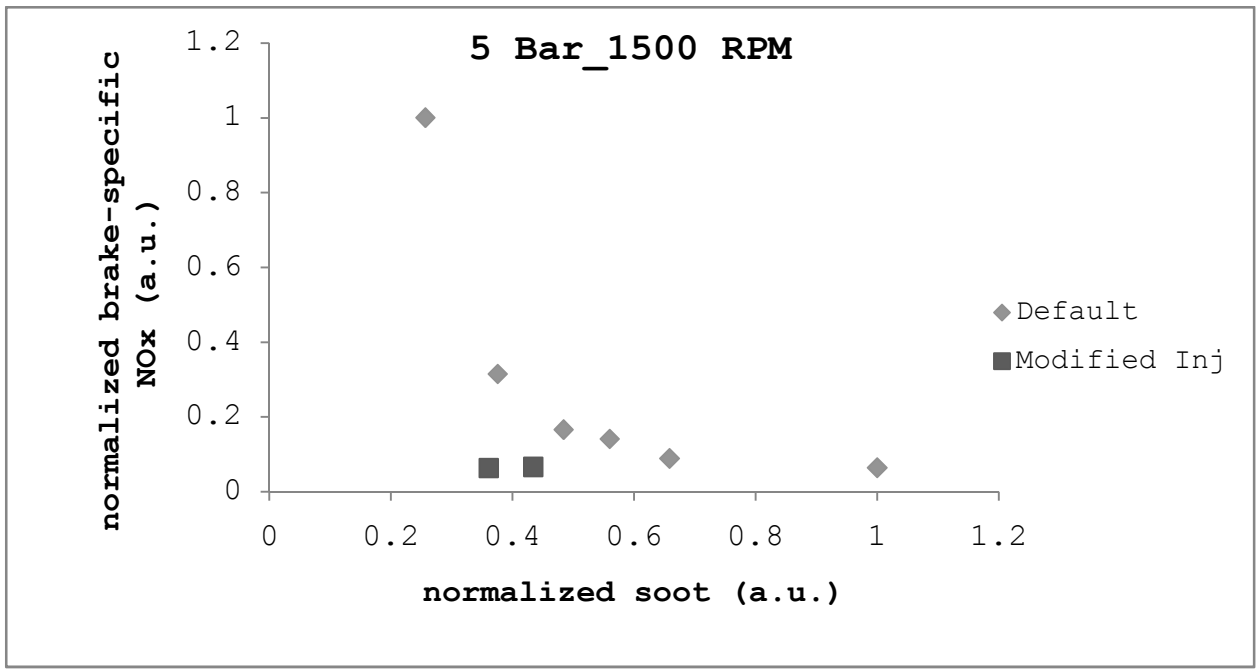


Figure 4.46: Soot-NOx tradeoff for 1500 rpm & 5 bar bmep

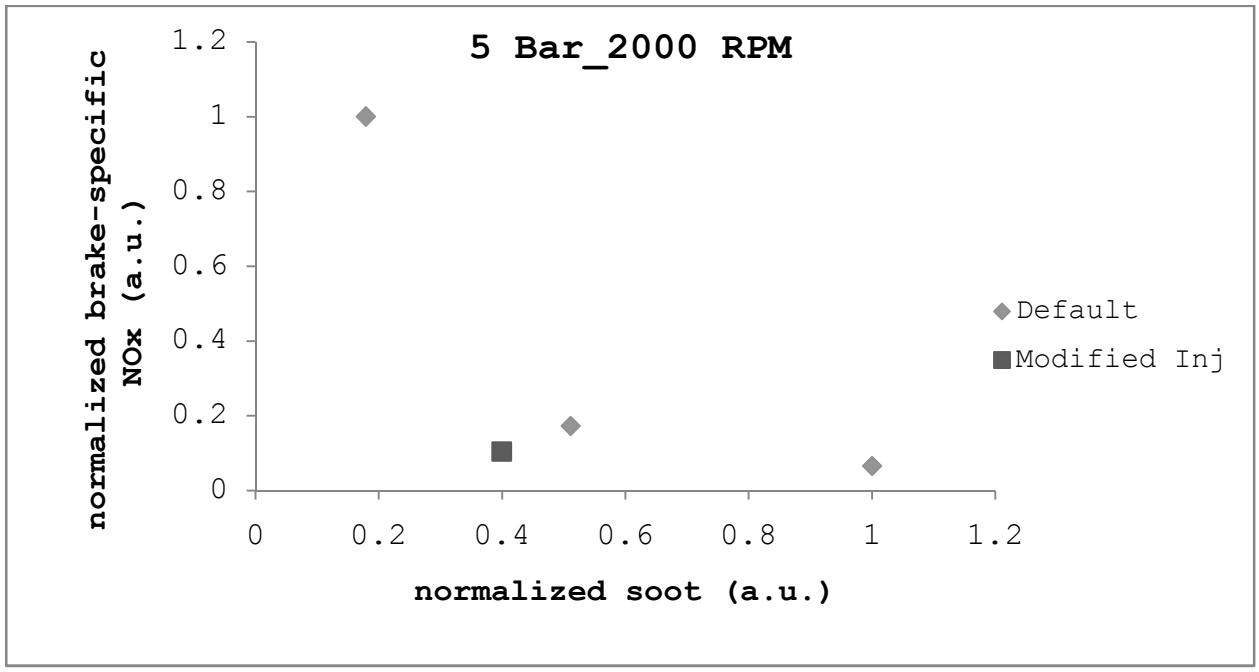


Figure 4.47: Soot-NOx tradeoff for 2000 rpm & 5 bar bmep

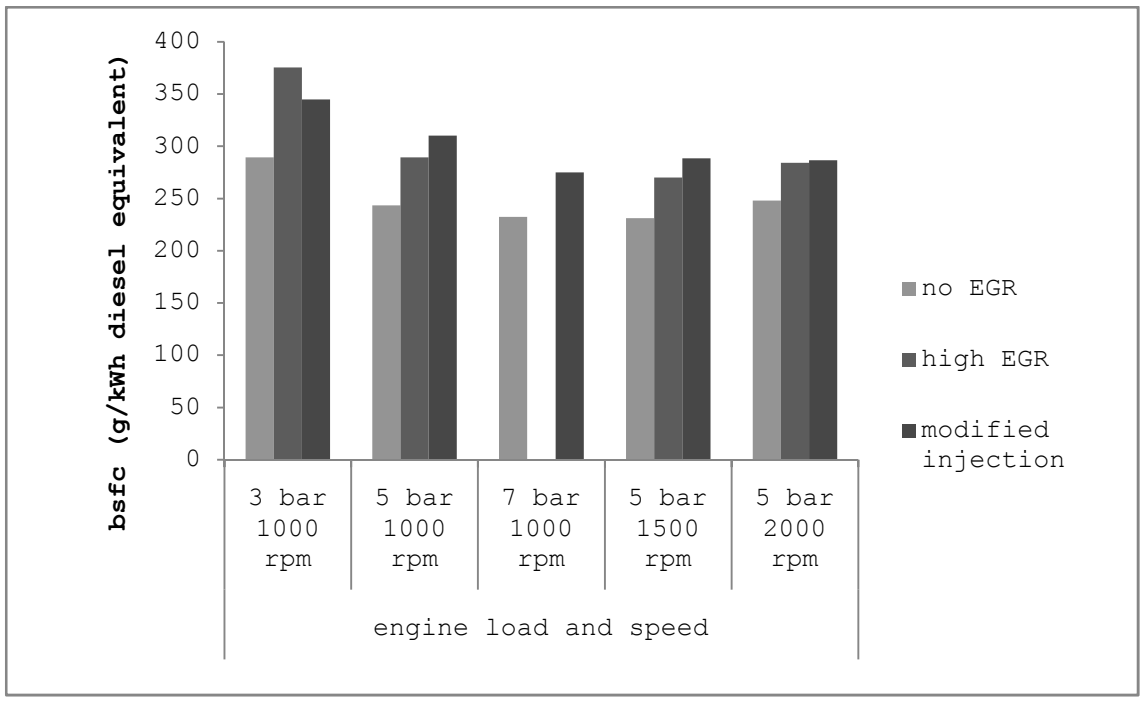


Figure 4.48: Brake-specific fuel consumption for modified injection strategy compared with the minimum (no EGR) and maximum (high EGR) bsfc for the default injection strategy

Chapter 5:
Conclusions and Future Work

Several aspects regarding the combustion of biodiesel have been considered in this work. First, the consequences of running biodiesel and its blends in an engine designed to run on diesel were observed. Due to the lower energy density of biodiesel, several engine operating parameters were seen to change by small amounts as specified by the default settings of the ECM. In this study, injection timings advanced, boost pressure increased, and EGR ratio decreased, though these trends may be different for other engines, depending on how they are set up. These changes together may be considered ECM calibration effects of using biodiesel. The combination of ECM calibration effects and fuel effects on NOx emissions ranged from little change to a near 50% increase.

Observing these effects of biodiesel on NOx emissions, different strategies were tested to optimize certain ECM parameters for use with biodiesel. Soot emissions were reduced significantly compared with diesel, so focus was placed on NOx and fuel efficiency. At low load conditions, it was found that an increase in EGR coupled with an advance in injection timing could provide NOx emissions at or below the level of diesel along with better fuel efficiency compared with the default operating conditions. At moderate load, a closer look was taken at the MAF setpoint tables and how they affect NOx emissions. In terms of simple equivalence ratio, higher blends of biodiesel were found to be running leaner than diesel (and with less EGR), corresponding to a large increase in NOx emissions. Adjusting the ECM's MAF setpoint tables based on stoichiometric air-fuel ratio eliminated the large-scale increase in NOx normally seen when running biodiesel with default settings in this engine. Similar conclusions held true for B50 in these conventional combustion studies.

Strategies were also developed for low temperature combustion of biodiesel in this engine. At low engine load, low temperature combustion could be achieved simply by increasing EGR to about 50% while using the ECM's default injection strategies. At higher load, low temperature combustion was achieved by first increasing the EGR to a level just lower than the point of combustion deterioration and then modifying the injection strategy to provide for lower in-cylinder temperatures. Specifically, the pre-injection was set to its minimum value without shutting it off completely, and the injection timing was delayed as needed in each case until the soot finally dropped off. Later injection timings were needed at higher engine load, resulting in a combustion phasing later than ideal. Overall, a tradeoff was seen between fuel efficiency and soot when attempting to achieve low temperature combustion by adjusting injection timings. Though the fuel consumption for low temperature combustion cases suffered somewhat compared with conventional combustion, the increase was reasonable given the substantial reductions in NOx and soot that were achieved.

Several possibilities remain for further study related to this work. The fuel pressures used in this study were the default values determined by the ECM, which may be rather low considering the general trend toward higher pressures in common-rail fuel systems. The influence of fuel pressure on emissions under high EGR conditions may be a useful study. Another interesting study would be the use of an optical engine with similar combustion chamber geometry to replicate some of the interesting cases from this study. This type of work could provide some valuable insight on the spray, mixing, and combustion processes underlying the engine-out emissions measured in this study.

References

1. Depcik C., Jacobs T., Hagena J., & Assanis D. Instructional use of a single-zone, premixed charge, spark-ignition engine heat release simulation. International Journal of Mechanical Engineering Education, 35 (1), 1 – 31, 2007.
2. Heywood J.B. *Internal Combustion Engine Fundamentals*. McGraw-Hill, Inc., New York, 1988.
3. Dec J.E. A conceptual model of DI diesel combustion based on laser-sheet imaging. SAE Paper 970873, 1997.
4. Flynn P.F., Durrett R.P., Hunter G.L., zur Loye A.O., Akinyemi O.C., Dec J.E., & Westbrook C.K.. Diesel combustion: an integrated view combining laser diagnostics, chemical kinetics, and empirical validation. SAE Paper 1999-01-0509, 1999.
5. Bowman C.T. Control of combustion-generated nitrogen oxide emissions: technology driven by regulation. Twenty-Fourth Symposium (International) on Combustion, The Combustion Institute, 859-878, 1992.
6. Richter H. & Howard J.B. Formation of polycyclic aromatic hydrocarbon and their growth to soot - a review of chemical reaction pathways. Progress in Energy and Combustion Science 26, 565-608, 2000.
7. Mansurov Z.A. Soot formation in combustion process. Combustion, Explosion, and Shock waves 41 (6), 727-744, 2005.
8. Maricq M. Chemical characterization of particulate emissions from diesel engines: a review. Aerosol Science 38, 1079-1118, 2007.

9. Hildemann L.M., Markowski G.R., & Cass G.R. Chemical composition of emissions from urban sources of fine organic aerosol. Environmental Science & Technology, 25, 744–759, 1991.
10. Guerrassi N. & Dupraz P. A common rail injection system for high speed direct injection diesel engines. SAE Technical Paper 980803, 1998.
11. Park C., Kook S., & Bae C. Effects of multiple injections in a HSDI diesel engine equipped with common rail injection system. SAE Technical Paper 2004-01-0127, 2004.
12. Ladommatos N., Abdelhalim S.M., Zhao H., & Hu Z. The effects of carbon dioxide in exhaust gas recirculation on diesel engine emissions. Proceedings of the I MECH E Part D Journal of Automobile Engineering 212 (1), 25–42, 1998.
13. Plee S.L., Ahmad T., Myers J.P. & Faeth G.M. Diesel NOx emissions - a simple correlation technique for intake air effects. Nineteenth International Symposium on Combustion, The Combustion Institute, 1495-1502, 1982.
14. Mitchell D.L., Pinson J.A., & Litzinger T.A. The effects of simulated EGR via intake air dilution on combustion in an optically accessible DI diesel engine. SAE paper 932798, 1993.
15. Ohigashi S., Kuroda H., Hayashi Y., & Sugihara K. Heat capacity changes predict nitrogen oxides reduction by exhaust gas recirculation. SAE paper 710010, 1971.
16. Durnholz M., Eifler G., & Endres H. Exhaust gas recirculation - a measure to reduce exhaust emissions of DI diesel engines. SAE paper 920725, 1992.
17. Wilson R.P., Muir E.B., & Pellicciotti F.A. Emissions study of a single-cylinder diesel engine. SAE paper 740123, 1974.

18. Ropke S., Schweimer G.W., & Strauss T.S. NOx formation in diesel engines for various fuels and intake gases. SAE paper 950213, 1995.
19. Lida N. Surrounding gas effects on soot formation and extinction - observation of diesel spray combustion using a rapid compression machine. SAE paper 930603, 1993.
20. Zheng M., Reader G.T., & Hawley J.G. Diesel engine exhaust gas recirculation - a review on advanced and novel concepts. Energy Conversion & Management 45 (6), 883-900, 2004.
21. Hawley J.G., Wallace F.J., Cox A., Horrocks R.W., & Bird G.L. Reduction of steady-state NOx levels from an automotive Diesel engine using optimized VGT/EGR schedules. SAE paper 1999-01-0835, 1999.
22. Kimura S., Aoki O., Ogawa H., Muranaka S., & Enomoto Y. New combustion concept for ultra-clean and high-efficiency small DI diesel engine. SAE Paper 1999-01-3681, 1999.
23. Yanagihara H. Simultaneous reduction of NOx and soot in diesel engines using a new mixture preparation method. JSME Intl. Journal, Series B 40 (4), 592-598, 1997.
24. Beatrice C., Avolio G., Bertoli C., Del Giacomo N., Guido C., & Migliaccio M. Oil & Gas Science & Technology 62 (4) 471-482, 2007.
25. Najt P.M. & Foster D.E. Compression ignition homogeneous charge combustion. SAE Paper 830264, 1983.
26. Glassman I. *Combustion*. 3rd edition, Academic Press, New York, 1996.
27. Kashdan J.T., Docquier N., & Bruneaux G. Mixture preparation and combustion via LIEF and LIF of combustion radicals in a direct-injection HCCI diesel engine. SAE Paper 2004-01-2945, 2004

28. Hildingsson L., Persson H., Joansson B., Collin R., Nygren J., Richter M., Alden M., Hasegawa R., & Yanagihara H. Optical diagnostics of HCCI and low-temperature diesel using simultaneous 2-D PLIF of OH and formaldehyde. SAE Paper 2004-01-2949, 2004
29. American Society for Testing and Materials (ASTM). Standard Specification for Biodiesel Fuel Blend Stock (B100) for Middle Distillate Fuels; ASTM: West Conshohocken, PA, 2009.
30. Ma F. and Hanna M.A. Bio-diesel production: a review. Bioresource Technology 70, 1-15, 1999.
31. Hill J., Nelson E., Tilman D., Polasky S., & Tiffany D. Environmental, economic, and energetic costs and benefits of biodiesel and ethanol biofuels. Proceedings of the National Academy of Science U.S.A. 103 (30), 11206–11210, 2006.
32. Sheehan J., Camobreco V., Duffield J., Graboski M. & Shapouri H. Life cycle inventory of biodiesel and petroleum diesel for use in an urban bus (National Renewable Energy Lab., Golden, CO), NREL Publ. No. SR-580-24089, 1998.
33. Mata T.M., Martins A.A., & Caetano N.S. Microalgae for biodiesel production and other applications: a review. Renewable and Sustainable Energy Reviews 14, 217–232, 2010.
34. United States Environmental Protection Agency (EPA). A comprehensive analysis of biodiesel impacts on exhaust emissions. EPA 420-P-02-001, 2002.
35. Boehman A.L., Morris D., and Szybist J. The Impact of Bulk Modulus of Diesel Fuels on Fuel Injection Timing. Energy and Fuels 18, 1877-1882, 2004
36. Zhang Y. & Boehman A.L. Impact of biodiesel on NOx emissions in a common rail direct injection diesel engine. Energy and Fuels 21 (4) 2003-2012, 2007.

37. Schonborn A., Ladommatos N., Allan R., Williams J., & Rogerson J. Effect of the molecular structure of individual fatty acid alcohol esters (biodiesel) on the formation of NOx and particulate matter in the diesel combustion process. SAE Paper 2008-01-1587, 2008.
38. Ban-Weiss G.A., Chen J.Y., Buchholz B.A., & Dibble R.W. A numerical investigation into the anomalous slight NOx increase when burning biodiesel; A new (old) theory. Fuel Processing Technology 88 (7) 659-667, 2007.
39. Musculus M. On the correlation between NOx emissions and the diesel premixed burn. SAE Paper 2004-01-1401, 2004.
40. Musculus M. Measurements of influence of soot radiation on in-cylinder temperature and exhaust NOx in a heavy-duty DI diesel engine. SAE Paper 2005-01-0925, 2005.
41. Knothe, G. Dependence of biodiesel fuel properties on the structure of fatty acid alkyl esters. Fuel Processing Technology 86, 1059–1070, 2005.
42. McCormick R.L., Graboski M.S., Alleman T.L., Herring A.M. Impact of biodiesel source material and chemical structure on emissions of criteria pollutants from a heavy-duty engine. Environmental Science & Technology 35 (9) 1742-1747, 2001.
43. Knothe, G. "Designer" biodiesel: optimizing fatty ester composition to improve fuel properties. Energy & Fuels 22, 1358–1364, 2008.
44. Eckerle W.A., Lyford-Pike E.J., Stanton D.W., Lapointe L.A., Whitacre S.D., & Wall C.W. Effects of methyl ester biodiesel blends on NOx emissions. SAE Paper 2008-01-0078, 2008.

45. Foong T.M. "Setup of Common-Rail Small-Bore High-Speed Direct Injection Diesel Engines for Biodiesel Combustion Studies." MS Thesis, Department of Mechanical Science and Engineering. Urbana, IL, University of Illinois at Urbana-Champaign, 2009.
46. Paul M.A. "A Direct-Injection Natural Gas Engine Laboratory for In-Cylinder Fuel/Air Mixing Studies." MS Thesis, Department of Mechanical and Industrial Engineering. Urbana, IL, University of Illinois at Urbana-Champaign, 1997.
47. Horiba. Non-sampling type NOx-A/F analyzer MEXA-720NOx: instruction manual. Kyoto, Japan: Horiba Ltd, 2003.
48. AVL. Smoke value measurements with the filter-paper-method: application notes. Graz, Austria: AVL LIST GmbH, 2005.

Appendix A:
Incomplete List of Useful INCA Parameters

Table A.1: Measurement Parameters*

Parameter	Description
fup	fuel pressure
maf	mass air flow per stroke
maf_kgh_mes	mass air flow rate
maf_slm	mass air flow per stroke used to calculate mf_slm
map	manifold absolute pressure
mf_main1	mass of fuel injected per stroke during the main injection
mf_prev2	mass of fuel injected per stroke during the pre-injection
mf_slm	maximum amount of fuel allowed to be injected per stroke (for soot control)
mf_tot	total mass of fuel injected per stroke
n	engine speed
soi_main1	start of injection for the main injection
soi_prev2	start of injection for the pre-injection
tba	boosted air temperature
tfu	fuel temperature
ti_main1_tu	duration of main injection
ti_prev2_tu	duration of pre-injection
tia	inlet air temperature
toil	oil temperature
tqi_sp	indicated engine torque
v_egrv[0]	control signal for left EGR valve (0.8~1.0V fully closed, ~4V fully open)
v_egrv[1]	control signal for right EGR valve (0.8~1.0V fully closed, ~4V fully open)

* includes direct measurements as well as values obtained through calibrations and calculations

Table A.2: Calibration Parameters

Parameter	Description
c_fac_ti_main1_tu[0-6]	allows adjustment of the duration of main injection for individual injectors
c_fac_ti_prev2_tu[0-6]	allows adjustment of the duration of pre-injection for individual injectors
lc_inj_prev2_on	toggle pre-injection on (1) and off (0)

Table A.3: Tabulated Adjustments

Parameter	x axis	y axis	Description
ip_egrvpwm_n_mafpwm	n	mafpwm	allows manual adjustment of EGR valve positions by setting all table entries for a given speed to the desired value
ip_maf_sp_bas	n	tqi_sp	allows adjustment of the maf setpoint value, which is used to control the amount of EGR
ip_mf_prev2	n	tqi_sp	allows adjustment of the amount of fuel injected during the pre-injection
ip_mf_slm_bas_dyn	n	maf_slm	allows adjustment of mf_slm based on the engine speed and amount of fresh air inducted
ip_soi_main1*	n	tqi_sp	allows adjustment of soi_main1
ip_soi_prev2_dif	n	tqi_sp	allows adjustment of soi_prev2 by specifying the difference between soi_main1 and soi_prev2

Appendix B:
Selected Operating Parameters for LTC Study

Table B.1: Selected Operating Parameters for 1000 rpm & 2 bar bmep

Intake Oxygen (%)	Start of Injection (deg ATDC)		Injected Fuel Mass (% of Total)		Injection Strategy
	Pre	Main	Pre	Main	
21.392	-16.3	2.58	10.12	89.88	Default
19.872	-16.3	2.58	10.12	89.88	Default
19.009	-16.3	2.58	10.12	89.88	Default
17.861	-16.3	2.58	10.12	89.88	Default

Table B.2: Selected Operating Parameters for 1000 rpm & 3 bar bmep

Intake Oxygen (%)	Start of Injection (deg ATDC)		Injected Fuel Mass (% of Total)		Injection Strategy
	Pre	Main	Pre	Main	
21.298	-15.69	2.43	9.1	90.9	Default
19.918	-15.69	2.43	9.14	90.86	Default
18.814	-15.69	2.43	9.15	90.85	Default
17.846	-15.69	2.43	9.15	90.85	Default
16.46	-15.69	2.43	9.15	90.85	Default
15.965	-15.69	2.43	9.15	90.85	Default
14.622	-15.69	2.43	9.15	90.85	Default
13.569	-15.69	2.43	9.15	90.85	Default
12.954	-15.69	2.43	9.15	90.85	Default
13.605	-13.32	5	9.15	90.85	Late Injection
13.719	-18.01	0.2	9.15	90.85	Early Injection
13.612	-15.75	2.46	6.02	93.98	Minimum Pre-injection
14.403	-15.75	2.46	6.02	93.98	Minimum Pre-injection

Table B.3: Selected Operating Parameters for 1000 rpm & 5 bar bmep

Intake Oxygen (%)	Start of Injection (deg ATDC)		Injected Fuel Mass (% of Total)		Injection Strategy
	Pre	Main	Pre	Main	
21.097	-16.18	2.11	7.72	92.28	Default
19.993	-16.18	2.11	7.72	92.28	Default
19.004	-16.18	2.11	7.72	92.28	Default
17.823	-16.18	2.11	7.72	92.28	Default
17.041	-16.18	2.11	7.72	92.28	Default
15.831	-16.18	2.11	7.72	92.28	Default
14.843	-16.18	2.11	7.72	92.28	Default
13.931	-16.18	2.11	7.72	92.28	Default
15.385	-10.82	7.46	4.52	95.48	Late Injection

Table B.4: Selected Operating Parameters for 1000 rpm & 7 bar bmep

Intake Oxygen (%)	Start of Injection (deg ATDC)		Injected Fuel Mass (% of Total)		Injection Strategy
	Pre	Main	Pre	Main	
21.409	-18.76	1.32	6.58	93.42	Default
15.568	-10.55	9.41	3.68	96.32	Late Injection
16.388	-10.57	9.4	3.68	96.32	Late Injection

Table B.5: Selected Operating Parameters for 1500 rpm & 5 bar bmep

Intake Oxygen (%)	Start of Injection (deg ATDC)		Injected Fuel Mass (% of Total)		Injection Strategy
	Pre	Main	Pre	Main	
22.06	-20.55	1.55	6.28	93.72	Default
19.1	-20.55	1.55	6.28	93.72	Default
17.776	-20.55	1.55	6.28	93.72	Default
17.055	-20.55	1.55	6.28	93.72	Default
15.936	-20.55	1.55	6.28	93.72	Default
14.459	-20.55	1.55	6.28	93.72	Default
15.16	-15.18	6.94	4.9	95.1	Late Injection
15.107	-16.18	5.94	4.9	95.1	Late Injection

Table B.6: Selected Operating Parameters for 2000 rpm & 5 bar bmep

Intake Oxygen (%)	Start of Injection (deg ATDC)		Injected Fuel Mass (% of Total)		Injection Strategy
	Pre	Main	Pre	Main	
21.971	-24.08	0.28	6.25	93.75	Default
18.364	-24.08	0.28	6.25	93.75	Default
14.658	-24.08	0.28	6.25	93.75	Default
16.984	-18.43	5.91	5.03	94.97	Late Injection